

Spring 2021

Design and Synthesis of Macrocyclic Peptide BRAF-WT Dimerization Inhibitors for the Treatment of Metastatic Melanoma

Chad Mulloy Beneker

Follow this and additional works at: <https://scholarcommons.sc.edu/etd>



Part of the [Pharmacy and Pharmaceutical Sciences Commons](#)

Recommended Citation

Beneker, C. M.(2021). *Design and Synthesis of Macrocyclic Peptide BRAF-WT Dimerization Inhibitors for the Treatment of Metastatic Melanoma*. (Doctoral dissertation). Retrieved from <https://scholarcommons.sc.edu/etd/6397>

This Open Access Dissertation is brought to you by Scholar Commons. It has been accepted for inclusion in Theses and Dissertations by an authorized administrator of Scholar Commons. For more information, please contact digres@mailbox.sc.edu.

DESIGN AND SYNTHESIS OF MACROCYCLIC PEPTIDE BRAF-WT
DIMERIZATION INHIBITORS FOR THE TREATMENT OF METASTATIC MELANOMA

by

Chad Mulloy Beneker

Bachelor of Science
Northern Kentucky University, 2015

Submitted in Partial Fulfillment of the Requirements

For the Degree of Doctor of Philosophy in

Pharmaceutical Sciences

College of Pharmacy

University of South Carolina

2021

Accepted by:

Campbell McInnes, Major Professor

Michael Wyatt, Committee Member

Eugenia Broude, Committee Member

John Lavigne, Committee Member

Thomas Dix, Committee Member

Tracey L. Weldon, Interim Vice Provost and Dean of the Graduate School

© Copyright by Chad Mulloy Beneker, 2021
All Rights Reserved.

DEDICATION

I would like to dedicate this work to my late grandfather, Donald Mulloy, who never stopped learning and encouraging me to do the same until his passing. I remember that no matter what was going on in my life or the world, he would always ask me about my studies and encourage me to do better and go further. The interest that he showed in my education encouraged me to do more and this drive only amplified after his loss. In life he just wanted me to pursue my dreams, be happy, and care about those that I hold dear. I think he would be proud of me today for the life and accomplishments that I have made, if only he were here to see it. Rest in peace Grandpa.

ACKNOWLEDGEMENTS

I would first and foremost like to acknowledge my mentor, Dr. Campbell McInnes, for giving me the chance at a graduate career, working with me over the years, and helping me learn and grow as a scientist. I would also like to acknowledge my committee members Dr. Michael Wyatt, Dr. Eugenia Broude, Dr. John Lavigne, and Dr. Thomas Dix, as well as Dr. Jill Turner who used to be on my committee, for helping me grow through all the meetings and career checkpoints throughout the years with insightful feedback and differing perspectives. Furthermore, I would like to acknowledge my collaborators who have ran the biological experiments including Dr. George Kontopidis and Dr. Magdalini in Greece and Dr. Tilman Brummer, Dr. Michael Röring, Dr. Simeon Galda, and Dr. Sandra Braun in Germany.

I would also like to acknowledge all my current and former labmates, Jessy Varghese, Li Zhang, Danda Chapagai, Robert Sears, Dr. Gurusankar Ramamoorthy, and Dr. Sandra Craig for all the support and insights over the years. Furthermore, I would like to acknowledge my colleges within the department who have been close friends of mine and have supported me as well through my journey, Dr. Nicole Reilly, Dr. Pamela Quizon, and Dr. Alexander Gasparian.

On a more personal note, I would like to acknowledge my husband, Kyle Graham, as well as my parents, Charles and Karen Beneker, and my grandmother, Roslyn Mulloy, for all being there with me throughout my journey and listening to me ramble, even

though you didn't know what I was talking about. I greatly appreciate all the love and support.

ABSTRACT

In cases of metastatic melanoma, BRAF is frequently mutated to the V600E oncoprotein causing uncontrolled cell proliferation driven by the MAPK-ERK pathway. There are several BRAF inhibitors, such as vemurafenib, which are FDA approved, but patients treated with these Type-I kinase inhibitors frequently observe relapse under mutant RAS and BRAF-wt conditions due to paradoxical activation. The mechanism of this resistance occurs through binding of the inhibitor to BRAF-wt initiating conformational changes which leads to BRAF dimerization. Once in the dimerized state, the inhibited monomer induces allosteric transactivation of the second monomer. This drug-induced activation of BRAF in cells with mutant RAS leads to uncontrolled cellular proliferation. In the context of mutant RAS/BRAF-wt cells treated with Type-I inhibitors, the MAPK/ERK pathway continually signals for initiation of cell proliferation, leading to mutant RAS-driven tumorigenesis. Currently there are no FDA approved treatments on the market for inhibiting RAS-driven tumorigenesis directly due to RAS family members having picomolar affinity for GDP/GTP. Recently there has been some progress in clinical trials of AMG510 (sotorasib), which binds outside of the catalytic GDP/GTP binding site. In a small cohort of 13 patients with KRAS-G12C-driven tumors, 7 patients observed partial responses to the target dose and 6 had stable disease.^{1,64} Though this clinical trial is exciting there is still a need for therapies targeted toward preventing paradoxical

activation in melanoma patients and for alternative therapies for patients suffering from mutant RAS-driven tumorigenesis. Herein we discuss the linear design of potent Type-IV BRAF inhibitors which have been seen to inhibit paradoxical activation of mutant RAS/BRAF-wt driven tumorigenesis.

Initially, the linear native sequence of peptides from the BRAF dimer interface (DIF) and variations of this were tested for direct binding using an intrinsic tryptophan fluorescence assay. Contributions of residue sidechains was further assessed through an alanine-scan of the truncated, linear sequence. Linear data combined with the crystal structure (PDB 4E26) contributed to the design of a 6-residue macrocyclic peptide which possessed enhanced binding. These alterations enhanced binding interactions giving a peptide with $K_d=0.06\mu\text{M}$ compared to the native sequence with $K_d=3.84\mu\text{M}$.

Cyclic peptides were then optimized to include physiochemical properties which agree with the beyond the rule of 5 guidelines for passive cell permeability of macrocycles larger than 500 Da. Further modifications consisted of REPLACEMENT of exocyclic sequences with more drug-like analogs which are uncharged and lipophilic in nature. Additional derivatization included N-methylation of the peptide backbone. The macrocyclic peptidomimetics described herein represent potential next generation BRAF therapeutics which have potent binding and have anti-tumor activity under paradoxical activation conditions.

TABLE OF CONTENTS

Dedication	iii
Acknowledgements.....	iv
Abstract.....	vi
List of Tables	ix
List of Figures	x
List of Abbreviations	xi
Chapter 1: Introduction	1
Chapter 2: Linear BRAF DIF Peptides Inhibit Paradoxical Activation.....	18
Chapter 3: Optimization of Cyclic BRAF DIF Peptides.....	44
Chapter 4: Optimization of Physicochemical Properties of Cyclic BRAF DIF Peptides for Passive Cell Permeability using REPLACE	62
Chapter 5: Off-Target Effects, Conclusions, and Future Directions.....	93
References	109
Appendix A: Characterization of Peptides	117
Appendix B: TC-NMR Data	120

LIST OF TABLES

Table 2.1 ITF Direct Binding Assay Data of Linear BRAF DIF Peptides.....	40
Table 3.1 ITF Direct Binding Assay Data of Cyclic BRAF DIF Peptides.....	58
Table 3.2 ITC Thermodynamics Data	59
Table 4.1 Passive Cell Permeability Guidelines.....	84
Table 4.2 Physicochemical Properties of Peptide for Cell Permeability	85
Table 4.3 Proton Assignment of Peptide 44	86
Table 4.4 Temperature Coefficients of Backbone Amide Protons of Peptide 44.....	87
Table 4.5 ITF Direct Binding Assay Data of BRAF DIF FLIPs.....	88
Table 4.6 N-Terminal and C-Terminal Capping Groups	89
Table A.1 LCMS Characterization of Synthetic Peptides.....	117

LIST OF FIGURES

Figure 1.1 MAPK Pathway Signaling Scheme.....	16
Figure 1.2 Linear Peptide Mimicking Reverse-Beta Turn of Native Sequence	17
Figure 2.1 Key DIF Peptide Binding Motifs	41
Figure 2.2 Inhibition of Paradoxical Activation with BRAF DIF Peptides	42
Figure 2.3 FAM-TAT-Peptides Diminish Cell Viability and Inhibit Downstream Transcription.....	43
Figure 3.1 BRAF DIF Peptide Cyclization Sites	60
Figure 3.2 ITC Data for Linear and Cyclic Peptides	61
Figure 4.1 REPLACE Strategy Scheme	90
Figure 4.2 2D NMR Spectra of Peptide 44	91
Figure 4.3 TC-NMR Spectra of Peptide 44	92
Figure 5.1 Homodimer DIF Interaction Energy Calculations	104
Figure 5.1 BRAF/hRIPK3 Heterodimer Interaction Energy Calculations.....	105
Figure 5.3 Human RIPK3 Homology Model and BRAF Crystal Structure	106
Figure 5.4 Heterodimer of BRAF and hRIPK3.....	107
Figure 5.5 Examples of Cyclic Peptides with potential Alternative Cyclization Methods for CPP Attachment	108
Figure B.1 TC-NMR Spectra of Peptide 17	120

LIST OF ABBREVIATIONS

ALLOC	Allyloxycarbonyl
ATP	Adenosine Triphosphate
BOC.....	tert-Butyloxycarbonyl
DIF	Dimer Interface
DIPEA.....	Diisopropylethylamine
DMF.....	Dimethylformamide
DQF-COSY.....	Double Quantum Filtered Correlated Spectroscopy
ERK	Extracellular Signal-Regulated Kinase
FMOC	9-Fluorenylmethoxycarbonyl
GTP	Guanine Triphosphate
MAPK.....	Mitogen-Activated Protein Kinase
MEK	Mitogen-Activated Protein Kinase Kinase
NMR	Nuclear Magnetic Resonance
RAF	Rapidly Accelerated Fibrosarcoma
RAS	Rat Sarcoma
ROESY	Rotating Frame Overhauser Effect Spectroscopy
RTK	Receptor Tyrosine Kinase
TC-NMR.....	Temperature Coefficient Nuclear Magnetic Resonance
TIPS.....	Triisopropylsilane
TOCSY	Total Correlation Spectroscopy

CHAPTER 1

INTRODUCTION

1.1 Historical Perspective on Cancer Treatment

The collective disease state of cancer is characterized as an uncontrolled proliferation of cells due to mutations in the genetic code. These mutations can then lead to changes in the conformation of proteins whose role is to regulate cell proliferation and programmed cell death known as apoptosis. With deregulated cell division and/or apoptosis, such mutations can lead to tumorigenesis and form tumors. In the case of malignant cancer types, these cells can break away from the original mass and travel to distant and unrelated areas of the body to start new tumors in other locations. Tumorigenesis in organs responsible for life sustaining functions, such as nutrient absorption in the intestines or gas exchange in the lungs, can become deadly by disrupting the function of that organ system. According to predictions published by the American Cancer Society, there will be an estimated 1.8 million new cases and about 600 thousand deaths from cancer in the United States alone in 2020; of which 5.5% of the predicted new cases (100,350 cases) are attributed to melanoma of the skin, with about 11,500 cases of skin cancer resulting in death.³

Chemotherapy refers to the treatment of a disease with a chemical drug, although the word is now usually most associated with cancer treatment specifically. The use of

chemotherapy drugs is a way of treating the whole body with the intent to cure, control, or ease the symptoms of a patient's disease state.² Furthermore, modern chemotherapy is usually administered as a neoadjuvant therapy i.e. to shrink the tumor prior to surgery or radiation treatment either due to size of the tumor or complexity around vital organs. Additionally, it can be used as an adjuvant therapy after surgery to prevent the reappearance of the resected tumor.

Traditional cancer chemotherapeutic drugs typically target the cell cycle. Many of the traditional drugs have been in use for decades starting with the discovery of the nitrogen mustards and the anti-metabolites in the 1940's.³ These drugs are classified into several classes: alkylating agents, antimetabolites, anti-tumor antibiotics, topoisomerase inhibitors, and mitotic inhibitors,³ and are toxic because they mostly target DNA similarly in normal and cancer cells. Although these drugs have the benefit of treating the whole body in contrast to the local treatments of surgery or radiation therapy, the risk factors associated with chemotherapy include the eminent danger of harming the normal, healthy cells and the potential incidence of leukemia and nerve or heart damage.³

1.2 Targeted Therapy of Kinases

In contrast to "chemotherapy", targeted therapy involves treating cancer patients based on their individualized type of cancer and the product of specific mutations which lead to constitutively active proteins or changes in protein levels which inherently cause the uncontrolled cell proliferation.⁵ In this sense, cells bearing specific cancer markers, containing upregulated protein levels, or mutations which enhance drug binding would

be affected solely or more significantly, therefore leaving the normal, healthy cells relatively unharmed. The product of the oncogene is targeted in this sense because the protein products are significantly different due to conformation, whereas the mutant versus non-mutant DNA is relatively similar. For example, trastuzumab is a monoclonal antibody which is used in the treatment of postmenopausal women who have HER2+ breast cancer.⁶ This antibody specifically binds to the HER2 receptor, which is overexpressed in 20-30% of breast cancer cases due to having extra copies of the gene encoding HER2. Due to the overexpression of the HER2 receptor, these cells are more susceptible to treatment with trastuzumab versus normal cells.

The kinase superfamily is a large group of proteins whose catalytic activity functions by phosphorylating its substrate, thus acting as a signal transducer. But kinases also have a large role in the non-catalytic, coordination of complex biological processes by scaffolding protein complexes, acting as competition for protein interactions, exerting allosteric effects on other enzymes, subcellular targeting, and DNA binding.^{7,8} For catalytic signaling of protein kinases, an upstream protein will bind to the kinase and phosphorylate the activation loop, thus converting the kinase to its active conformation. In the presence of ATP, a kinase can bind and phosphorylate the downstream substrate by adding a phosphate to the substrate serine, threonine, or tyrosine residue, depending on the class of kinase, while converting the ATP to ADP, thus either activating or inhibiting the target substrate's catalytic activity. In this sense, a phosphorylation cascade can propagate, and a signal can be conveyed from one portion of the cell to another and a response can be triggered. Furthermore, kinases not only can propagate a signal, but

catalytic activity of kinases can inversely inhibit cellular functions as well. In the cancer disease state kinases which promote cell proliferation and survival can become dysregulated and continually signal, thus promoting tumorigenesis and making them ideal targets of therapeutic intervention for inhibiting the uncontrolled signaling from oncogenic kinases. Furthermore, kinases consume adenosine triphosphate (ATP) for catalytic activity by cleaving the γ -phosphate for phosphorylation of its substrate. Historically, most kinase drug discovery involves the design of a small molecule which binds to the ATP binding site with higher affinity than the native substrate to prevent the kinase's catalytic activity, this is the mechanism for Type I-III inhibitors as described below. Overall, the benefits of inhibiting a kinase would be the ability to directly interfere with the dysregulated pathway which drives tumorigenesis by means of small molecule inhibitors. Potential drawbacks of this approach include lack of selectivity for more than 500 known kinases encoded by the genome, with similar ATP binding pockets. Therefore, kinase inhibitors utilizing the ATP binding site have the potential to have off-target effects which may be counterproductive to the therapeutic intent.

Kinase inhibitors are chemical compounds with the therapeutic ability to interfere with kinase activity. The first clinical approval for use of a kinase inhibitor was the approval of fasudil in Japan for the indication of patients suffering from cerebral vasoplasm.⁹ Later, the drug was determined to be inhibiting Rho kinase II which prevents activation of pathways controlling vascular smooth muscle contraction.¹⁰ In 2001, the first US FDA approved kinase inhibitor in oncology was imatinib (Gleevec) used for the treatment of chronic myelogenous leukemia (CML).¹¹ After the 5 year follow-up on

patients initially treated with imatinib, the majority of patients maintaining a continuous therapy of imatinib treatment had a complete cytogenetic response ($P < 0.001$) and there was minimal risk of disease progression.¹² Furthermore, continuous treatment with imatinib from initial diagnosis produced a survival rate of 89% which is higher than that of any prior study of CML treatment. Currently there are 48 US FDA approved small molecule kinase inhibitors, most of which are orally bioavailable and are indicated for treatment of malignancies.¹³ For a compound to inhibit a kinase, the compound must be able to bind to either the ATP binding site, co-factor binding site, or a regulatory protein-protein binding site. Currently there are six types of kinase inhibitors which are categorized by their mechanism of inhibition and they are defined as follows:¹⁴

- Type I: Bind to the active conformation (DGF-in/ α C-in) and occupy some of the ATP binding site with hydrogen bonds to the hinge region
- Type I $\frac{1}{2}$: Bind to the inactive conformation (DGF-in) and occupy some of the ATP binding site with hydrogen bonds to the hinge region
- Type II: Bind to the inactive conformation (DGF-out) and occupy some of the ATP binding site with hydrogen bonds to the hinge region
- Type III: Bind adjacent to the ATP binding site and allosterically blocks ATP from binding.
- Type IV: Bind to an allosteric site which is not the ATP binding site nor the substrate binding site
- Type V: Bivalent compounds which bind to two different sites of the enzyme

Stratification of types of kinase inhibitors has to do with selectivity as well as combatting disease resistance mechanisms. As for selectivity, a mutation may cause the target to be locked in the active conformation, thus a Type II inhibitor would not work since it binds to the inactive conformation. Furthermore, if treatment with a Type I inhibitor leads to dimerization dependent resistance, then an allosteric Type IV inhibitor may be of use to combat the resistance mechanism by blocking dimerization.

1.3 MAPK Pathway

The mitogen-activated protein kinase (MAPK)/ERK pathway is responsible for cell proliferation and differentiation in the cell.¹⁵⁻¹⁷ Through this pathway, extracellular signals are carried to nucleus to initiate transcription of proteins necessary for cell proliferation. The principal proteins associate with this pathway are RAS, RAF, MEK, and ERK.

Signal transduction is initiated upon binding of extracellular growth factors (e.g. epidermal growth factor) to their respective receptor tyrosine kinase (RTK; e.g. epidermal growth factor receptor). This leads to the recruitment of guanine nucleotide exchange factors to the cell membrane to facilitate the exchange of GDP for GTP on the membrane localized RAS protein (KRAS, NRAS, or HRAS)(**Figure 1.1**). This exchange activates the RAS protein and allows it to bind to a RAF monomer (ARAF, BRAF, or CRAF). Once the RAS-GTP-RAF complex is formed, the RAF catalytic domains associate through the dimerization interface (DIF). The activation site of one protomer is phosphorylated, causing conformational changes in the regulatory spine (R-spine) and DIF, resulting in the

phosphorylation of the second protomer in the dimeric complex. The dimeric form of RAF kinase is catalytically active and initiates the phosphorylation cascade on to MEK and ERK, which ultimately activates the downstream transcription factors required for cell proliferation.¹⁸

The MAPK/ERK pathway is largely involved in cell proliferation, differentiation, and survival of the cell, therefore, members of this pathway frequently are dysregulated in cancer. Upstream abnormalities include frequently overexpressed or mutated RTK's which can lead to an increased degree of signaling due to growth factor binding.¹⁹⁻²¹ Furthermore, activating mutations in the RAS GTPase²²⁻²⁴ which functions as a molecular switch are frequently observed as well, leading to the activation of the MAP3K (RAF) for this signaling pathway. Downstream influences include the loss of neurofibromin²⁵, the protein product of the NF1 gene which is a negative feedback mechanism of the MAPK/ERK pathway. NF1 is a tumor suppressor protein which is transcribed by the MAPK/ERK pathway and inhibits the activity of RAS. Loss of this NF1 gene removes the negative feedback regulation step and can be a factor of tumorigenesis by dysregulating upstream catalytic enzymes. Furthermore, RAF acts as the gatekeeper kinase of the MAPK/ERK pathway and gain-of-function point mutations are frequently observed in malignancies.^{18,26,27} Dysregulation of this kinase allows for the initiation of the phosphorylation cascade and thus uncontrolled cell proliferation. The most frequent RAF mutation is the BRAF V600E point mutation which mimics activation loop phosphorylation^{26,28}, thus allowing the kinase to not only function without upstream activation, but it also allows the kinase to have catalytic activity as a monomer. This

mutation removes two of the regulatory mechanisms from the native kinase, locking it in the active conformation and producing uncontrolled activity, thus leading to tumorigenesis.

The RAF kinase has three isoforms in the human context, ARAF, BRAF, and RAF-1 (i.e. CRAF). The RAF kinases all share three highly conserved regions:

- CR1: RAS-GTP binding domain (RBD) and Cysteine-rich domain (CRD)
- CR2: 14-3-3 protein binding site
- CR3: Catalytic domain and Dimer interface (DIF)

The CR1 RBD contains a conserved arginine residue (R188 in BRAF) which facilitates its recruitment to the membrane and RAS-GTP binding.²⁶ Mutation of this residue (R188L) inhibits upstream activation via RAS interaction and abrogates downstream phosphorylation events. The 14-3-3 protein binds to phosphorylated S365 in BRAF in the CR2 and stabilizes the inactive, closed conformation in which the N-terminal and C-terminal domains are clamped together.²⁶ Dissociation of this protein and subsequent dephosphorylation of the serine residue represents a key regulatory step in BRAF activation, opening up the conformation for RAS-GTP binding. The catalytic CR3 domain contains the N-region, Phosphorylation Loop (P-Loop), Activation Loop (A-Loop), and the DIF, where the latter facilitates the side-to-side dimerization step required for RAF activation. One protomer of the loosely dimerized RAF kinase has its activation site (T⁵⁹⁹VKS⁶⁰²) phosphorylated which causes a conformational change, involving the

regulatory spines and dimer interface and then leads to allosteric phosphorylation of the second, inactive protomer and a fully active RAF complex.^{18,26}

In cases of metastatic melanoma, as well as hairy cell leukemia and colorectal carcinoma²⁹, BRAF is mutated in about 45% of cases³⁰ with the most frequent being the V600E point mutation. This substitution mimics BRAF phosphorylation by introducing a negatively charged glutamate residue near the point of phosphorylation on the activation loop, rendering the kinase locked in a constitutively active conformation. By mimicking the A-loop phosphorylation, the monomer is without need of RAS binding and can initiate the phosphorylation cascade without extracellular initiation.

1.4 Paradoxical Activation and Resistance

In 2011, the FDA-approved drug Zelboraf[®] (vemurafenib)¹⁵, was approved for the indication of melanoma patients bearing the BRAF V600E mutation. This drug is a Type I ½ kinase inhibitor which potently binds to the ATP binding site of mutant BRAF V600E and initially created significant enthusiasm by therapeutically reducing the tumor size in patients exhibiting this mutation. This enthusiasm diminished as drug-induced resistance appeared in patients after 23 weeks of treatment with the drug.³¹ This resistance was later identified as paradoxical activation, in which the drug would inhibit ATP binding to the first protomer of BRAF-wt protein in the presence of oncogenic RAS but induce catalytic activity of the second protomer in the dimeric RAF complex.³²⁻³⁴ In these cases, oncogenic RAS allowed for unregulated signaling through the now activated BRAF protomer, resulting in proliferation of undruggable, mutant RAS-driven tumors.

The undesirable clinically observed response to vemurafenib sparked the drive to create second line therapies for patients who have developed resistance for the drug. The FDA approval of the MEK inhibitor trametinib as a combination therapy for patients with mutant melanoma yielded significant improvement, but MEK inhibitors have toxicity issues which make treatment difficult.¹¹ The idea behind this combination was to target the initial BRAF-driven tumor with vemurafenib, and then to inhibit drug-induced progression of upstream RAS-driven tumorigenesis by inhibiting the downstream MEK kinase. Furthermore, the sequential combination of BRAFi/MEKi therapy followed by immunotherapy with the anti-CTLA4 antibody ipilimumab or anti-PD1 antibodies nivolumab and pembrolizumab has yielded improvements but not without multiple mechanisms of escape from immunotherapy.³⁵ For this combination, adjuvant therapy with either anti-CTLA4 or anti-PD1 antibodies allows for the production and immune response via T-cells which have the ability to kill cancer cells. The idea is that after initial treatment with small molecule inhibitors, immunotherapy activates the T-cells to attack overly prolific cells, thus maintaining a smaller tumor size and increasing the survival rate of the patient.

1.5 Hypothesis and Rationale

The drug-induced dimerization of BRAF-wt and proliferation of mutant RAS-driven tumorigenesis can be inhibited by a macrocyclic, Type IV kinase inhibitor designed around the reverse β -turn sequence (**Figure 1.2**) of the BRAF dimer interface. In the treatment of BRAF V600E mutant melanoma, there is also a high frequency of mutations leading to

oncogenic RAS, i.e. about 30% of all human cancers.²⁹ In previous attempts to treat patients with this mutation, Type I BRAF inhibitors proved to be effective in the mutant BRAF context, but in the wild-type BRAF context, the inhibitor induced BRAF homo-/heterodimerization and subsequent paradoxical activation of the second monomer. In the case of the presence of oncogenic RAS and wild-type BRAF, a drug-resistant tumor forms, for which there is not effective therapy. The treatment of patients with the proposed Type IV BRAF DIF inhibitor should prevent the paradoxical activation of BRAF and therefore avoid the promotion of the RAS-driven tumor while treating with vemurafenib.

1.6 Rationale for targeting the dimer interface of RAF kinases

In 2001, the significance of RAF heterodimerization was demonstrated for the first time,³⁶ then there was the discovery that the naturally occurring R732H mutation, in *Drosophila* KSR (Kinase Suppressor of RAS), which abolished KSR-induced RAF activation and subsequent MEK phosphorylation in S2 cells.³⁷ Based on that discovery, Rajakulendran et al. described the side-to-side dimerization of RAF/KSR and deemed the BRAF DIF a potential therapeutic target.³⁸ This work was based on the analysis of KSR and RAF crystal structures, from which R732 of KSR was found to be conserved throughout the KSR and RAF kinase families. Further investigation of the crystal structures showed that KSR and BRAF have similar dimer interfaces and through dimerization, R732 of KSR engages the α C-helix of BRAF, a known regulatory structure required for catalytic activity. Furthermore, in an analytical ultracentrifugation experiment, DRAF-wt (RAF isoform of

Drosophila) was able to form dimers, whereas DRAF-R481H (equivalent to KSR R732H) was only found as a monomer in solution, thus demonstrating the dimer inhibitory effects of the R481H mutation. Dimerization was further identified as a key step to catalytic activity in a KSR-RAF-MEK co-overexpression assay where mutations in either the KSR or RAF dimer interface abrogated MEK (direct catalytic substrate of RAF) phosphorylation, whereas mutations distant from the DIF did not, thus further demonstrating the catalytic relevance of RAF dimerization for activity.

Roring et al. has done extensive work with characterizing the BRAF dimer interface and has further identified binding determinants for BRAF homo-/heterodimers through cellular studies analyzing substrate level phosphorylation of downstream targets.²⁶ The DIF is described as a central cluster of residues in the form of a reverse- β -turn located between the α C-helix and the β 4-sheet (**Figure 1.2**). The R481H substitution (R509H in BRAF) in DRAF^{EVKD}, a synthetic mutant with similar activity to BRAF V600E, was shown to ablate downstream MEK phosphorylation according to Rajakulendran et al.³⁸ Roring et al. found that the BRAF-R509H substitution and the 3x mutant (3x: R509H, L515G, and M517W) had a similar inhibitory effect in the BRAF-wt context with a reduced cellular MEK phosphorylation potential of >60 and 90%, respectively, but Class I high activity BRAF-V600E, BRAF-insT, and BRAF-G469A were insensitive to the DIF mutations.²⁶ Furthermore, BRAF DIF mutations inhibited paradoxical MEK/ERK phosphorylation induced by D594A mutation, sorafenib, or PLX 4720, but heterodimerization with CRAF was not abolished, which suggests that inhibition of the dimerization motif could be a therapeutic target to combat drug-induced paradoxical activation of BRAF-wt.

Additionally, although the CRAF-R401H (equivalent to BRAF-R509H) mutation impaired MEK phosphorylation, CRAF homodimers were still formed, suggesting that RAF activation consists of a two-step mechanism consisting of dimerization and then DIF-mediated transactivation. This data directly supports the idea that disruption of the DIF in the BRAF-wt context can prevent downstream MEK phosphorylation events and provide an alternative therapeutic for preventing mutant RAS-driven tumorigenesis during the treatment of patients bearing the BRAF-V600E mutation.

In a study conducted by Freeman et al., RAF heterodimerization versus homodimerization was explored among the three RAF isoforms.³⁹ In this study, it was found that BRAF and CRAF heterodimerization was the major activating complex for MEK phosphorylation, and ARAF had only marginal heterodimerization with BRAF, but not CRAF. Heterodimerization of BRAF/CRAF was observed to be more crucial for CRAF activity when removal of BRAF decreased CRAF-driven activity by 90% compared to basal level. In the reverse case, removal of CRAF only decreased BRAF-driven activity by 50%. Furthermore, BRAF was shown to exhibit some homodimerization, as well as CRAF homodimerization was observed to a lower extent. Additionally, through the use of mutational experiments, alterations in the BRAF and CRAF dimer interface were tested for catalytic activity in which the R509H mutation previously shown to inhibit BRAF catalytic activity was confirmed for both BRAF and CRAF (R401H), of which the CRAF mutant also exhibited a decreased basal level activity, whereas BRAF was only an inhibition of EGF-induced activity. This mutation was also demonstrated to inhibit BRAF/CRAF homodimer activity as well. Additionally, as a primary proof-of-concept for

the use of DIF peptides as dimerization inhibitors, the GFP-tagged DIF peptide, GFP-DI1 (GVLKTRHVNILLFMGYST), was expressed in cells and inhibited BRAF/CRAF heterodimerization as well as RAF-mediated MEK phosphorylation. Moreover, NSCLC cells were treated with TAT-DI1, and was shown to inhibit cell viability compared to the TAT-Scram negative control peptide (GRINKGRHTFLLVVMYSL). Taken together, heterodimerization of BRAF and CRAF appears to be the driving force for RAF-catalyzed MEK phosphorylation and this work is the first to demonstrate the ability to inhibit MEK phosphorylation using a BRAF DIF peptide sequence.

While this research was being accomplished, there was another article published by Gunderwala et al. which provides a secondary proof-of-concept for the approach of inhibiting BRAF dimerization using DIF peptides.⁴⁰ In this study, linear DIF peptides (Braftide; BRAF residues 508-517; TRHVNILLFM) were computationally designed and tested for their ability to inhibit full length BRAF catalytic activity in solution using the ELISA assay. The data was obtained by measuring MEK phosphorylation and resulted in $IC_{50} = 364$ nM and 172 nM for BRAF-wt and BRAF-G469A, respectively. Mutation of the arginine residue in the braftide to histidine (R/H-braftide; THHVNILLFM) resulted in data consistent with findings from Roering et al. with $IC_{50} = 1.5$ μ M and 2.5 μ M for wild-type and G469A respectively. Furthermore, TAT-Braftide constructs in the BRAF-wt and non-V600 BRAF mutant (BRAF-G469A) context using HEK293 cells transfected with the protein of interest were tested as a cellular experiment while being co-treated with dabrafenib, a type I BRAF kinase inhibitor. This data confirms the ability of DIF peptides to inhibit MEK phosphorylation under the paradoxical activation conditions as well as its application in

treatment of cancer driven by non-V600 BRAF mutants. Interestingly, BRAF and MEK were observed to be proteolytically degraded upon treatment with TAT-Braftides, the authors attributed this to a non-catalytic function of BRAF kinase. Furthermore, the TAT-Braftides were tested for cell viability in HCT116 and HCT-15 cell lines, which both contain the KRAS-G13D gain-of-function mutation, while cells were co-treated with clinically relevant BRAF inhibitors. The resulting EC_{50} = 7.1 and 6.6 μ M respectively, with the TAT sequence alone acting as the negative control with no observable cell death up to 100 μ M, demonstrating that DIF peptides can inhibit mutant RAS-driven tumorigenesis in the clinically relevant paradoxical activation context. Taken together, this data demonstrates the proof-of-concept for the inhibition of paradoxical activation using BRAF DIF inhibitors to dissociate BRAF homo-/heterodimers of BRAF-wt for the clinical application of preventing drug-induced resistance to type I BRAF kinase inhibitors.

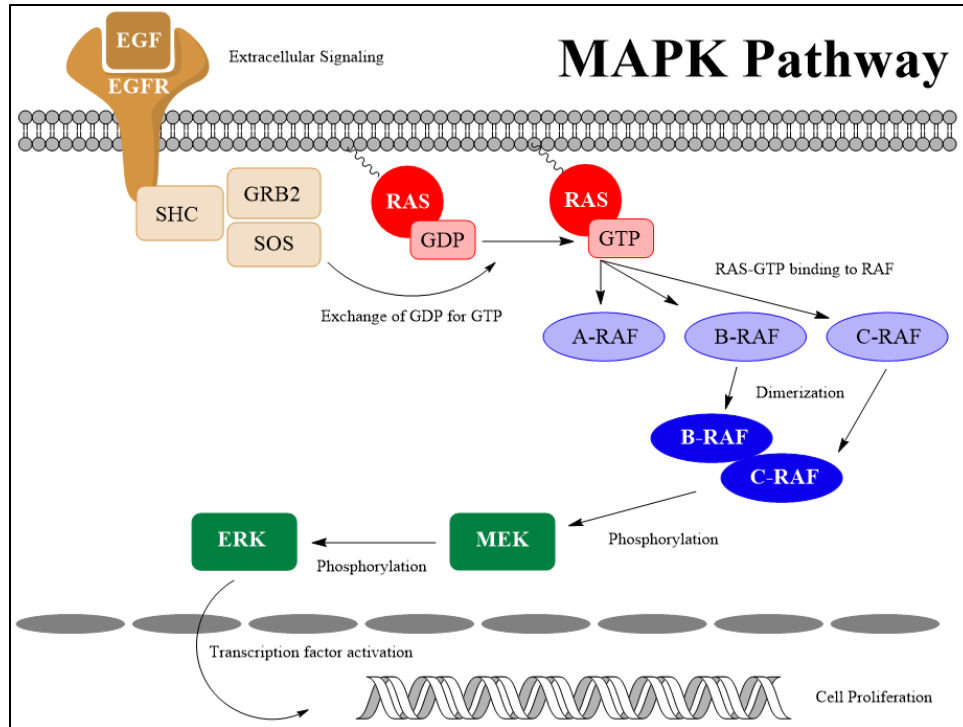


FIGURE 1.1: MAPK PATHWAY SIGNALING SCHEME: Extracellular signaling initiates the MAPK pathway by binding of EGF to EGFR, thus activating the SOS complex to catalyze the exchange of GDP for GTP on membrane localized RAS protein. RAS then phosphorylates a RAF isoform, triggering dimerization and propagation of the phosphorylation cascade through MEK and ERK to activate transcription factors in the nucleus and eventually lead to cell proliferation.

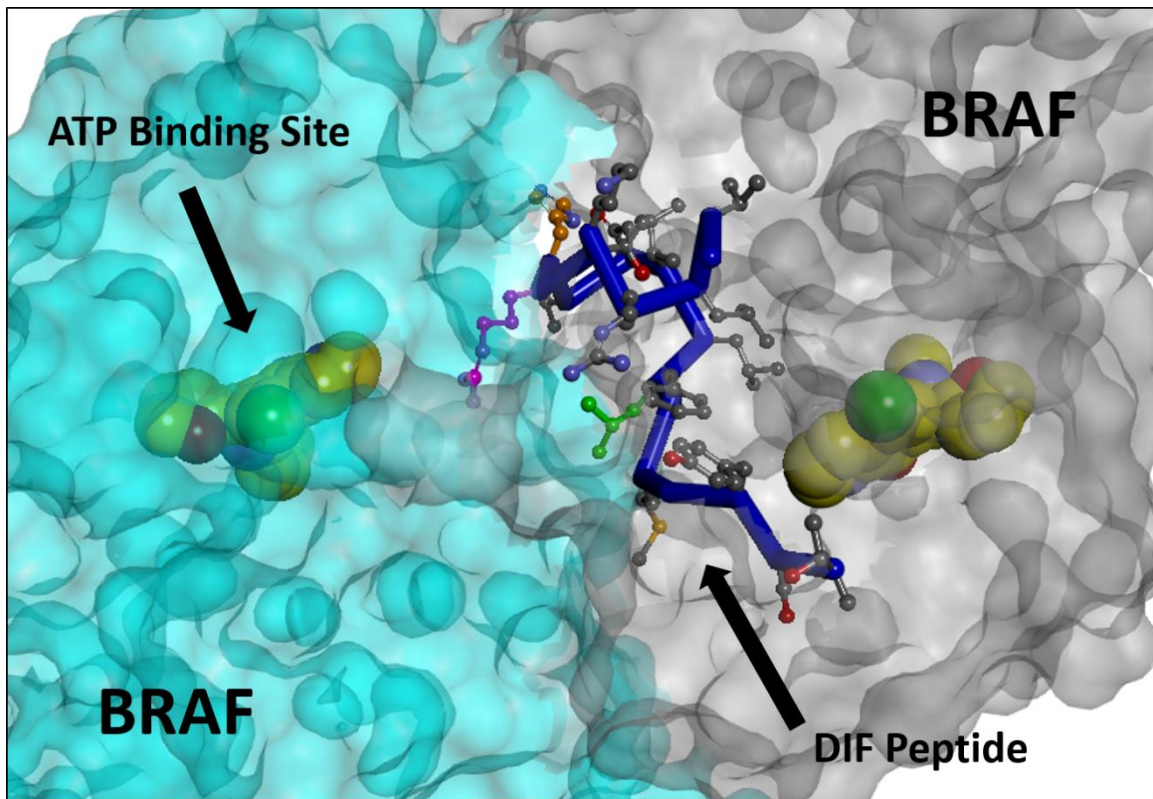


FIGURE 1.2: DIF PEPTIDE MIMICKING REVERSE-BETA-TURN OF NATIVE SEQUENCE: Solvent surface of BRAF homodimer crystal structure where the DIF peptide (blue) is truncated from BRAF (grey) native sequence to bind the target BRAF (cyan). Key linear residues R509 (magenta), H510 (orange), and L515 (green) highlighted in linear sequence and ATP (yellow) highlighted for perspective.

CHAPTER 2

LINEAR BRAF DIF PEPTIDES INHIBIT PARADOXICAL ACTIVATION

2.1 Introduction

The MAPK/ERK pathway, controls cell proliferation and differentiation and in the cancer disease state, this pathway frequently encounters gain-of-function mutations which dysregulate signaling and lead to tumorigenesis. Of these mutations, RAF-driven malignancies have a high frequency in cases of metastatic melanoma, to which Type I kinase inhibitors have been FDA approved, but unfortunately lead to the resistance mechanism known as paradoxical activation which is catalyzed by stabilization of the active conformation of the drug-free protomer in the dimeric complex of wild-type BRAF through the BRAF dimer interface. In cases of metastatic melanoma there is also a high frequency of oncogenic RAS, and through this mechanism oncogenic RAS-driven tumorigenesis can proliferate through dysregulation of the gatekeeper BRAF kinase, thus leading to a tumor type of which the driving oncogenic protein has no efficient therapeutics.

Previous studies outlined in Chapter 1 have demonstrated the requirement of the dimer interface for paradoxical activation and have started the development of peptidic BRAF dimer interface inhibitors using the native sequence as a proof-of-concept for therapeutically inhibiting BRAF dimerization and thus preventing the paradoxical

activation mechanism. In the following chapter, the use of DIF peptides for the inhibitor of clinically relevant disease-state signaling will further be demonstrated using cellular studies exhibiting inhibition of substrate level phosphorylation as well as inhibition of cell viability. Furthermore, the BRAF-wt dimer interface and the contributions of DIF peptides to binding will further be examined using a direct binding assay for a library of probing linear peptides designed to explore the binding contributions of each peptidic residue.

For the initial design of the peptidic dimer interface inhibitors, inspirations were brought in from literature-based peptides as well as in silico computational modeling. The natural dimer interface sequence was probed by point mutations and an alanine-scan in order to simulate the most favorable alterations to enhance binding potency. Quantitative data from minimization and interaction energy calculations were retrospectively fruitless, but based on the qualitative data obtained from the modeling experiments, a linear peptide library was designed and ordered from GenScript for experimental testing. Linear peptides were tested using the intrinsic tryptophan fluorescence (ITF) assay which measures direct binding of the peptide to BRAF-wt. The experimental and computational data were compared to determine key binding interactions of the DIF peptides with the dimer interface to facilitate the design of potent, cyclic peptides for BRAF dimer inhibition (Chapter 3).

2.1.2 Crystal Structure

The crystal structure for the full length BRAF homodimer has recently been solved (PDB 4e26) and was used in the design of the Type IV BRAF inhibitors using the Discovery

Studio 3.0 software. The BRAF dimer interface is characterized as having a short, continuous sequence consisting of BRAF residues 503-521 which form a reverse- β -turn and facilitate the side-by-side dimerization of BRAF. Based on literature evidence, R509 is a key binding determinant as exemplified by mutational experiments described in Chapter 1. Further inspection of this binding motif using the crystal structure revealed an arginine-handshake motif where R509 binds to the induced negative charge of the α C-helix of the complementary protein in a mirror-like fashion (**Figure 2.1A**). Further examination of the DIF binding surface revealed a deep, lipophilic pocket directly adjacent to the R509 binding site, to which L515 localizes (**Figure 2.1B**). Based on initial minimizations, H510 appears to be stabilizing the reverse-turn through an intramolecular hydrogen bonding network involving the N512 side-chain and L514 backbone amide as well as displaying hydrogen bonding interactions with the complementary H477 backbone carbonyl (**Figure 2.1C**). Other characteristics of the DIF binding surface utilize hydrophobic residues such as V511, F516, and M517 which interact with the generally hydrophobic binding surface (**Figure 2.1D**). These qualitative observations were directly extrapolated from the 4e26 BRAF homodimer crystal structure and required further quantitative analysis to more accurately characterized the landscape of the BRAF DIF binding surface.

2.1.3 Direct Binding Assay

Experimental testing of the direct binding potency of the peptides to the BRAF-wt dimer interface (DIF) was accomplished using the intrinsic tryptophan fluorescence (ITF)

assay. There are other aromatic residues in proteins such as phenylalanine (Phe) but its contribution is negligible due to low absorptivity and very low quantum yield, the ratio of photons emitted versus photons absorbed. There is also tyrosine (Tyr), which has a quantum yield similar to that of tryptophan (Trp), but the magnitude of Trp absorbance is higher due to the indole group of the Trp sidechain being the dominant source of UV absorption at 280 nm.⁴¹ Tryptophan when excited at 280 nm has a specific emission wavelength at 350 nm and when solvent exposed on the protein emits a baseline fluorescence. In the binding site of the DIF is W450, upon binding of the peptide to the binding site, the micro-environment of W450 is changed and this residue is no longer solvent exposed and the overall fluorescence of the BRAF protein after excitation at this specific wavelength is reduced. With titration of the DIF peptide and the measured decrease in intrinsic fluorescence at 350 nm, a dose-response curve was generated, and the dissociation constant (K_d) was determined from each compound. Data from these experiments gave quantitative experimental data to confirm binding determinants which were previously predicted by the computational modeling of DIF peptides.

2.2 Results

2.2.1 Electroporated DIF Peptides inhibit BRAF-wt signaling under paradoxical activation conditions

The nature of drug-induced paradoxical activation requires dimerization of BRAF-wt to allow for the activation of the second monomer.³²⁻³⁴ In this case the BRAF-wt homodimer forms as a side-by-side protein-protein interaction, of which the crystal

structure has recently been solved (PDB: 4e26). The majority of the dimer interface is composed of a single continuous sequence with no gaps, residues 503-521 (**1**; **Figure 2.1**), which makes up the reverse- β -turn located between the α C-helix and the β 4-sheet, therefore allowing for a single peptide to be generated to inhibit BRAF dimerization. It was hypothesized that treatment with a peptide representing this native sequence would disrupt the BRAF-wt homodimer and therefore inhibit downstream phosphorylation events in the paradoxical activation context.

In an experiment, conducted by the Brummer lab, to determine the effects of the DIF peptide **1** on substrate level phosphorylation under the paradoxical activation conditions, this peptide was synthesized. SBcl2 cells containing the NRAS Q61K gain-of-function mutation were electroporated in the presence of Peptide **1** and were then treated with PLX4032 (vemurafenib) to simulate the paradoxical activation mechanism. After lysis, immunoprecipitating, and western blotting, the result shows that Peptide **1** causes a dose dependent decrease of MEK and ERK phosphorylation in the presence of PLX4032 and NRAS Q61K (**Figure 2.2**). In contrast, the positive control (lane 2) where the NRAS Q61K mutant cells are treated with PLX4032 alone, there is an observed enhanced phosphorylation of MEK and ERK compared to the baseline phosphorylation in lane 1 where the cells are treated with vehicle alone. These results suggest that inhibition of downstream phosphorylation is due to the disruption of the BRAF-wt dimerization event by Peptide **1** binding, and thus preventing the activation of the second monomer in the presence of PLX4032. This data provides proof of concept for inhibition of downstream

MEK/ERK phosphorylation by disruption of the BRAF-wt dimer interface by treatment with a peptidic DIF inhibitor.

2.2.2 FAM-TAT-DIF Peptides inhibit cell viability in a dose-dependent manner

In an experiment, conducted by the Brummer lab, to investigate the effects of DIF peptides on cell viability and visualize entry, N-terminal 5-carboxyfluorescein (5-FAM) labeled trans-activating transduction (TAT) fusion peptides were used to treat SbCl₂ melanoma cells. As seen in **Figure 2.3A**, treatment of cells exposed to a 3.6 μM peptide solution displayed fluorescence in contrast to the lower concentration which only exhibited background autofluorescence. Cells treated with the active FAM-TAT-Pep17 peptide (BRAF 504-518, loop forming residues from DIF contact surface) tended to form smaller colonies than the cells treated with the FAM-TAT-Pep6AlaNC3 (GRKKRRQRRR-(PEG2)-GVLAATAAVNALLFAGYST) negative control (residues contacting the other monomer mutated to alanine). Furthermore in the colony forming assay in **Figure 2.3B**, it can be seen that treatment with FAM-TAT-Pep17 had an inhibitory effect as low as 1.8 μM with complete absence of colonies at 3.6 μM, whereas no inhibitory effect for FAM-TAT-Pep6AlaNC3 was observed until cells were treated with the 7.2 μM solution.

2.2.3 FAM-TAT-DIF Peptides inhibit downstream substrates of ERK kinase

The Brummer lab performed further experiments using these FAM-labeled TAT-fusion peptides in same SbCl₂ cells (NRAS-Q61K), co-treatment with FAM-TAT-Pep6AlaNC3 and PLX4032 elicited an enhanced phosphorylation of MEK/ERK (**Figure 2.3C**). In contrast, treatment with FAM-TAT-Pep17 in the presence of PLX4032 exhibited

a decrease of the enhanced downstream phosphorylation induced by PLX4032. To monitor further downstream effects of MEK/ERK inhibition, the expression and phosphorylation of FRA1 was analyzed. ERK directly activates the transcription of the FOSL1 gene to make FRA1, and down regulation of this protein is thus a direct readout for inhibition of ERK activity as would be expected by BRAF DIF peptides. As seen in **Figure 2.3C**, FAM-TAT-Pep17 downregulated the expression and phosphorylation of FRA1 compared to cells treated with FAM-TAT-Pep6AlaNC3, thus demonstrating inhibition of ERK activity. Taken together, the data from these cellular studies supports the hypothesis that BRAF DIF-based peptides can inhibit downstream phosphorylation events driven by oncogenic RAS and PLX4032.

2.2.6 Experimental Testing of BRAF 503-521 Linear Peptide Analogs

Using the previously mentioned ITF assay, a library of linear peptides was tested for direct binding potency by the Kontopidis lab (**Table 2.1**). In the preliminary biological data, the native BRAF DIF sequence containing BRAF residues 503-521 (**1**) was tested in cells and was shown to exhibit a dose-dependent inhibition of MEK/ERK phosphorylation. This sequence when tested in the ITF assay was shown to have $K_d = 3.84 \pm 0.32 \mu\text{M}$ and was therefore used as the baseline sequence for the experimental determination of the peptidic binding determinants for the BRAF-wt dimer interface. Furthermore, a negative control peptide containing the 3x mutation²⁶ from Roering et al. in the BRAF 503-521 residue context (**2**) was tested and was determined to have no binding. In contrast, another negative control peptide containing a scrambled sequence³⁹ as reported by

Freeman et al. in the BRAF 503-521 context (**3**) was tested in the ITF assay and interestingly displayed a $K_d = 2.96 \pm 0.18 \mu\text{M}$, which is enhanced compared to the native sequence. After assessing the BRAF-wt 503-521 native sequence (**1**) and the two negative controls from literature sources (**2** and **3**), a library of linear peptides containing single point mutations in the BRAF 503-521 sequence was generated and tested in the ITF assay to experimentally explore the binding determinants of the DIF peptide.

Based on the crystal structure (PDB 4e26), L505 was not thought to contribute to binding as evident by the L505A (**4**; $3.89 \pm 0.53 \mu\text{M}$) showing binding equipotent peptide **1** (**Table 2.1**). Charge repulsion interactions between R506 and K507 were predicted to electronically diminish the interaction of K507 with the DIF binding site. As expected, the R506E (**5**; $1.09 \pm 0.29 \mu\text{M}$) and R506L (**6**; $0.54 \pm 0.11 \mu\text{M}$) peptides showed enhanced binding owing to the elimination of the observed cation-cation repulsion of the Arg and Lys side-chains. Substitution of T508, whose side-chain is in close proximity to the opposite side of the reverse-turn and does not directly contact the binding surface, with Asp (**7**; $2.20 \pm 0.83 \mu\text{M}$) and Ala (**8**; $2.80 \pm 0.29 \mu\text{M}$) exhibited a marginally enhanced binding affinity. In contrast, the H510F (**9**; NB) substitution ablated binding of the peptide. The V511A mutation (**10**; $4.75 \pm 1.7 \mu\text{M}$) marginally decreased potency while L514A (**11**; $9.80 \pm 1.6 \mu\text{M}$) more significantly hindered binding. Replacement of L515 with Ile (**12**; $4.10 \pm 1.1 \mu\text{M}$) slightly decreased potency while replacement with homoleucine (**13**; $1.25 \pm 0.36 \mu\text{M}$) enhanced binding. The F516 side-chain was computationally determined to bind above the protein R509 residue and mutation to Asp (**14**; NB) was predicted to enhance binding through electrostatic interactions but experimentally demonstrated no binding.

2.2.7 Truncation Study of BRAF DIF Peptides

The combined data from the crystal structure and the previously described experimental data suggest that the entire BRAF 503-521 residue sequence is not required for binding to the dimer interface. In this section, the truncation of the 503-521 sequence was evaluated to minimize unnecessary residues from the DIF peptide sequence, all experiments involving the ITF assay were carried out by the Kontopidis lab (**Table 2.1**). Truncation to the 503-518 BRAF sequence (**15**; $1.88 \pm 0.36 \mu\text{M}$) showed an enhanced binding after elimination the YST sequence from the C-terminus. Removal of one residue from either side in the further truncation to the 504-517 BRAF sequence (**16**; $5.75 \pm 1.2 \mu\text{M}$) showed diminished binding. The addition of G518 (**17**; $0.13 \pm 0.04 \mu\text{M}$) to the sequence enhanced the binding potency with almost a 30-fold increase in binding compared to the initial BRAF 503-521 sequence. Synthesis of the same BRAF 504-518 sequence with an amide C-terminus (**18**; $0.48 \pm 0.09 \mu\text{M}$) resulted in diminished potency compared to **17**. Furthermore, acetylation of the BRAF 504-518 N-terminus (**19**; $0.80 \pm 0.08 \mu\text{M}$) showed an even further decrease in potency compared to the free amine. From this data, the BRAF 504-518 sequence was determined to be the ideal scaffold for further investigation into the binding determinants of the BRAF DIF peptides.

2.2.8 Alanine Scan of BRAF 504-518

Now that an optimum truncated sequence required for BRAF binding has been identified, the individual contribution of each residue's side-chain has been experimentally evaluated using the same ITF assay as previously described. For this

section, each of the residues were individually replaced with alanine as a method of removing the functionality of the side-chain while the chirality of the residue was maintained. From this experiment (**Table 2.1**), the results show that L505A (**20**; $0.45 \pm 0.03 \mu\text{M}$), R506A (**21**; $0.36 \pm 0.03 \mu\text{M}$), F516A (**28**; $0.57 \pm 0.08 \mu\text{M}$), and M517A (**29**; $0.54 \pm 0.15 \mu\text{M}$) are relatively insensitive to mutation. In contrast, K507A (**22**; ND), R509A (**23**; $2.4 \pm 0.35 \mu\text{M}$), H510A (**24**; $2.7 \pm 0.40 \mu\text{M}$), N512A (**25**; NB), and I513A (**26**; $2.69 \pm 0.35 \mu\text{M}$), and to a lesser degree L514A (**27**; $1.02 \pm 0.14 \mu\text{M}$), had either diminished, very weak, or no binding detected. Residues T508, V511, and L515 were excluded from this study since the alanine mutation was already addressed for T508 and V511 in the BRAF 503-521 context and as L515 is known to bind to a deep, lipophilic pocket.

2.3 Discussion

There is a significant need for a combination therapy for patients with tumors bearing the BRAF-V600E mutation to prevent the development of mutant RAS-driven resistance mechanisms to Type I BRAF inhibitors. These RAS-driven tumors display an enhanced proliferation while the patient is treated with Type I BRAF inhibitors due to paradoxical activation of the second monomer in the wild-type BRAF dimer complex. The proposed method of preventing this enhanced proliferation is through treatment with BRAF-wt dimerization inhibitors. The initial data shows that co-treatment of human melanoma SbCl2 cells, containing the NRAS-Q61K gain-of-function mutation, by electroporation with Peptide **1** (BRAF DIF residues 503-521) and PLX 4032 (vemurafenib), a Type I BRAF inhibitor, showed a dose-dependent decrease in phosphorylation of the

downstream kinases, MEK and ERK (**Figure 2.2**) whereas treatment of these cells with PLX 4032 alone induced an enhanced ability to phosphorylate MEK/ERK compared to vehicle alone. This dose-dependent decrease in downstream substrate phosphorylation indicates that DIF peptides can disrupt the dimerization of BRAF and inhibit tumorigenesis under the disease-state conditions. Furthermore, cellular FAM-TAT-Peptide assays have shown repeated diminishing phosphorylation of downstream kinases MEK/ERK, as well as decreased transcription of FRA1, the transcription product of FOSL1, a transcription factor activated by ERK (**Figure 2.3C**). Additionally, treatment with these peptides has shown decreased cell viability of internalized, fluorescent peptides compared to negative controls (**Figure 2.3A/B**).

Taken together, this data demonstrates on several accounts for the proof-of-concept of use of BRAF DIF peptides to inhibit the phosphorylation of downstream MEK/ERK, expression and phosphorylation of FRA1, and a decreased cell viability, all under the paradoxical activation disease-state conditions. Furthermore, the comparison between FAM-TAT-Pep17 and FAM-TAT-Pep6AlaNC3 demonstrates the requirement for peptide side-chain functionality for residues which directly interact with the DIF binding surface and therefore alludes that the binding potency can therefore be optimized. Additionally, with the native conformation of the DIF sequence forming the reverse- β -turn secondary structure, the potency, proteolytic stability, and cell penetrating ability of the DIF peptide can further be enhance through cyclization to rigidify the structure and lock it in the bioactive conformation. The development of BRAF-wt DIF peptides has the potential to be used as a second-line therapy for patients with drug-induced resistance to

Type I BRAF inhibitors as well as a potential therapy for patients exhibiting mutant RAS-driven tumorigenesis.

Computational modeling of the linear DIF peptides using the crystal structure did not prove to be quantitatively useful, but there was proof-of-concept for the binding of peptides to BRAF-wt and disruption of downstream phosphorylation from the initial biological data (**Figure 2.2**); DIF peptides of BRAF 503-521 including the native sequence (**1**), 3x mutant reported by Roering et al. (**2**), and the scrambled peptide sequence reported by Freeman et al. (**3**) were tested experimentally in the ITF direct binding assay.^{26,39} As a baseline for this experiment, Peptide **1** exhibited $K_d = 3.84 \pm 0.32 \mu\text{M}$ and the 3x mutant (**2**) expectedly had no binding detected (**Table 2.1**). Interestingly, the scrambled peptide analog (**3**), which was reported as a negative control in the activated RAS and impaired activity in the BRAF-G466V context, exhibited a better binding than **1**. This retention of binding affinity could be due to the conservation of R509 and H510 in the scrambled sequence which have been demonstrated to be key binding determinants in the linear context, but the exact explanation for why the binding potency is enhanced was not examined.

Next, a series of probing mutations to the BRAF 503-521 sequence and subsequent ITF assay testing were completed (**Table 2.1**). L505 was determined to not be required for DIF binding by the equipotent binding L505A (**4**) compared to **1**. It was speculated that the cationic sidechain of R506 energetically disfavored the binding of the adjacent K507 residue to the DIF. Mutation of R506 to an anionic glutamic acid (**5**) or a

lipophilic leucine (**6**) both significantly increased the binding potency by about 4-fold and 8-fold, respectively. T508 does not come into direct contact with the DIF binding surface, but it is close in proximity to the other side of the reverse- β -turn. The testing of T508D (**7**) and T508A (**8**) resulted in a marginally enhance binding, indicating that this residue is relatively unaffected by mutation making it a prime residue for cyclization. Replacement of H510 with a phenylalanine (**9**) resulted in the complete loss of binding, probably since H510 is the central portion of the intramolecular hydrogen bond network with the peptidic backbone amides which support the formation of the reverse- β -turn conformation in the linear context. Without this network, the reverse turn in not energetically favorable and due to an increased entropic cost of binding, the peptide loses all binding ability. The substitution of alanine for V511 (**10**) and L514 (**11**) resulted in a decreased binding potency, with the latter being more significant, though the decrease in binding of L514A is difficult to explain since it does not contact the binding surface. As probed in the molecular modeling, here too L515 and its deep hydrophobic pocket were analyzed. Conversion of L515 to its isostere isoleucine (**12**) had a marginal hinderance on binding, but substitution to homoleucine (**13**; 1.25 μ M) resulted in a 3-fold increase in binding potency as expected by lengthening the alkyl side-chain and sterically filling the deep, lipophilic binding pocket adjacent to the R509 binding pocket. F516 binds just above the BRAF protein R509 in the minimized crystal structure and mutation to aspartic acid (**14**) to mimic the negative dipole of the α C-helix was expected to increase binding by interacting with the protein R509, but it resulted in no detectable binding. Taken together, it was determined by this experimental set that there are energetically

unfavorable adjacent residues with R506-K507, H510 is required in the linear peptide context to maintain the bioactive conformation, and that the deep, lipophilic pocket of L515 can be optimized to improve peptide binding.

After probing the BRAF 503-521 sequence with conservative mutations, it was necessary to reduce the overall size of the linear peptide due to the fact that terminal portions of the sequence do not directly contact the dimer interface and smaller compounds are correlated with better oral availability. Size reduction which improves drug likeness was accomplished by truncation to the core reverse-turn sequence which directly binds to the BRAF DIF (**Table 2.1**). Truncation of the three C-terminal residues, YST, resulted in **15**, which is roughly a 2-fold increase in potency compared to **1**. Further truncation of one residue from each end resulted in **16** and about a 3-fold decrease in binding potency. Upon reintegration of the N-terminal Gly gave **17** and a 14-fold increase in potency compared to **15**. Based on these observations, it is thought that the relative length of the backbone in **17** and the proximity of the C-terminus to the R506 side-chain created a pseudo-cyclic conformation of the linear peptide, making it energetically favorable to preemptively assume the bioactive conformation. The pseudo-cyclic conformation thus decreases the entropic cost of binding and significantly increases the direct binding potency. To test this theory, **18** was tested containing BRAF residues 504-518 and an amide C-terminus. The resulting peptide exhibited a 4-fold decrease in binding potency compared to its carboxylate counterpart. Since the C-terminus is an amide instead of a carboxylate, there is no negative charge on the C-terminus thus dampening its ability to assume the pseudo-cyclic conformation, but the amide nitrogen

is still able to interact with the R506 side-chain, thus not completely eliminating the effect. From the observations obtained from this experiment, it was decided to continue with the truncated sequence containing BRAF residues 504-518 for the following experiments.

The alanine-scan in the computational model was lacking significant utility for the design of more potent linear peptides, to better assess the contribution of each residue an alanine-scan was performed on the linear BRAF sequence containing residues 504-518 with direct binding assessed by the ITF assay (**Table 2.1**). Residues L505, R506, F516, and M517 were relatively insensitive to alanine mutation. In contrast, mutation of K507 and N512 resulted in no detectable binding. K507 is expected to make an electrostatic interaction with D448 in the protein binding site based on the crystal structure, the K507A mutation was expected to hinder binding but not necessarily abolish it completely. In regard to N512A, based on the crystal structure, the Asn side-chain makes hydrogen bonds with the adjacent H510 which help to stabilize the reverse- β -turn in the linear context, but again it was not expected to completely lose binding after mutation to alanine. Furthermore, the mutation of R509 and H510 exhibited a diminished binding potency as expected with R509 being a key binding determinant as reported by Roering et al. and H510 composing the central participant in the hydrogen bond network maintaining the reverse- β -turn in the linear peptide context.²⁶ From the results, residues 507-515 (excluding T508) which make up the residues adjacent to the reverse- β -turn appear to be highly sensitive to mutation and their side-chain functionality seems to be important for potent binding in the linear peptidic context.

2.4 Conclusion

Based on the biological application of the DIF peptides, either with or without the FAM-TAT moiety, in the mutant RAS, BRAF wild-type context, co-treatment of cells with type I kinase inhibitors and DIF peptides resulted in decreased downstream signaling. Furthermore, treatment of cells in the same context showed a dose dependent decrease in cell viability, thus inhibiting cell proliferation in the disease state context. This data in addition to that previously described in Chapter 1 further indicates that the BRAF dimer interface could be therapeutic target for treatment of patients with metastatic melanoma which exhibit paradoxical activation-induced resistance to type I BRAF kinase inhibitors.

The direct binding assay results of probing mutations, truncation peptides, and the alanine-scan of the core sequence were enlightening by determining the structure activity relationship of residues in the linear context, such as which residues in the linear context were crucial for binding and which were relatively insensitive to mutation or elimination. From this data, it was confirmed that R509 is indeed a key residue for binding of the linear peptide to the BRAF DIF as literature predicted.²⁶ Furthermore, the combination of the 503-518 truncation sequence and the core His-Val-Asn-Ile sequence composing the predicted hydrogen bonding network of the reverse- β -turn may help to stabilize the reverse- β -turn bioactive, pseudo-cyclic conformation and are therefore appear to be crucial for binding in the linear context. Though these residues are important for binding in the linear context, if the peptide was covalently cyclized then this leaves room for additional optimization of reverse-turn residues for binding site affinity

rather than stabilization of the predicted pseudo-cyclic conformation. Additionally, the deep hydrophobic pocket which L515 binds can be exploited for optimization of binding by elongating the aliphatic chain to fill this part of the dimer interface.

Taken together, this data supports our hypothesis of disrupting BRAF dimerization with a peptide to prevent paradoxical activation induced by Type I BRAF inhibitors. It also shows that there is room for optimization of the DIF peptides for the inhibition of downstream phosphorylation events through cyclization, key binding determinant optimization, as well as repurposing conformation stabilizing residues for binding affinity optimization. Furthermore, residues which are relatively tolerant to mutation and do not directly interact with the binding surface have been identified and present the opportunity to optimize for physicochemical properties which make the peptide more drug-like for cell permeability. In the next chapter, cyclization of the DIF peptides through non-interacting residues is explored as a method of stabilizing the reverse- β -turn, bioactive conformation via side-chain-to-side-chain cyclization methods which will in turn result in a decrease in the entropic cost of binding and therefore lead to a more potent DIF peptide.

2.5 Experimental

2.5.1 Peptide Synthesis

Linear peptides were synthesized and purified to greater than 95% purity by GenScript.

2.5.2 Electroporated Peptide 1 in SbCl₂ cells in the presence of PLX4032²⁹

SbCl₂ cells were electroporated with the BioRad GenePulser XCell™ in the presence of the indicated concentrations of peptide **1**. Following recovery at 37°C for 30 min, the cells were treated with 1 μM PLX4032 for 1 hr. or dimethyl sulfoxide (DMSO) as a vehicle control. Subsequently, the cells were harvested, lysed using radioimmunoprecipitation assay (RIPA) buffer, and analyzed by Western blotting using the indicated antibodies, as described previously.²⁶

2.5.3 FAM-TAT-Peptide Internalization²⁹

SbCl₂ cells were plated in tissue culture vessels (6-well format) and grown in the presence of the indicated concentrations of FAM-labeled TAT peptides. Medium with freshly added peptides was changed every 3–4 days. Shown are micrographs taken 2 weeks after seeding.

2.5.4 FAM-TAT-Peptide Colony Forming Assay²⁹

Five thousand SbCl₂ cells were seeded onto 6-well plates and grown in the presence of the indicated peptide concentrations for 2 weeks. Medium with freshly added peptides was changed every 3–4 days. Cells were stained with Giemsa solution. Shown is a representative result from two independent biological replicates with comparable outcomes.

2.5.5 FAM-TAT-Peptides in SbcI2 cells in the presence of PLX4032²⁹

NRAS Q61K mutant human SbcI2 melanoma cells were incubated with 3.60 μ M FAM-TAT-pep6AlaNC3 (control) or FAM-TAT-pep17 for 3 days. Four hours prior to harvest, the cells were treated with 1 μ M vemurafenib (PLX4032) or the same volume of DMSO as vehicle control. RIPA buffer lysates were subjected to Western blotting using the indicated antibodies. Detection of HSP90 serves as a representative loading control.

2.5.6 Tissue Culture²⁹

The generation of MCF-10Atet cells, a subline of the human mammary epithelial cell line MCF-10A, was described previously.⁴² MCF-10Atet cells were grown at 37 °C in a water-vapor saturated 5% CO₂ atmosphere in conventional tissue culture plastic vessels (Sarstedt, Nürnberg, Germany) containing Dulbecco's modified Eagle medium/F12 medium (PAN-Biotech GmbH, Aidenbach, Germany) supplemented with 5 vol % horse serum (PAA, Cölbe, Germany), 1 vol % glutamine (PAN-Biotech GmbH, Aidenbach, Germany), 1 vol % HEPES (PAN-Biotech GmbH, Aidenbach, Germany), 1 vol % penicilline/streptomycine (PANBiotech GmbH, Aidenbach, Germany), 250 μ g of hydrocortisone (Sigma-Aldrich, Munich, Germany), 50 μ g of cholera toxin (Sigma- Aldrich, Munich, Germany), 10 μ g of human recombinant epidermal growth factor (R&D Systems, Wiesbaden-Nordenstadt, Germany), and 4.858 mg of human recombinant insuline (Actrapid Penfill solution, Novo Nordisk Pharma GmbH, Mainz, Germany). Cells were passaged twice a week or upon reaching confluency and detached by trypsin/ethylenediaminetetraacetic acid (EDTA) solution. Five hundred cells were plated

onto 6-well plates and grown for 24 h prior to peptide treatment. For the experiments with Sbcl2 cells, we used the stably transfected pool Sbcl2ecoR, which expresses the receptor for murine retroviruses. These cells were cultivated as the parental cell line⁴³ and generated using the pQCXIN/ecoR plasmid, as described for other cell lines previously.²⁶

2.5.7 Western Blotting²⁹

NRAS-Q61K-mutant SbCl2 melanoma cells were electroporated with BioRad GenePulser XCell in presence of the indicated concentrations of peptide. Following recovery at 37 °C for 30 min, cells were treated with 1 µM PLX4032 for 1 h with DMSO as a vehicle control. Subsequently, the cells were harvested, lysed using RIPA buffer, and analyzed by Western blotting using the indicated antibodies as described previously.²⁶ Sbcl2 cells were lysed in RIPA buffer (50 mM Tris/HCl, pH 7.4; 1% Triton X-100; 137 mM NaCl; 1% glycerin; 1 mM sodium orthovanadate; 0.5% sodium deoxycholate, 0.1% sodium dodecyl sulfate, 0.5 mM EDTA; 0.01 µg/µL leupeptin, 0.1 µg/µL aprotinin, 1 mM AEBSF). Lysates were cleared by centrifugation, mixed with the sample buffer, and analyzed by Western blotting using 10% sodium dodecyl sulfate polyacrylamide gel electrophoresis gels, as described previously,²⁶ using the following antibodies: anti-BRAF (F-7) and anti-RAF-1 (C-12) purchased from Santa Cruz Biotechnology; anti-phospho-FRA1 (S265; D22B1), anti- FRA1 (D80B4), anti-HSP90 (#4874), anti-phospho-MEK1/2 (pS217/221), anti-MEK1/2, anti-p42/p44 MAPK, and anti-phospho-MAPK (pT202/pY204), and ERK1/2 purchased from Cell Signaling Technologies. Protein concentration determination was performed via bicinchoninic acid assay (Thermo Fisher Scientific, Germany). Equal protein

amounts were loaded for PAGE. Blotted proteins were visualized with a Fusion Solo chemiluminescence reader (Vilber Lourmat, Germany).

2.5.8 Dissociation Constant (K_d) Determination from ITF and ITC Measurements²⁹

The dissociation constant is an indicator of the binding strength between two molecules. For the reaction: $P + L \leftrightarrow PL$

$$\text{Equation 1: } K_d = \frac{[P][L]}{[PL]}$$

where [P] is the concentration of free Protein, [L] is the concentration of free Ligand, and [PL] is the ligand-bound protein.

Fluorescence intensity was measured with a Hitachi F-2500 fluorescence spectrophotometer. Briefly, 1.6 mL of protein solution (0.5 μM) was placed in a cuvette and equilibrated at 15 °C for 1 h. After equilibration, small increments (2–15 μL) of the ligand solution were injected in the cuvette. The ITF experiments were performed in 20 mM N-(2-hydroxyethyl)piperazine-N-ethanesulfonic acid (HEPES) buffer (pH 7.5), 10 mM MgCl₂, and 30 mM NaCl. For certain ligands that were insoluble in aqueous media, 5–10% DMSO was added to increase its solubility. The slits were set at 10 nm for the excitation and emission wavelengths. To determine the dilution effect of BRAF (due to ligand addition) and any fluorescence effect by the unbound ligand, a blank sample containing Trp with the same fluorescence signal was titrated with ligand additions, as described above. The sample absorbance was kept below 0.1 to minimize the inner filter effect.⁴⁴ The K_d of BRAF/ligand was calculated by fitting fluorescence data using the one-site binding site model in Origin 7 as follows:

Equation 2: $[L_{total}] = \frac{2\theta[P_{total}]}{K_b \left(-K_{diss} \sqrt{K_{diss}^2 - 4K_{diss}[P_{total}](\theta - 1)} \right)} + \theta[P_{total}]$

TABLE 2.1: ITF DIRECT BINDING ASSAY DATA OF LINEAR BRAF DIF PEPTIDES

ID	BRAF Residues	Mutations	Sequence	Kd (μM)
1	503-521	N/A	GVLKTRHVNILLFMGYST	3.84 \pm 0.32
2	503-521	R509H, L515G, M517W	GVLKTHHVNIIGFWGYST	NB
3	503-521	Scrambled	GRINKGRHTFLLVVMYSL	2.96 \pm 0.18
4	503-521	L505A	GVARKTRHVNILLFMGYST	3.89 \pm 0.53
5	503-521	R506E	GVLEKTRHVNILLFMGYST	1.09 \pm 0.29
6	503-521	R506L	GVLLKTRHVNILLFMGYST	0.54 \pm 0.11
7	503-521	T508D	GVLKDRHVNILLFMGYST	2.20 \pm 0.83
8	503-521	T508A	GVLKARHVNILLFMGYST	2.80 \pm 0.29
9	503-521	H510F	GVLKTRFVNILLFMGYST	NB
10	503-521	V511A	GVLKTRHANILLFMGYST	4.75 \pm 1.70
11	503-521	L514A	GVLKTRHVNIALFMGYST	9.80 \pm 1.60
12	503-521	L515I	GVLKTRHVNILIFMGYST	4.10 \pm 1.10
13	503-521	L515homoleucine	GVLKTRHVNIL[HL]FMGYST	1.25 \pm 0.36
14	503-521	F516D	GVLKTRHVNILLDMGYST	NB
15	503-518	N/A	GVLKTRHVNILLFMG	1.88 \pm 0.36
16	504-517	N/A	VLKTRHVNILLFM	5.75 \pm 1.20
17	504-518	N/A	VLKTRHVNILLFMG	0.13 \pm 0.04
18	504-518	N/A	VLKTRHVNILLFMG-NH ₂	0.48 \pm 0.09
19	504-518	N/A	Ac-VLKTRHVNILLFMG	0.80 \pm 0.08
20	504-518	L505A	VARKTRHVNILLFMG	0.45 \pm 0.03
21	504-518	R506A	VLAKTRHVNILLFMG	0.36 \pm 0.03
22	504-518	K507A	VLKTRHVNILLFMG	ND
23	504-518	R509A	VLKTAHVNIILLFMG	2.40 \pm 0.35
24	504-518	H510A	VLKTRAVNIILLFMG	2.70 \pm 0.40
25	504-518	N512A	VLKTRHVAILLFMG	NB
26	504-518	I513A	VLKTRHVNALLFMG	2.69 \pm 0.35
27	504-518	L514A	VLKTRHVNIALFMG	1.02 \pm 0.14
28	504-518	F516A	VLKTRHVNILLAMG	0.57 \pm 0.08
29	504-518	M517A	VLKTRHVNILLFAG	0.54 \pm 0.15

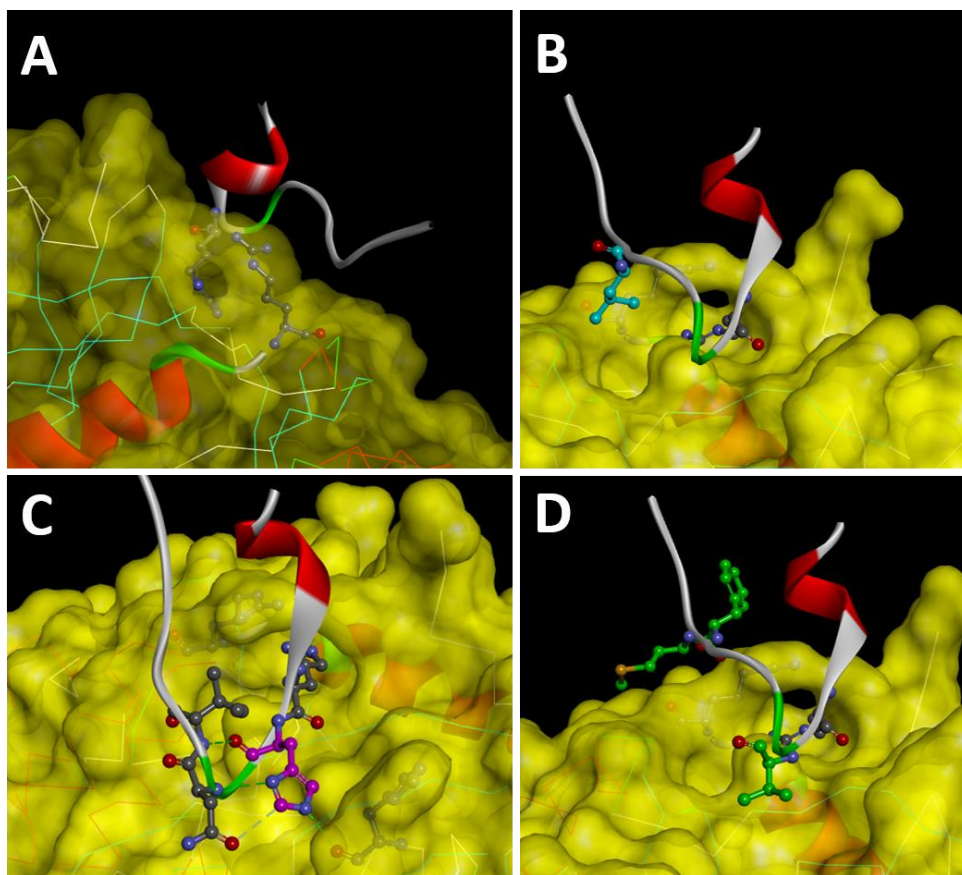


FIGURE 2.1: KEY DIF PEPTIDE BINDING MOTIFS: Minimized crystal structures (PDB 4E26) of BRAF DIF peptides docked into BRAF dimer interface, highlighting key residues for design of potent inhibitors. A.) The chemical structure of protein and peptide R509 residues highlighted (grey) in arginine-handshake motif. B.) L515 (cyan) highlighted to show deep hydrophobic binding pocket. C.) Contribution of H510 (magenta) in stabilization of the hydrogen bonding network which makes up the reverse- β -turn of residues BRAF 510-514. D.) Hydrophobic residues V511, F516, and M517 (green) shown to interact with the neutral binding surfaces of the BRAF DIF.

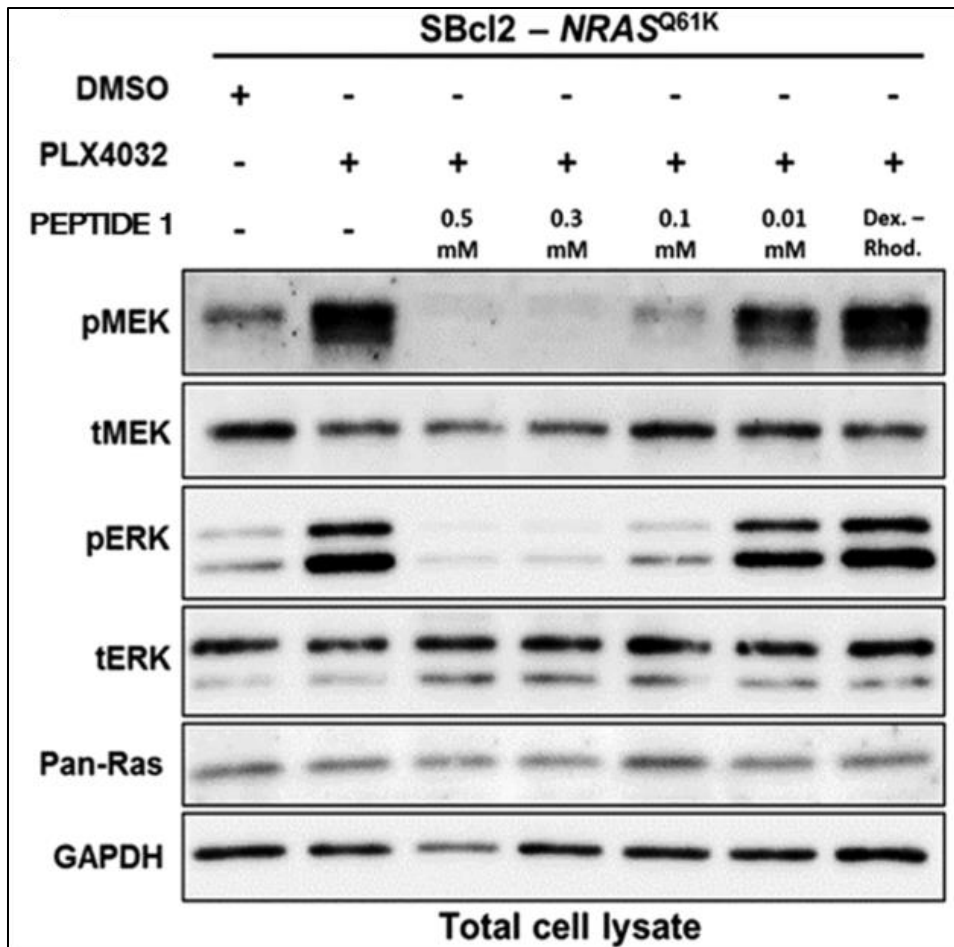


FIGURE 2.2: INHIBITION OF PARADOXICAL ACTIVATION WITH BRAF DIF PEPTIDES: Treatment of metastatic melanoma cells SBcl2 under paradoxical activation conditions with NRAS-Q61K and PLX4032 (vemurafenib) and electroporated with BRAF DIF peptides. Co-treatment of cells with PLX4032 and BRAF DIF Peptide 1 exhibit a dose-dependent decrease in downstream MEK/ERK phosphorylation compared to the enhanced phosphorylation of MEK/ERK under paradoxical activation conditions exhibited by PLX4032 treatment alone. Experiment was carried out by the Brummer lab.

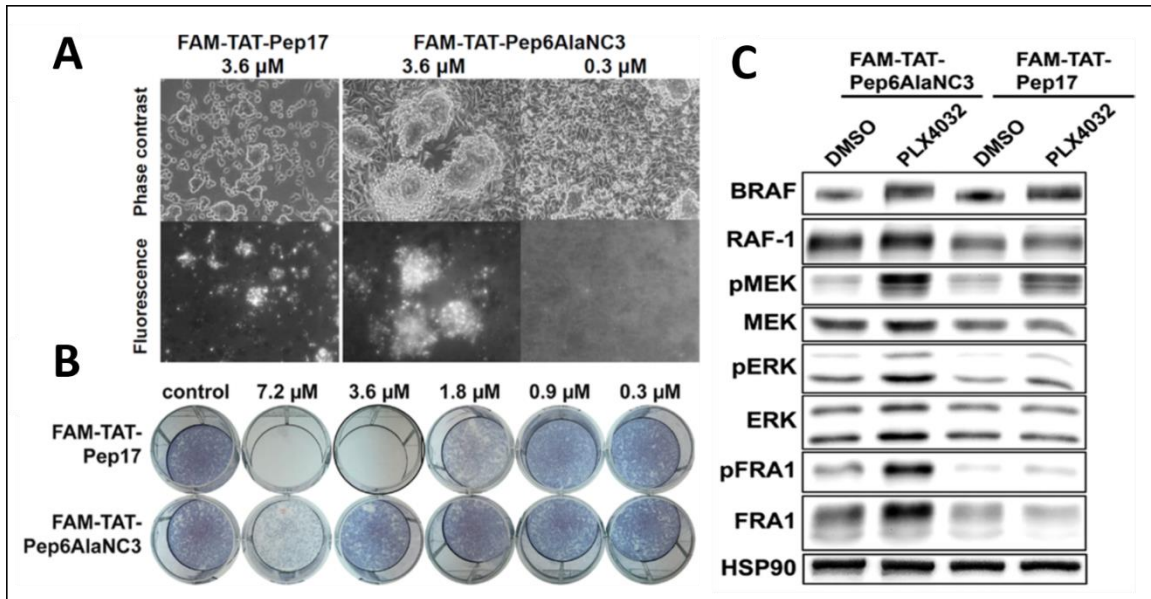


FIGURE 2.3: FAM-TAT-PEPTIDES DIMINISH CELL VIABILITY AND INHIBIT DOWNSTREAM TRANSCRIPTION: SbCl₂ melanoma cells treated with FAM-TAT-Peptides, Pep17 and Pep6AlaNC3 as the positive and negative samples respectively. A.) Confocal microscopy of cells treated with FAM-TAT-Peptides indicating that 3.6 μ M the fluorescent FAM label is visible in the cells, whereas the 0.3 μ M treatment merely shows a faint autofluorescence. B.) Cell viability assay showing diminished cell viability in cells treated with 1.8 μ M FAM-TAT-Pep17 and a 4-fold increase in concentration is needed for FAM-TAT-Pep6AlaNC3 to see the same effect. C.) Western blot of SbCl₂ cells co-treated with PLX4032 and FAM-TAT-tagged peptides to show down regulation of FRA1 expression as a result of inhibiting BRAF and therefore the downstream products of ERK activation using FAM-TAT-Pep17. Experiments were carried out by the Brummer lab.

CHAPTER 3

OPTIMIZATION OF CYCLIC BRAF DIF PEPTIDES

3.1 Introduction

Until recently in drug discovery, small molecule inhibitors were the gold standard for intercellular drug targets and mainly focused on out competing protein substrates such as ATP and protein cofactors. With the exponential increase in cases of drug resistance to small molecule cancer therapeutics, and as a way to expand the number of available drug targets, attention has been turned to inhibiting protein-protein interactions (PPIs) to disrupt signaling pathways. Macrocyclic peptides are defined as compounds which are primarily composed of amino acid segments which form a ring bridging several residues in the sequence. In recent years, the field of macrocyclic peptide drug discovery has been increasingly pursued due to the ability of such molecules to bind to large, flat, and featureless protein target surfaces of PPI interfaces. PPIs are generally not amenable to small molecule development due to smaller surface area and requirement for deep binding pockets for a therapeutic response.

Due to the biopolymeric nature of peptides, being composed of easily interchangeable amino acids using straightforward synthetic strategies, large libraries can be synthesized in an efficient manner making them advantageous for early stage development of PPI inhibitors. Additionally, cyclization of peptide sequences allows for

the compound to mimic the secondary structure of the target's native substrate where the conformational restraint decreases the entropic cost of binding and therefore increases the peptide's potency. Taken together, macrocyclic peptide drug discovery involves straightforward synthetic means for development of compound libraries to optimize potently binding sequences for inhibition of PPIs to which small molecule inhibitors cannot efficiently bind. A drawback of peptide drug discovery is the fundamental lack of cell permeability of peptides which can be overcome using macrocycles and will be addressed in detail in Chapter 4.

In the previous chapters, proof-of-concept for the application of a peptide as a BRAF dimerization inhibitor for the prevention of PLX 4032-induced paradoxical activation was demonstrated in cellular studies. Furthermore, in Chapter 2 the linear peptide sequence was examined, and key binding determinants were identified as being the core sequence surrounding the reverse- β -turn secondary structure of the BRAF protein dimer interface (DIF). The contents of this chapter highlights the process of optimizing the lead linear peptide (**17**) to create a macrocyclic peptide which potently binds the BRAF DIF.

3.2 Results

3.2.1 Design and Location of Peptide Cyclization Linker

From the previous linear truncation study, truncation of the BRAF 503-521 sequence to BRAF 504-518 significantly increased the potency of the peptide and was attributed to the electrostatic interaction between the C-terminus of G518 and the side-chain of R506, creating a pseudo-cyclic conformation. This potential pseudo-cyclic

conformation, along with the reverse- β -turn of the DIF from the crystal structure strongly suggest that cyclization of the DIF peptides would greatly enhance binding ability by rigidifying the peptide to the bioactive conformation, thus reducing the entropic cost of binding. Residues 506 and 518 were therefore highlighted as a potential location for introducing a cyclization linker and would result in a 13-residue macrocycle. The minimized crystal structure (4e26) of the linear DIF peptide in the BRAF dimer interface was examined for additional cyclization sites. The characteristics that were sought for were the close proximity of two residues, with one on either side of the reverse-turn moiety, and for the sidechain to not participate in direct binding to the DIF surface. Based on these properties, two sites were chosen, side-chain cyclization between residues L505-F516 or between T508-I513 (**Figure 3.1**). The first case would result in a 12-residue macrocycle and the later in a 6-residue macrocycle.

3.2.1 Initial Cyclization Site Testing

All peptides were either cyclized using lactam cyclization linkers or disulfide bridges between orthogonally protected residues during on-resin synthesis and the ITF assay was carried out by the Kontopidis lab. The cyclization of BRAF residues 505-519 using cyclization residues 506 and 518 and either an 8 or 9 atom lactam linker resulted in **30** and **31** which were both insoluble and were not tested for binding (**Table 3.1**). When BRAF residues 504-517 were cyclized through a disulfide bond at residues 505 and 516, the resulting peptide (**32**) exhibited a $K_d = 0.36 \mu\text{M}$. Cyclization of BRAF residues 505-518 at residues 508 and 513 using an 8-atom linker (**33**) resulted in a $K_d = 0.78 \mu\text{M}$. Extension

to a 9-atom linker resulted in **34** with $K_d = 1.89 \mu\text{M}$. When combining the 8-atom linker with the N512A substitution, **35** was made and displayed a $K_d = 0.46 \mu\text{M}$. Incorporating the N512A substitution into the 9-atom linker sequence resulted in **36** with $K_d = 0.06 \mu\text{M}$. As proof-of-concept for the utility of the cyclization, **37** was tested with the same sequence as **35**, but without cyclization and the resulting peptide showed no binding to BRAF DIF. Peptide **38** was made as a trial for the idea of a bicyclic peptide by cyclizing through the 505-516 site and the 508-513 site using two lactam cyclization linkers and resulted in $K_d = 0.37 \mu\text{M}$.

3.2.2 Cyclic Peptides Show Decreased Entropic Cost of Binding

As a method of confirming the results from the ITF assay and to explore the thermodynamics of BRAF DIF peptides binding, isothermal titration calorimetry experiments performed by the Kontopidis lab were completed for a few select peptides. Testing of the 19-residue linear peptide **7** (**Figure 3.2**) resulted in a moderate difference in binding affinity ($K_d = 14.9 \pm 10.8 \mu\text{M}$; $\Delta H = -34.8 \text{ kJ/mol}$; $\Delta S = -28.4 \text{ J/(mol K)}$) compared to that observed in the ITF assay ($K_d = 2.20 \pm 0.83 \mu\text{M}$), though the error was larger for ITC. The binding data of the 15-residue peptide **17** had a similar binding affinity ($K_d = 0.35 \pm 0.17 \mu\text{M}$; $\Delta H = -199 \text{ kJ/mol}$; $\Delta S = -567 \text{ J/(mol K)}$) to that determined by the ITF assay ($K_d = 0.13 \pm 0.04 \mu\text{M}$). Furthermore, it appeared that both linear peptides were enthalpically driven to bind based on their favorable ΔH and their unfavorable ΔS terms. The cyclic peptide **35** was confirmed to also have a similar binding potency in the ITC experiment ($K_d = 0.31 \pm 0.16 \mu\text{M}$; $\Delta H = -9.41 \text{ kJ/mol}$; $\Delta S = 92.05 \text{ J/(mol K)}$) compared to that of the ITF assay ($K_d = 0.46 \pm 0.04 \mu\text{M}$). Furthermore, this

peptide appeared to be entropically driven to bind, which is in line with the rationale of creating the cyclic peptide, based on the favorable value of the ΔS term determined by ITC.

3.2.3 Probing and Truncation of 508-513 Cyclized Peptides

In the previous section, substitution of N512 for alanine showed an enhanced binding effect in the context of the 508-513 cyclized peptide (**36**). In this section, the 6-residue cyclic peptide is further examined for enhanced binding opportunities when tested in the ITF assay by the Kontopidis lab (**Table 3.1**). In Chapter 2, L515 was described as a prospect for enhanced binding due to the lipophilic binding pocket. A peptide containing a 6-residue macrocycle with an 8-atom linker, the N512A mutation, and L515 is substituted for homoleucine, resulted in peptide (**39**) and exhibited a $K_d = 0.43 \mu\text{M}$. In the same scaffold, when L515 is substituted for Nle (norleucine), the resulting peptide (**40**) has an enhanced $K_d = 0.17 \mu\text{M}$. In the 9-atom cyclized peptide (508-513), reducing the number of hydrogen bond donors through N-methylation of R509 to make **41** resulted in $K_d = 0.39 \mu\text{M}$, of which binding is slightly diminished compared to the non-methylated counterpart but reduction of HBDs aids in passive cell permeability. Truncation of the 9-atom linker construct from the N-terminus gives peptide **42** with $K_d = 0.59 \mu\text{M}$. With the addition of the V511P mutation (**43**) to stabilize the reverse- β -turn with the rigid, cyclic proline residue, potency was enhanced 3-fold ($K_d = 0.19 \mu\text{M}$). Further truncation of the C-terminus of the **42** sequence to make **44** resulted in $K_d = 0.30 \mu\text{M}$.

3.3 Discussion

The key binding determinants of the linear DIF peptide have been examined using computational modeling as well as an experimental direct binding assay. From that data, there is evidence of enhanced binding through maintaining the bioactive conformation of the native BRAF protein. For example, mutating either H510 or N512 resulted in either diminished binding or no binding detected in the linear context (**Table 2.1**). This is thought to be due to these residue's role in the intramolecular hydrogen bonding network which supports the stability of the bioactive conformation. Furthermore, truncation of the sequence to BRAF residues 504-518 (**17**) resulted in a 30-fold increase in potency compared to Peptide **1** (**Table 2.1**), this is suspected to result from a pseudo-cyclic conformation emerging from the electrostatic interaction between the C-terminus and side-chain of R506. This section aims to examine the implications of covalently cyclizing the peptide sequence to allow for enhanced binding to the BRAF DIF.

The first aspect of peptide cyclization which was examined was the location (**Figure 3.1**) and type of cyclization linker used. First it was decided that the method of cyclization would be through using orthogonally protected acid and amine residues to create a lactam cyclization linker once deprotected, this method was used for most of the cyclic peptides. Then the location needed to be determined, drawing inspiration from the pseudo-cyclic linear peptide (**17**) and from the conformation of the truncated DIF in the reverse- β -turn secondary structure in the crystal structure, the BRAF sequence 505-519 was cyclized by a lactam linker through residues 506 and 518. There were two peptides

made using either an 8-atom or 9-atom linker, **30** and **31** respectively, unfortunately, both peptides were insoluble and were not tested. Peptide **32** was cyclized through the side chains of residues 505 and 516 due to their proximity (**Figure 3.1**) and their lack of direct binding to the DIF surface. This peptide was a 12-residue macrocycle with side-chain cyclization through a disulfide bridge (**32**; **Table 3.1**) and was slightly less potent than the pseudo-cyclic linear peptide **17** (**Table 2.1**), but more importantly, this peptide had a 15-fold greater affinity compared to its linear counterpart peptide **16** thus supporting the rationale of cyclization. Furthermore, considering the overall goal of this project, a large macrocycle such as this one may have issues when it comes to drug-likeness. With trying to make the most potent and smallest cyclic peptide as possible, peptide **33** was made by cyclizing the peptide at residues 508 and 513 to make a 6-residue macrocycle. This peptide was cyclized using an 8-atom lactam linker and exhibited a decreased binding affinity compared to **32** but the core macrocycle was smaller giving it more potential for drug-likeness optimization. While trying to improve the linker length, **34** was made with a 9-atom lactam linker and resulted in diminished binding compared to the 8-atom linker counterpart, which is even further reduced compared to the pseudo-cyclic linear peptide (**17**). Furthermore, 6-residue macrocycles were made using both lactam linkers and replacing N512 with alanine due to the lack of need for the hydrogen bonding network in the cyclic context. Interestingly, **35** with the 8-atom linker had equipotent binding as **32** and was improved over the original native sequence. Peptide **36** with the 9-atom linker exhibited an increase in potency and is 6-fold more potent than the disulfide cyclized **32**. Overall, two peptide cyclization sites were discovered (505-516 and 508-513) and have

shown proof of concept for the utility of cyclizing the peptide to stabilize the reverse-turn bioactive conformation for enhanced affinity.

As a proof-of-concept for the validity of peptide cyclization, the **35** sequence was made in the linear context (**37**) and resulted in no binding to the BRAF DIF (**Table 3.1**), thus demonstrating that cyclization is significantly benefiting the DIF-peptide interaction. To further investigate the cyclization of the DIF peptide sequence, a bicyclic peptide (**38**) was made where the inner macrocycle was connected by a 9-atom lactam linkage at the 508-513 site, and the outer macrocycle was connected by a 5-atom lactam linkage at the 505-516 site. The resulting peptide exhibited equipotent binding as the large macrocycle alone in peptide **32**. Based on these results, it seems that the optimum fit for the cyclization of BRAF residues 505-518 were through the 508-513 site using a 9-atom lactam linker creating a 6-residue macrocycle which strictly encompasses the reverse-turn motif and can further be enhanced through sequence optimization now that the reverse-turn residues are no longer required for secondary structure stabilization.

A few different mutations were explored in the cyclic context of the DIF peptide. Using the 508-513 cyclized peptide with the 8-atom linker, the mutation of L515 was explored by mutation to homoleucine (hL) and norleucine to sterically fill the deep lipophilic binding pocket. In the first case, **39** exhibited an equipotent binding coefficient to the original sequence (**Table 3.1**), whereas the norleucine substitution resulted in **40** with enhanced binding affinity by 2-fold when compared to **35**. This is interesting because in the linear 503-521 context, the L515hL mutation (**13**) gave a 2-fold increase in potency,

but now in the cyclic context the mutation does not benefit the binding. Additionally, in the peptide **36** context, the N-methylation of the backbone amide of R509 (**41**), for cell permeability enhancement by decreasing the overall number of hydrogen bond donors, resulted in a 6-fold decrease in binding affinity. Based on interactions in the crystal structure, the decreased affinity cannot be explained since the NH does not play a direct role in binding to the BRAF DIF. Furthermore, the α NH bond of R509 points to the exterior of the macrocycle, disputing its role in intramolecular hydrogen bonding. Additional alterations of the sequence of **36** include truncation of the exocyclic C-terminus, residues 505-507, resulting in a 10-fold drop in potency (**42**). This peptide, though it did lose a relatively significant affinity, it also demonstrated that the exocyclic C-terminus retained respectable activity. Furthermore, the residue V511 was mutated to proline since it could potentially stabilize the reverse turn. Testing of **43** indicated a 3-fold increase in binding compared to **42**, demonstrating that the initial drop in potency of **42** can be recovered by sequence optimization and confirming that stabilization of the reverse- β -turn is important even in the cyclic context. In a further truncation study, exclusion of both the exocyclic C-/N-terminus to generate **44** resulted in a 2-fold increase compared to just the C-terminus truncation alone (**42**), additionally this peptide is equipotent to the larger macrocycle (**32**) and more potent than the much longer linear peptides, demonstrating the optimum conformation of this small macrocycle with fewer points of contact. Interestingly, this peptide excludes the L515 hydrophobic interaction which was thought to be crucial in the linear context but perhaps plays a lesser role in the cyclic form. It is also possible that incorporation of the exo-cyclic C-terminus reduces the overall flexibility

of the bound macrocycle, thus hindering the binding conformation. Taken together, it appears that optimization of L515 binding could be beneficial to binding in the cyclic context may not be necessary based on the truncation study. Furthermore, it appears that the exocyclic truncation of the peptide results in retained binding, thus reducing the overall size and increasing the drug-likeness of the peptide, and through sequence optimization of the truncated cyclic peptide **44**, potency can be recovered while maintaining a smaller, more drug-like macrocycle.

3.3 Conclusion

The rationale for developing potent BRAF inhibitors was to take advantage of the reverse- β -turn in the DIF sequence in order to develop a cyclic peptide which binds the BRAF dimerization interface with high affinity. Optimization of the cyclization method for the peptide has resulted in cyclization through the side chains of residues 508 and 513 and a 9-atom lactam linker. The ITF and ITC experiments have provided experimental proof of concept for the benefit of cyclization by decreasing the entropic cost of binding in cyclic peptides. This concept is exemplified by the comparison of **16** and **32** where cyclization produced a 15-fold increase in binding affinity as well as in the comparison of **37** and **35** where the cyclic **35** displayed enhanced affinity and the linear counterpart produced no binding. Overall, optimization has achieved **36** which has 64-fold more binding affinity for the BRAF DIF than peptide **1**. Furthermore, it appears that the cyclic sequence can be improved further by optimization of the L515 residue for deep binding into a hydrophobic pocket and the V511P substitution can be used to further stabilize the

reverse-turn, rescuing the diminished binding from exocyclic truncation. Additionally, truncation of the exocyclic peptide sequence has yielded a small macrocycle which maintains relatively high affinity at a third of the DIF contact area, thus making the peptide more drug-like and a prime scaffold for design of BRAF DIF inhibitors.

3.4 Experimental

3.4.1 Standard Fmoc Chemistry Solid Phase Peptide Synthesis Protocol

The linear peptide sequence was synthesized on a solid support resin, usually Rink Amide ChemMatrix resin, using N α -Fmoc protected amino acids with acid-labile side-chain protecting groups, 1-[Bis(dimethylamino)methylene]-1H-1,2,3-triazolo[4,5-b]pyridinium 3-oxid hexafluorophosphate (HATU) as the coupling reagent, and diisopropylethylamine (DIPEA) as the base. Resin was allowed to swell in DMF for 30 min with shaking. For resin loading, the first amino acid (2 eq), HATU (2 eq), and DIPEA (4 eq) were dissolved in DMF, added to the resin, and allowed to shake for 4 hours. Following the reaction, the vessel was drained and the addition was repeated once more. After coupling of the first residue, the resin was drained, rinsed three times each with DMF, DCM, and DMF again, and then the resin was tested for primary amines using the Kaiser test. The resin was then Fmoc deprotected by treatment with piperidine (20% in DMF) two times 10 min. The resin was then drained, washed, and again Kaiser tested. The process was then repeated with the next residue, using 2 hour coupling times, in the sequence until the intended peptide sequence was complete.

3.4.2 Kaiser Test Protocol⁴⁵

A small portion of the resin beads were added to a test tube, to which three drops each of the Kaiser test solutions (as described by the AAPPTec Kaiser Test recipe) were added and the solution was heated at 100°C in an oil bath for 5 min. The solution was then removed from heat, the solution was decanted, and the beads were washed once with ethanol. The color of the beads indicates whether there are free amines on the resin; clear beads indicate that there are no free amines and blue or purple beads indicate that there are free amines.

3.4.3 Solid Phase Peptide Synthesis of Cyclic Peptides

The linear sequence of peptides were synthesized using standard Fmoc chemistry as described in Section 3.4.1. Coupling reactions were completed by treatment with the Fmoc-N α -amino acid, HATU, and DIPEA 2x 2 hours and Fmoc deprotection reactions were completed by treatment with piperidine (20% in DMF) 2x 10 min (the final residue was left Fmoc-protected). After the linear synthesis of the intended sequence, orthogonally protected cyclization residues (Alloc and Allyl protecting groups) were deprotected by treatment with tetrakis(triphenylphosphine)palladium (*cat.*) and phenylsilane (100 μ L) dissolved in DCM 4x 5 min. The resin was then washed ten times with DCM to remove all catalyst. The peptide was then cyclized by treatment with HATU (4 eq) and DIPEA (8 eq) dissolved in DMF overnight. The resin was then washed three times each with DMF, DCM, and DMF again, and the final residue was Fmoc deprotected as previously described. The peptide was then cleaved from the resin by treatment with a solution of TFA/TIPS/H₂O

(94/5/1) for 2-4 hours. The solution was then collected along with a TFA rinse, and the sample was dried via evaporation at reduced pressure.

3.4.4 Purification of Synthetic Cyclic Peptides

After cleavage from the resin, peptides were concentrated to a minimal volume of trifluoroacetic acid (TFA) and were placed on ice. The peptide was then precipitated with cold diethyl ether (~5 mL) and were spun down using a centrifuge and the solution was decanted. The remaining solid was dissolved in DMSO and the peptide was purified via semi-preparative LCMS using the Phenomenex Luna 5u C18(2) 100Å column which was 250x10.00 mm with a 5 micron pore size. Peptides were separated using a water/acetonitrile/0.1% formic acid mobile phase on a 5-40%B over 40 min gradient. The sample was obtained through mass-based collection methods. Fractions were re-analyzed by analytical LCMS to determine pure fractions, which were then combined, rotovapped to remove the organic solvent, lyophilized, and weighed.

3.4.5 Intrinsic Tryptophan Fluorescence (ITF) Assay²⁹

See section 2.5.8.

3.4.5 Isothermal Titration Calorimetry (ITC)²⁹

ITC was measured with an Affinity ITC instrument (190 µL cell volume, TA Instruments, USA) at 15 °C with stirring speed 170 rpm. The ITC experiments were performed in 20 mM N-(2-hydroxyethyl)piperazine-N-ethanesulfonic acid (HEPES) buffer (pH 7.5), 10 mM MgCl₂, and 30 mM NaCl. For certain ligands that were insoluble in

aqueous media, 5–10% DMSO was added to increase its solubility. The sample cell was loaded with the solution of 6.5–10 μM of protein and the 50–1000 μM peptide inhibitor solution was placed in the injection syringe. In a typical experiment, 12 injections of 2 μL aliquots of the peptide were added into the calorimeter cell. Data analysis was performed using NanoAnalyze software according to model of the single set of identical independent sites. Also two “blank” experiments were performed with the above settings.

TABLE 3.1: ITF DIRECT BINDING ASSAY DATA OF CYCLIC BRAF DIF PEPTIDES

ID	BRAF Residues	Mutations	Sequence	Kd (μM)
30	505-519 (c506-518)	R506K, G518E	LKKTRHVNILLFMEY	INS
31	505-519 (c506-518)	R506O, G518E	LOKTRHNVILLFMEY	INS
32	504-517 (c505-516)	L505C, F516C	VCRKTRHVNILLCM	0.36 \pm 0.32
33	505-518 (c508-513)	T508O, I513E	LRKORHVNELLFMG	0.78 \pm 0.01
34	505-518 (c508-513)	T508K, I513E	LRKKRHVNELLFMG	1.89 \pm 0.33
35	505-518 (c508-513)	T508O, N512A, I513E	LRKORHVAELLFMG	0.46 \pm 0.04
36	505-518 (c508-513)	T508K,N512A, I513E	LRKKRHVAELLFMG	0.06 \pm 0.01
37	505-518	T508O, N512A, I513E	LRKORHVAELLFMG	NB
38	504-518 (c505-516) (c508-513)	L505Dab, T508K, N512A, I513E, F516D	V-Dab-RKKRHVAELLDMG	0.37 \pm 0.03
39	505-518 (c508-513)	T508O, N512A, I513E, L515homoleucine	LRKORHVAEL-hL-FMG	0.43 \pm 0.03
40	505-518 (c508-513)	T508O, N512A, I513E, L515Nle	LRKORHVAEL-Nle-FMG	0.17 \pm 0.06
41	505-518 (c508-513)	T508K, R509MeR, I513E	LRKK-MeR-HVAELLFMG	0.39 \pm 0.02
42	508-518 (c508-513)	T508K,N512A, I513E	KRHVAELLFMG	0.59 \pm 0.02
43	508-518 (c508-513)	T508K, V511P, N512A, I513E	KRHVAELLFMG	0.16 \pm 0.02
44	508-513 (c508-513)	T508K,N512A, I513E	KRHVAE	0.30 \pm 0.03

TABLE 3.2: ITC THERMODYNAMICS DATA

Peptide	Sequence	ITF Kd (μM)	ITC Kd (μM)	ΔH (kJ/mol)	ΔS (J/(mol K))
Pub #8	GVLTKARHVNILLFMGYST	2.80	14.9 \pm 10.8	-34.8	-28.4
11	VLRKTRHVNILLFMG	0.13	0.35 \pm 0.17	-199.0	-567.0
31	LRKORHVAELLFMG	0.46	0.31 \pm 0.16	-9.4	92.1

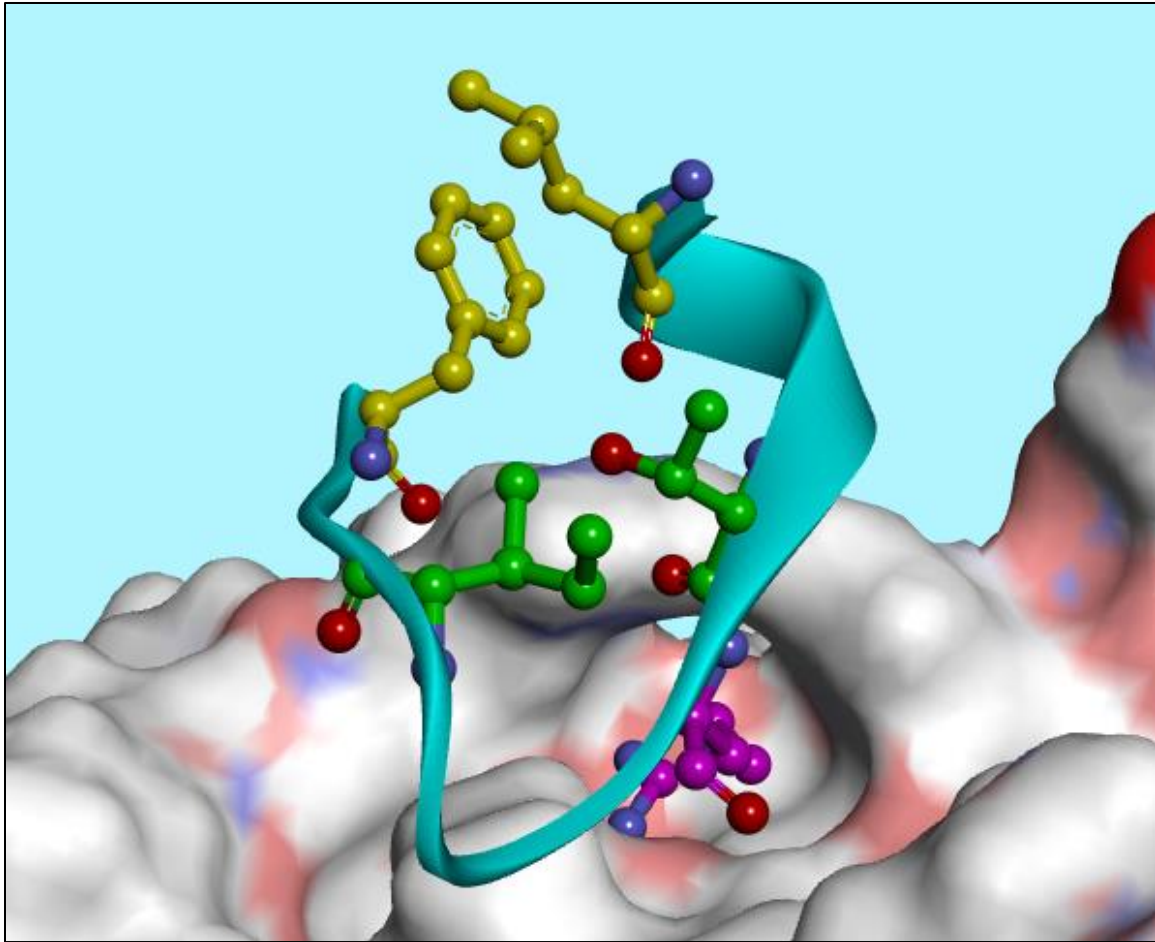


FIGURE 3.1: BRAF DIF PEPTIDE CYCLIZATION SITES: Shown above is the truncated DIF peptide (residues 504-518) with two cyclization sites. Site 1 makes a larger 12 residue macrocycle between L505 and F516 (yellow) and site 2 makes a 6 residue macrocycle between T508 and I513 (green), R519 is shown in magenta for perspective.

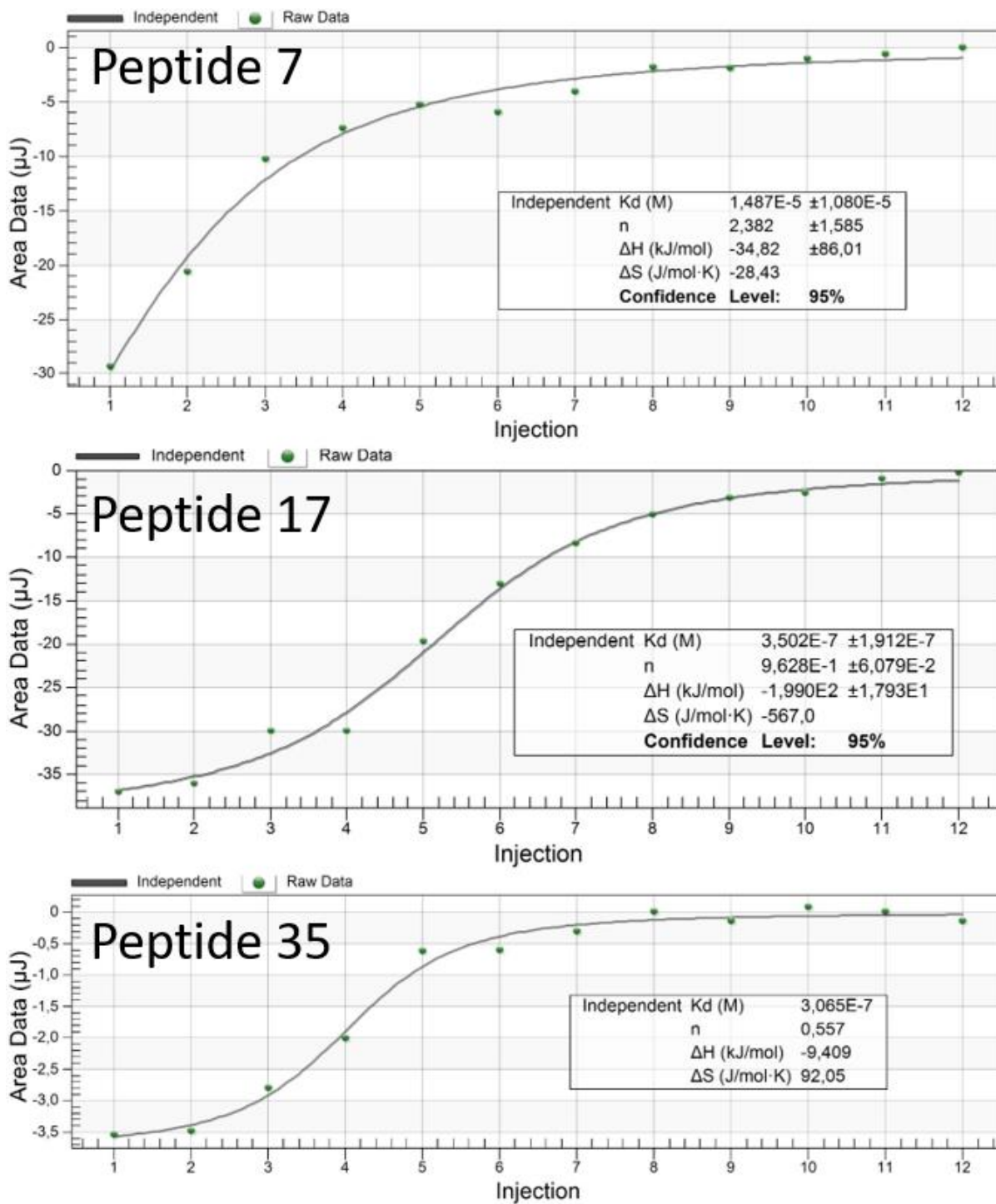


FIGURE 3.2: ITC DATA FOR LINEAR AND CYCLIC PEPTIDES

CHAPTER 4

**OPTIMIZATION OF PHYSIOCHEMICAL PROPERTIES OF CYCLIC BRAF DIF PEPTIDES FOR
PASSIVE CELL PERMEABILITY**

4.1 Introduction

4.1.1 The Growing Need for Drug Space Beyond Small Molecule Therapeutics

Drugs are designed to be taken by patients in order to cause a physiological effect which is therapeutic in nature. Most medications are administered to the patient orally which means that the drug must be able to be absorbed through the gastrointestinal tract and travel through the body to the therapeutic target. In the context of cancer therapeutics, most of the drug targets are located within the cells of the tumor, and therefore the drug must be able to pass through the phospholipid bilayer of the cell membrane in order to reach its target to cause a therapeutic effect.

Due to their favorable absorption, small molecules such as Type I kinase inhibitors continue to be used as therapeutic tools to invoke a physiological response by out-competing adenosine triphosphate (ATP) or other co-factors to inhibit oncogenic proteins for the treatment of cancer. With the growing need for second-line therapies for drug resistant malignancies, novel therapeutic targets are needed for efficacious treatment of advanced stage cancers which inhibit oncogenic targets potently and selectively.

In recent years, therapeutically targeting protein-protein interactions (PPIs) has become a growing field in drug discovery as a method of inhibiting the interaction of oncogenic proteins with either upstream effectors or downstream substrates. This method of inhibition allows for the design of compounds which are selective for the target protein's binding surface rather than the ATP ligand pocket which is relatively conserved across the kinase families, though inhibiting PPIs can be utilized for other protein families as well. A hindrance to the development of PPI inhibitors is that binding interfaces tend to be quite large, flat, and featureless and therefore requiring the need for larger compounds to block these interactions. The development of larger and more complex compounds as therapeutics fundamentally violates the guidelines oral availability which were originally established by Lipinski et al. and later revised by Veber et al. owing to the idea that with increased size there will be an increase in polarity which will inhibit compounds from crossing the lipophilic membrane passively (**Table 4.1**), thus complicating the situation with the question, how can larger compounds, greater than 500 Da, enter the cell to inhibit these protein-protein interactions in a therapeutic manner?

4.1.2 Hallmarks of Cell Permeability

In the field of drug design, Lipinski's Rule of Five (Ro5) was previously regarded as the gold standard for design of small molecule drugs which are orally available. This rule came from Christopher Lipinski's publication in 1997 which was written in the *Advanced Drug Delivery Reviews* journal outlining the chemical properties which a substance should have in order to be orally bioavailable.⁴⁶ The rule states that the compound should have

a molecular weight less than 500 Da, less than 5 hydrogen bond donors, less than 10 hydrogen bond acceptors, and a water-octanol partition coefficient less than 5 (**Table 4.1**).

Later, in 2002, a paper by Veber et al. was published in the Journal of Medicinal Chemistry which took another look at the requirement of a compound for cell permeability.⁴⁷ Veber et al. stated that the better molecular properties for the prediction of oral availability were the number of rotatable bonds as a measurement of molecular flexibility and the polar surface area (defined as the sum of hydrogen bond donors and acceptors) of the compound. The article also stated that the molecular weight does not impede cell permeability, but in a general sense, with increased molecular weight there is an increased number of rotatable bonds and polar surface area which determines cell permeability. In this article, the oral bioavailability of 1100 drug candidates were analyzed in rats and it was determined that having fewer than 10 rotatable bonds and a polar surface area of less than 140 Å² (less than 12 total hydrogen bond acceptors and donors) was an effective predictor of cell permeability independently of molecular weight (**Table 4.1**).

With the growing enthusiasm of targeting protein-protein interactions, there is also an enhanced need to explore the drug space beyond the realm of small molecule drugs. In recent years there has been several articles which have extensively screened large libraries of macrocyclic compounds for their ability to be cell permeable even

though they have molecular weights which exceed the restraint defined in Lipinski's rule of five.⁴⁸⁻⁵⁰

4.1.3 Cell Permeability of Macrocyclic Peptides

With the intent to inhibit protein-protein interactions, it is likely that larger compounds with a broad binding surface will be needed to bind the large, flat, and rather featureless surfaces of one of the partners and compete with the other for binding. Since the ligand of PPI binding sites are other proteins, generation of peptide libraries has grown in popularity as screening methods for PPI inhibitor hit or partial hit discovery. Partial hits can then be combined with post-synthesis modifications which can enhance binding if the ligand sequence is not contiguous for the PPI interaction.⁵¹⁻⁵⁴ While optimization of binding using peptidic sequences as potential drug leads sounds advantageous, peptides in themselves have several drawbacks to being used as drugs including fast clearance, low proteolytic stability, and low cell permeability which negatively affects their therapeutic utility as drugs.^{48,50,55} The following section will focus on examples of cyclic peptides which have the ability to permeate the cell as well as the modifications which can be used to promote cell permeability of designer peptides for therapeutic applications.

A recent review states that there are several methods for to improve cell permeability through passive diffusion, active transport, direct translocation or endocytosis.⁵⁶ Passive diffusion (PD) is energy-independent and the main mechanism by which small molecule therapeutics gain entry into a cell and for which the Ro5 defines

acceptable physicochemical parameters . PD is possible where the lipophilicity of the compound enables desolvation to enter the membrane and then resolvation to exit into the cytosol in an energy efficient manner. Active transport (AT) involves the energy-dependent uptake of drugs and takes advantage of integral transporter proteins whose key role is to transport nutrients and metabolites into the cell. AT can also involve solute carrier proteins (SLC) known to transport a variety of different compounds into the cell. Direct translocation is another mechanism poorly defined and where at high concentrations, peptides can directly transverse the membrane directly into the cytosol. Cell penetration of peptides can also occur through endocytosis of positively charged peptides followed by endosomal escape into the cytosol. Here we focus on the passive diffusion of cell permeability of cyclic peptides as the main route of cellular entry.

The fundamental issue hindering passive diffusion of peptides across the cell membrane is their high polarity. They typically have a large number of hydrogen bond donor (HBD) and hydrogen bond acceptors (HBA) giving a large overall polar surface area (PSA), an unfavorable characteristic to allow passage through the hydrophobic conditions inside the membrane phospholipid bilayer. In particular, the polarity contributed by the HBDs/HBAs of the amide backbone contributes to the energy required to desolvate the amide groups during the transition from the aqueous to the lipophilic environment as established by Burton et al.⁵⁷ Masking the HBDs of the amide backbone is therefore an effective approach for promoting cell permeability of peptides and methods of doing this include N-methylation of amide nitrogens, incorporation of bulky aliphatic groups as amino acid sidechains, increased frequency of proline residues, and incorporation of

peptoid functionalization. All of these methods will either replace the amide proton and decrease the PSA or sterically hinder the formation of hydrogen bonds between the amide proton and the aqueous environment, thus decreasing the desolvation energy required for the peptide to enter the lipophilic environment of the cell membrane.

A classic example of a cyclic peptide which is cell permeable is Cyclosporine A (CsA), an immunosuppressive drug which can be taken orally and is used to prevent organ transplant rejection as well as treat rheumatoid arthritis and psoriasis. Cyclosporin A is a head-to-tail cyclized peptide which is 11 residues in length and is made up of mainly natural, hydrophobic, aliphatic residues. The key structural features of CsA leading to its cell permeability is the pattern of N-methylation of the amide backbone and the intramolecular hydrogen bond network which occurs upon introduction of the peptide to a hydrophobic environment. In a study analyzing the contribution of cyclization for the cell permeability of CsA, a 10-residue cyclic analog, and the acyclic precursor was studied.^{53,58} Of these samples the truncated analog and the linear analog were iso-lipophilic based on the experimental polar surface area and had the ability to form the same intramolecular hydrogen bond network. Based on the RRCK values representing cell permeability rates, the acyclic peptide was 20-fold less permeable than its cyclic counterpart. This decrease in permeability was attributed to the linear analog occupying significantly greater conformational space than the cyclic analog. This study showed that there is more that dictates the cell permeability of peptides than just the physiochemical properties, and that restricting the peptide to the cyclized conformation decreased the

entropic cost of energy for desolvation of the peptide to form the intramolecular hydrogen bond network required for passive diffusion.

A recent review by Nielsen et al. recognized the need for peptide cyclization as a way of orienting the sidechains of the peptide in a manner to shield the polar functional groups for cell permeability.⁵⁰ Nielsen et al. analyzed the physiochemical properties associated with cell permeability of 125 cyclic peptides with reported bioavailability in order to probe the chemical space beyond the rule of five (bRo5). From this study, they found that the limit on molecular weight (MW) can be increased in this context with reported bioavailability from peptides with MW of 500-1350 Da. As for the number of hydrogen bond donors (HBDs), this property is roughly consistent with the Ro5 with cyclic peptides exhibiting bioavailability with HBDs of 1-6. In the case of hydrogen bond acceptors (HBAs) and water-octanol partition coefficient (LogP), bioavailable peptides were seen with HBA ranging from 5-20 and LogP of 1-8, which extends the Ro5 (**Table 4.1**). Furthermore, comparing with Veber's extension to the rule, peptides containing 5-20 rotatable bonds and a topological polar surface area of $< 300 \text{ \AA}^2$ were seen to have ample bioavailability, almost doubling the acceptable tPSA and number of rotatable bonds. Thus, there is more to be considered than the original Ro5 parameters when trying to predict cell permeability of cyclic peptides.

4.1.4 Peptide to Peptidomimetic REPLACEMENT

REPLACE (Replacement with Partial Ligand Alternatives through Computational Enrichment) is a validated strategy for conversion of peptides to drug-like compounds

which inhibit protein-protein interactions (PPIs).⁵⁹⁻⁶¹ The REPLACE strategy iteratively substitutes peptide segments for small molecule fragments deemed favorable through the use of computational methodology as a platform for broadening the landscape of PPI inhibitor technology (**Figure 4.1**). In a sense, the structure activity relationship is initially optimized through the generation of peptide libraries which are screened for direct binding affinity. A peptidic sequence is then truncated and Partial Ligand Alternatives (PLAs) are docked into the binding site using computational methods, replacing the initial segment. High scoring PLAs are then synthetically ligated to the truncated peptide to generate FLIPs (Fragment Ligated Inhibitory Peptides) which are then tested for binding efficiency. PLAs which are highly active and recapitulate the affinity of the native peptide in the FLIP context are kept and the process is repeated with the next peptidic segment until the entire peptide is converted to a drug-like compound with optimized binding. The iterative conversion of the sequence to a can enhance the binding affinity and cell permeability, thus resulting in a more drug-like compound.

4.2 Results

4.2.1 Passive Cell Permeability of BRAF DIF Peptides

The peptide library was gradually optimized include physiochemical properties which might promote passive cell permeability based on the bRo5 guidelines for cell permeable cyclic peptides (**Table 4.1**).⁵⁰ Peptide **1** consisted of BRAF residues 503-521 (Kd = 3.84 μ M) and had a MW of 2205.66 g/mol, 28 hydrogen bond donors, 26 hydrogen bond acceptors, and a topological polar surface area of 885 \AA^2 (**Table 4.2**). Truncation to

residues 505-518 and optimized cyclization (**36**; $K_d = 0.06 \mu\text{M}$) resulted in a dramatic increase in potency and an overall decrease in size (MW = 1679.12 g/mol; HBD = 20; HBA = 18; cLogP = -3.78; tPSA = 651 Å²). Truncation of exocyclic sequences after cyclization (**44**; $K_d = 0.30 \mu\text{M}$) resulted in a compound with good affinity while decreasing its size, the number of HBD/HBAs, and its topological polar surface area (MW = 719.85 g/mol; HBD = 10; HBA = 9; cLogP = -3.94; tPSA = 330 Å²), however with a similar cLogP. The REPLACE strategy was used to design exocyclic capping groups more druglike in nature (**53**) and largely within bRo5 guideline ranges (MW = 1014.24 g/mol; HBD = 10; HBA = 11; cLogP = 1.94; tPSA = 328 Å²). Further optimization of the macrocyclic sequence resulted in a lead peptide in terms of affinity (**54**; $K_d = 0.017 \mu\text{M}$) while meeting all bRo5 criteria except the number of HBD (MW = 960.19 g/mol; HBD = 7; HBA = 10; cLogP = 3.13; tPSA = 286). Further optimization of the cyclic sequence for cell permeability was attempted by replacement of the “aPA” sequence in 54 with an alkyl chain to generate a compound meeting all of the bRo5 guidelines (MW = 862.13 g/mol; HBD = 6; HBA = 7; cLogP = 3.71; tPSA = 237 Å²).

4.2.2 Temperature Coefficient NMR Study of BRAF DIF Peptides

One of the leading theories explaining the cell permeability of cyclic peptides involves the chameleon effect which the peptide structure allows for dynamic conversion of cyclic peptides between an aqueous conformation where the backbone amide protons are solvent exposed and a lipophilic conformation where these participate in intramolecular hydrogen bonds. Temperature Coefficient NMR (TC-NMR) can be used to

determine if the amide protons are participating in intramolecular hydrogen bonds (IMHBs) under lipophilic conditions by determining how far the peaks shift in response to temperature change. First a suite of 2D-NMR experiments were ran on Peptide **44** to fully assign the amide proton chemical shifts (**Table 4.3; Figure 4.2**) then the TC-NMR technique was used to determine whether or not amide protons were participating in IMHBs under the lipophilic conditions of 30% TFE-d₃ (a solvent known to induce peptide secondary structures) in D₂O (**Table 4.4; Figure 4.3**). Using this temperature sensitivity analysis, if amide protons move less than -2.5 ppb/K then they are potentially participating in IMHBs, but if they move more than -4.5 ppb/K then they are not likely to be involved in IMHBs.⁶² Based on the suite of 2D-NMR experiments (DQF-COSY; TOCSY; ROESY) the 5 backbone and the cyclization linker amide protons were assigned in addition to others of importance. Upon running the TC-NMR experiment from 295-320°K, the temperature coefficient for all amide protons were greater than the -4.5 ppb/K cut-off described by literature, indicating that none of these participate in IMHBs under lipophilic conditions.

4.2.3 Optimization of BRAF 508-513 Cyclized DIF Peptide for Passive Cell Permeability using REPLACE

After significantly truncating the cyclic peptide to the BRAF 508-513 cyclic sequence while retaining reasonable activity (**44; Table 3.1**), a compound suitable for further application of REPLACE was obtained. Using the REPLACE method to identify fragment replacements for the exocyclic sequences was attempted to recover lost affinity

while also increasing the lipophilicity of the overall compound. N-terminal and C-terminal capping groups were initially tested in the linear FLIP context of the BRAF 505-518 sequence, using the ITF assay carried out by the Kontopidis lab, in order to efficiently determine contribution of the FLIP without complicated cyclization and purification methods, respectively replacing the exocyclic sequence of the native sequence with the desired PLA capping group (**Table 4.5**).

The first N-terminal capping group to be used was benzoic acid (N1; **Table 4.6**) coupled to the N-terminal amine replacing the “LRK” sequence. Others included those incorporating extra methylenes to optimize the position of the phenyl ring to the W450 side-chain. The incorporation of N1 in the FLIP **45** ($K_d = 0.050 \mu\text{M}$; **Table 4.5**) resulted in an enhancement of binding compared to **1**. The N2 FLIP (**46**; $K_d = 0.084 \mu\text{M}$) slightly hindered binding but was still better than peptide **1**. FLIPS containing the N3 and N4 PLAs (2 and 3 methylenes respectively; FLIPs **47** and **48**) were determined to be insoluble under testing conditions.

Potential C-terminal capping groups were also tested in the linear FLIP context, replacing the LLFMG sequence of BRAF (residues 505-518) with fragment analogs of 2-(4-(isopentyloxy)phenyl)ethan-1-amine (**Table 4.6**). The incorporation of C2 (**49**), C3 (**50**), and C4 (**51**) PLA capping groups resulted in linear FLIPs exhibiting a K_d of 0.020, 0.380, and 0.570 μM respectively (**Table 4.5**). The incorporation of all the N-/C-terminal capping groups in the linear FLIP context resulted in sub-micromolar direct binding affinities similar to results obtained for the cyclic peptides.

FLIP **52** combining the N2 and C4 capping groups in the linear context was synthesized and tested. This compound had a $K_d = 0.280 \mu\text{M}$ (**Table 4.5**), in which the high potency of the N2 group rescued the weak binding interaction of the C4 capping group. . FLIP **54** included the two highest affinity capping groups identified in the linear context along with NMe-Arg and the reverse- β -turn stabilizing sequence “aPA” and yielded a K_d of $0.017 \mu\text{M}$. This data resulted in the new lead peptide sequence for direct binding and was designed to have both reduced size and increased lipophilicity required for passive cell permeability (**Table 4.2**).

4.2.4 Study of Passive Cell Permeability

The passive permeability of peptides was tested using a PAMPA (Parallel Artificial Membrane Permeability Assay) assay kit where compounds are incubated in a two well system divided by an artificial membrane and cell permeability is assessed via UV detection of the receiver well after incubation. Peptides **17**, **36**, **44**, and **55**, along with the low, medium, and high permeability controls, were tested in this assay for passive diffusion and results were accessed by UV absorption using a plate reader. As described in the kit, the controls performed as expected but the results obtained from the peptide samples were more ambiguous due to interference of the DMSO absorbing at the lower wavelengths. The experiment was repeated for peptides **44**, **54** and **55**, using LCMS to determine the compound concentration in the acceptor cell solution, and there was no detectable signal for any of those tested. Furthermore, peptides **54** and **55** which modified in the hope of making them cell permeable by incorporation of lipophilic capping

groups and through N-methylation and substitution of proline, or through complete replacement of some contiguous but less important residues with an alkyl chain, were tested in the PAMPA assay. Using an LCMS analysis these none of these compounds were detected in the acceptor cell.

4.3 Discussion

The objective of this chapter was to optimize the physiochemical properties of the lead peptides so that they better adhere to the beyond rule of 5 (bRo5) guidelines for passive cell permeability of macrocyclic peptides.⁵⁰ In a study conducted by Nielsen et al. a large library of orally bioavailable cyclic peptides was examined for bRo5 characteristics. This study observed that peptides with molecular weight (MW) up to 1300 daltons, a LogP range from 1-8, a maximum of 6 hydrogen bond donors (HBDs) and 20 hydrogen bond acceptors (HBAs), and a topological polar surface area (tPSA) of $<300\text{\AA}^2$ had the greatest oral availability (**Table 4.1**), meaning that when the drug was administered orally, then a certain percentage of the administered dose makes it to the therapeutic target.⁵⁰ The statistic of oral bioavailability is dependent on several parameters including absorption, metabolism, stability, and cell permeability. Though cell permeability is only one factor of oral bioavailability based on these properties and ability to hydrogen bond, or lack there of, the original BRAF DIF **peptide 1** was modified as follows.

After identifying an effective peptidic inhibitor (**1**) of BRAF dimerization, the three main characteristics where which needed to be addressed in order to generate a more drug-like compounds, were reduction of MW, increasing its lipophilicity, and

conformational flexibility of **1** (Table 4.2). Starting with cyclization to reduce the number of rotatable bonds, several macrocyclic peptides were designed and tested resulting in **36** which was connected by a nine atom lactam bridge between residues 508 and 513. This peptide possessed a $K_d = 0.06 \mu\text{M}$ and became the lead compound for the development. Further modifications to make the peptide more drug-like included reducing the size of the macrocycle by a series of exocyclic truncations. Based on these experiments, **44** was identified as the core macrocycle sequence containing only the cyclic residues of 508-513 from the precursor peptide **36**. Peptide **44** had a $K_d = 0.30 \mu\text{M}$, which although resulted in a 5-fold decrease in affinity relative to **36**, reduced the molecular weight to within the bRo5 guidelines and provided the basis for further optimization and application of the REPLACE strategy.

Based on bRo5 guidelines, further optimization was attempted by increasing lipophilicity of the peptide and decreasing the number of HBDs and HBAs all of which will address issues with a high tPSA. As mentioned, there are several studies which attribute cyclic peptide's cell permeability to "the chameleon effect".⁵³ This phenomenon occurs due to a peptide's ability to solvent expose polar groups under aqueous conditions and to be flexible enough to change conformation and sequester these to allow entry to the cell membrane, thus desolvating in an energy efficient manner. Furthermore, the peptide must be able to favorably resolvate upon exiting the cell membrane into the cytosol for example as occurs with cyclosporine A. As such, cell permeability is attributed to the ability of peptides to form intramolecular hydrogen bonds (IMHBs) transversely across the macrocycle. This sequesters polar groups (HBD/HBAs) from the lipophilic

environment and is complemented by N-methylated of amide NH's that do not form IMHBs thus making the compound more lipophilic.

To assess whether the core macrocycle **44** can form IMHBs, the peptide was analyzed via TC-NMR (Temperature Coefficient NMR; **Figure 4.3**; **Table 4.4**) after a suite of 2D-NMR techniques (**Figure 4.2**; **Table 4.3**) was used for chemical shift assignment. This technique is used to analyze the temperature dependence of backbone amide protons in a solvent such as trifluoroethanol-d₃ (TFE-d₃), which is thought to mimic the hydrophobic environment of a membrane and also to induce peptide secondary structure. If the NH proton in question is participating in an IMHB then the proton will exhibit less of a temperature-dependent change in the chemical shift (0 to -2.5 ppb/K) since its solvent exchange is decreased by hydrogen bonding. Conversely, protons not participating in IMHBs will shift more dramatically (greater than -4.5 ppb/K) with an increase in temperature. When **44** was tested in this experiment, all amide protons exhibited temperature-dependent shift characteristics suggesting that none of them participate in IMHBs (**Table 4.4**). This result indicates that the backbone amide nitrogens could be N-methylated as long as they don't play a role in BRAF binding. Incorporation of an N-methylated arginine at position 509 (**41**) did not significantly compromise binding and a proline at position 511 (**43**) resulted in enhancement of binding potency (due to stabilization of the reverse- β -turn), each while reducing the number of hydrogen bond donors (**Table 4.5**).

N and C-terminal truncation (“LRK” on the N-terminus and “LLFMG” on the C-terminus) of **36** to generate **44** resulted in loss of important binding interactions with BRAF-W450 and the deep hydrophobic pocket to which peptidic L515 bound. The REPLACE strategy (Replacement with Partial Ligand Alternatives through Computational Enrichment) was used in order to discover more drug-like alternatives for the truncated exocyclic sequences. In order to develop N-/C-terminal capping groups, small molecule libraries were searched for appropriate compounds which would provide pi-stacking interactions on the N-terminus with W450 as well as a lipophilic interaction with the hydrophobic pocket to which L515 originally bound. Capping groups were then computationally modeled in their appropriate location to assess the feasibility of incorporating them into the peptide sequence. The capping groups were then initially tested experimentally in the context of the truncated linear peptide for ease of synthesis and purification (**Table 4.5**). The peptides were then tested in the ITF assay to assess direct binding affinity for the BRAF DIF. N-terminal capping groups were varied by increasing the number of methylene groups in the benzoic acid portion (**Table 4.6**), of which the two longest were insoluble with the optimal of these being benzoic acid itself (**45**) and its face-to-edge pi-stacking conformation with the protein W450 resulted in $K_d=0.05 \mu\text{M}$. The C-terminal groups were analogs of 2-(4-(isopentyloxy)phenyl)ethan-1-amine (**Table 4.6**). The tightest binding C-cap was C2 with a para substituted phenol ether (**49**) and a $K_d=0.02 \mu\text{M}$ (**Table 4.5**). Interestingly, all linear, capped peptides had direct binding affinities on par with the best cyclic peptides. Furthermore, when the poorly binding C4 group and tightly binding N2 group were combined in the linear context, the

resulting peptide **52** had a relatively equivalent binding potency to the cyclic, uncapped version (**44**). This shows that the N2 cap rescued the inefficiently binding C4 cap thus confirming the utility of these non-peptidic capping groups.

After further optimization, the development of **36** produced the lead peptide, **54** for this study in terms of binding affinity and modifications predicted to both increase affinity and cell permeability. Furthermore, a peptidomimetic **55** which replaced the “aPA” sequence of **54** with an octyl linker was synthesized to realize cell permeability by increasing the overall lipophilicity and decreasing the number of HBD/HBAs. Several peptides and FLIPS including **1**, **36**, **44**, **54**, and **55** were tested for passive cell permeability in the PAMPA assay. After incubation of the peptides as described, the acceptor cell was analyzed via LCMS to determine the rate of passage through the membrane. Based on the results of the PAMPA assay, there was no evidence of passive permeability of any of the peptides or FLIPS. This may be due to the compounds not being able to efficiently transition between hydrophilic and hydrophobic conformations which allow for masking of the remaining polar surface area. Additional work should be completed to mask HBD/HBAs while still maintaining aqueous solubility.

4.4 Conclusion

In efforts to convert DIF peptide **1** (GVLKTRHVNILLFMGYST) into a drug-like and ultimately an orally available compound, the native sequence has been modified through cyclization and truncation to reduce the overall size and number of rotatable bonds of the initial sequence, resulting in **44** (KRHVAE) which contains less than half of the original size

and significantly fewer rotatable bonds compared to **Peptide 1**. Further investigation into the ability of the cyclic peptide to change conformation when passing through a lipophilic environment was evaluated using TC-NMR methods. The data suggests that none of the backbone amide protons participate in intramolecular hydrogen bonds with the trans-cyclic carbonyls under lipophilic conditions. This affects the peptide's ability to dynamically pass through the cell membrane by way of energetically favorable conformational changes that mask hydrogen bond donors. Results suggest that N-methylation of the backbone amide groups can be undertaken to increase lipophilicity. Furthermore, the REPLACE method was utilized in the generation of FLIPS capped with small molecule fragments which enable more efficient binding and increased lipophilicity. All FLIPs had sub-micromolar binding affinity in the linear context, suggesting successful and effective replacement of the exocyclic sequences. Furthermore, incorporation of both groups (N2 and C4) in the same compound was shown to recapitulate the lost binding affinity from truncation of the exocyclic sequences in the linear context (**52**). The PAMPA assay was used to assess passive permeability of the lead peptides and FLIPS however no detectable passage through the artificial membrane was observed. Though unsuccessful by this measure, significant progress has been made in the optimization of DIF peptide physiochemical properties, ability to tightly bind BRAF, and obtaining proof of concept for inhibiting BRAF mediated paradoxical activation. Future endeavors will involve further N-methylation studies of the 508-513 macrocycle, further REPLACEMENT of the cyclic sequence of FLIP **54**, and incorporation of cell penetrating peptide moieties through tri-functional cyclization linkers.

4.5 Experimental

4.5.1 Temperature Coefficient NMR Spectroscopy

The peptide sample was dissolved in minimal DMSO-d₆ and was then diluted with a solution of 30% trifluoroethanol-d₃ (TFE-d₃) and D₂O. The 1D spectra were obtained using a Bruker 400 MHz NMR equipped with a cryoprobe using a pre-saturation pulse sequence designed to suppress the signal of the water peak. The experiments were run using the TFE-d₃ as the lock solvent and were ran for 16-32 scans each at 295, 300, 305, 315, and 320° K. Following runs, spectra were checked for the presence of the correct number of amide proton doublets between 7.0-9.0 ppm. To determine the temperature coefficient of each amide proton, **Equation 3** was used, where “S” is the chemshift (ppb) of each respective amide peak at either 295° K or 320° K and “ΔT” is the change in temperature between the two extremes. The need for full characterization through a suite of 2D NMR spectra was dependent on clarity of the 1D spectrum at any given temperature.

$$\text{Equation 3: } TC = \left[\frac{(S_{320K} - S_{295K})}{\Delta T} \right]$$

4.5.2 Characterization of Peptides by 2D NMR Spectroscopy

For the characterization of peptides, the same sample and instrument were used as for the TC-NMR experiments. First a 1D H¹ NMR was obtained using the pre-saturation pulse sequence, then a double quantum filter correlated spectroscopy (DQF-COSY) experiment was ran to identify the amide protons and their adjacent αCH protons. In this

experiment, there was no correlation for the N-terminal residue due to rapid exchange of the deuterium isotope on the amine. Once the amide and α CH protons were identified, a total correlation spectroscopy (TOCSY) experiment was ran. This experiment was used to identify each residue based off of their spin system pattern which is representative of the consecutive adjacent protons in the residue side-chain. Lastly, a rotating frame overhauser effect spectroscopy (ROESY) experiment was ran which correlates α CH protons which are close in space to the adjacent residue's amide proton. In this experiment, the sequence of the peptide can be identified, resolving the identity of any duplicate residues which may be present in the sequence.

4.5.3 PAMPA Assay

The PAMPA assay was accomplished using a PAMPA assay kit purchased from BioAssay Systems, which included the donor plate, acceptor plate, UV plate, lecithin, dodecane, and high, medium, and low permeability controls. Each tested compound was dissolved in DMSO to make a 10 mM stock solution (standards were already 10 mM in DMSO) which was diluted with phosphate-buffered saline (PBS) to give a 500 μ M solution of the test compounds and standards. The lecithin was dissolved in dodecane as instructed by the kit protocol to make a 4% lecithin in dodecane solution, this solution was then used to wet the membrane at the bottom of the donor wells. The acceptor plate was then loaded with 300 μ L of PBS and the acceptor wells were loaded with the 500 μ M test compound solutions (200 μ L). The donor plate was then stacked onto the acceptor plate so that the acceptor PBS solution made complete contact with the bottom

side of the membrane. The plates were then covered and allowed to incubate at 38° C for 18-24 hours. The following day, the donor and acceptor solutions were collected from the plate to stop the experiment.

The kit suggests quantification of acceptor well concentration using the included UV plate, but the low absorbance wavelength of the peptides in conjunction with the interference of the DMSO made it impossible. The concentration of the acceptor well was quantified by LCMS methods. Solutions of test compounds and standards were made at 500, 250, and 125 μM and 20 μL aliquots were injected onto the LCMS. The combined absorbance of the sample peak at 215 and 254 nm were plotted verses concentration to establish each sample concentration curve. The acceptor and donor well solutions were then injected onto the LCMS and the concentration was determined based on the detected absorbance peak.

4.5.4 Synthesis of Double Capped Cyclic Peptides (FLIPS)

Compounds which were designed to be capped on both the N-/C-terminus were synthesized on a chlorotriyl chloride (CTC) polystyrene resin which allows for cleavage of the peptide under very mild conditions without deprotection of sidechains. The peptide was loaded onto the resin by 2x 5 hour treatments with the AA (2 eq) and DIPEA (4 eq) dissolved in a 1:1 solution of DMF and DCM. After loading, the unfunctionalized groups on the resin were capped by treatment with a solution of DCM/MeOH/DIPEA (80:15:5) for 30 min. The resin was then washed 3x each with DMF, DCM, and DMF again. The rest of the linear synthesis was completed as previously stated in section 3.4.1 except that the

coupling reactions were completed in a 1:1 DMF/DCM solution to promote swelling of the resin.

The N-terminal capping group was attached by treating the free amine N-terminus 2x 2 hours with a solution containing DIPEA (4 eq) and the respective acid chloride capping group (2 eq). The resin was then washed 3x each with DMF and DCM. The cyclization residues were then Alloc/Allyl deprotected by 4x 10 min treatments with a solution of tetrakis(triphenylphosphine)palladium catalyst (*cat.*) and phenylsilane (100 μ L) in DCM. The resin was then washed 10 times with DCM to remove all of the catalyst. The peptide was then cyclized by treatment with HATU (2 eq) and DIPEA (4 eq) in 1:1 DMF/DCM overnight. In the morning the sample was washed 3x each with DMF and DCM.

The peptide was then mildly cleaved from the resin by treatment with a 1% TFA in DCM solution 2x for 5 min each. The solution was then collected and immediately rotovapped to minimize sidechain deprotection. The C-terminus was capped with its corresponding amine by treatment with the amine capping group (1 eq), HATU (1 eq), and DIPEA (4 eq) for 8-12 hours. The reaction was then rotovapped to dryness, dissolved in DMSO, and was flash purified on the Biotage Sfar C18 12g column using mass-directed collection methods. Following purification, fractions were combined, rotovapped, and were then treated with the deprotection solution TFA/TIPS/H₂O (94:5:1) for 1-12 hours to remove sidechain protecting groups (duration depends on which protecting groups are to be removed). The solution was rotovapped off and the final peptide was purified by semi-preparative LCMS as described in Section 3.4.4.

TABLE 4.1: PASSIVE CELL PERMEABILITY GUIDELINES

	Lipinski	Veber	Nielsen
MW (g/mol)	< 500	---	500-1300
HBD	< 5	---	1-6
HBA	< 10	---	5-20
LogP	< 5	---	1-8
tPSA	---	< 10	< 300
RotB (Å)	---	< 140	5-20

Guidelines were developed by authors above with Lipinski⁴⁶ and Veber⁴⁷ referring specifically to passive permeability of small molecules and Nielsen⁵⁰ is describing passive permeability of cyclic peptides.

TABLE 4.2: PHYSIOCHEMICAL PROPERTIES OF PEPTIDES FOR CELL PERMEABILITY

ID	Sequence	Type	MW (g/mol)	HBD	HBA	cLogP	tPSA
1	GVLKTRHVNILLFMGYST	Linear	2205.66	28	26	N/A	885
36	LRKKRHVAELLMFG	Cyclic	1679.12	20	18	-2.34	651
42	KRHVAELLMFG	Cyclic	1281.59	15	14	-1.06	476
43	KRHVAELLMFG	Cyclic	1278.7	14	14	-1.50	467
44	KRHVAE	Cyclic	719.85	10	9	-3.94	330
52	N2-TRHVNI-C4	Linear	1032.26	11	12	0.98	363
53	N1-KRHVAE-C2	Cyclic	1014.24	10	11	1.94	328
54	N1-K-MeR-a-PAE-C2	Cyclic	960.19	7	10	3.13	286
55	N1-K-MeR-Octyl-E-C2	Cyclic	862.13	6	7	3.71	237

Description of physiochemical properties of key peptides and FLIPs as assessed by Lipinski's rule of 5 as well as the more relevant beyond the rule of 5 criteria.

TABLE 4.3: ITF DIRECT BINDING ASSAY DATA OF BRAF DIF FLIPS

ID	BRAF Residues	Sequence	Kd (μM)
45	508-518	N1-TRHVNILLFMG	0.050 \pm 0.006
46	508-518	N2-TRHVNILLFMG	0.084 \pm 0.024
47	508-518	N3-TRHVNILLFMG	----
48	508-518	N4-TRHVNILLFMG	----
49	505-513	LRKTRHVNI-C2	0.020 \pm 0.010
50	505-513	LRKTRHVNI-C3	0.380 \pm 0.096
51	505-513	LRKTRHVNI-C4	0.570 \pm 0.092
52	508-513	N2-TRHVNI-C4	0.280 \pm 0.088
53	508-513	N1-KRHVAE-C2	----
54	508-513	N1-K-MeR-a-PAE-C2	0.017 \pm 0.006

Direct binding coefficients of FLIPs which are going through iterative REPLACEMENT of exo-cyclic sequences to make the peptides more drug-like.

**TABLE 4.4: TEMPERATURE COEFFICIENTS OF
BACKBONE AMIDE PROTONS OF PEPTIDE 44**

Residue	ppm @ 295°	ppm @ 320° K	TC (ppb/K)
Lys*	7.595	7.466	-5.16
Arg	8.675	8.532	-5.72
His	8.502	8.368	-5.36
Val	7.903	7.758	-5.80
Ala	7.919	7.797	-4.88
Glu	7.994	7.856	-5.52

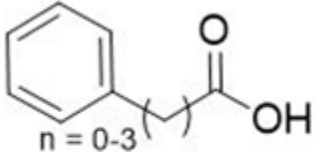
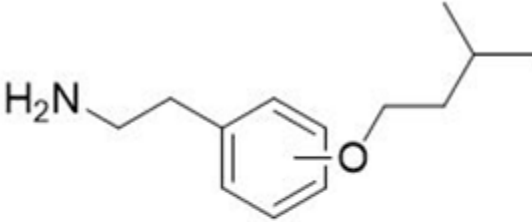
TC values greater than -4.5 ppb/K indicate non-participation in intramolecular hydrogen bonds (IMHBs) and TC values of 0 to -2.5 ppb/K indicate participation of amide protons in IMHBs. The symbol (*) indicates that the value is representative of the side-chain amide in the cyclization linker.

TABLE 4.5: PROTON ASSIGNMENTS OF PEPTIDE 44

Residue	Proton Assignments (ppm)						
	α NH	α CH	β H	γ H	δ H	ϵ H	ζ H
Lys	N/A	N/A	1.829	1.326	1.473	3.170	7.466
Arg	8.532	4.333	1.783	1.666	3.139	7.051	
His	8.368	4.562	3.317; 3.170				
Val	7.758	4.034	1.829	1.473; 1.326			
Ala	7.797	4.232	1.336				
Glu	7.856	4.237	1.880	2.296; 2.123			

The chemshifts were determined from the suite of 2D NMR experiments ran at 320° K in 30% TFE and water using the pre-sat pulse sequence on Bruker 400 MHz NMR equipped with a cryoprobe.

TABLE 4.6: N-TERMINAL AND C-TERMINAL CAPPING GROUPS

			
N-Term PLA	n	C-Term PLA	Position
N1	0	C2	para
N2	1	C3	ortho
N3	2	C4	meta
N4	3		

N-terminal capping groups were designed for pi-stacking interactions with BRAF-W450 and C-terminal groups were designed to bind a deep hydrophobic pocket adjacent to the R509 binding pocket.

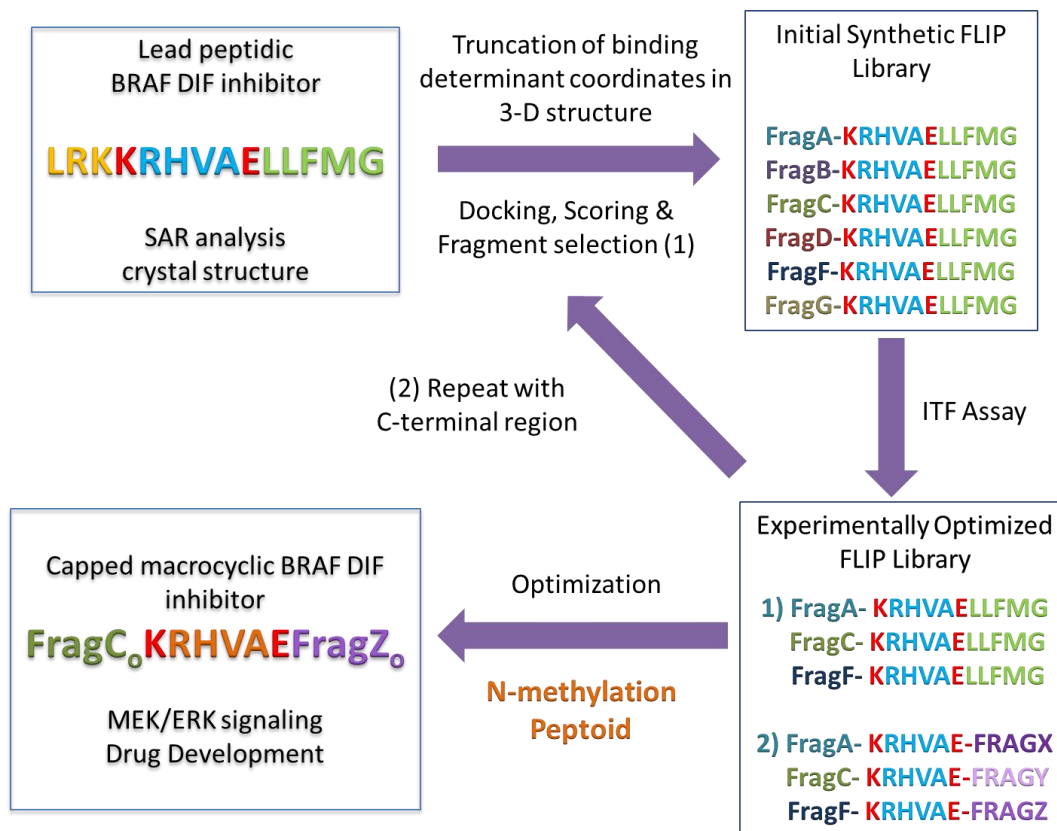


FIGURE 4.1: REPLACE STRATEGY SCHEME: Systematic conversion of segmented peptides into more drug-like compounds by iterative conversion using computationally designed partial ligand alternatives (PLAs) to make fragment ligated inhibitory peptides (FLIPs).

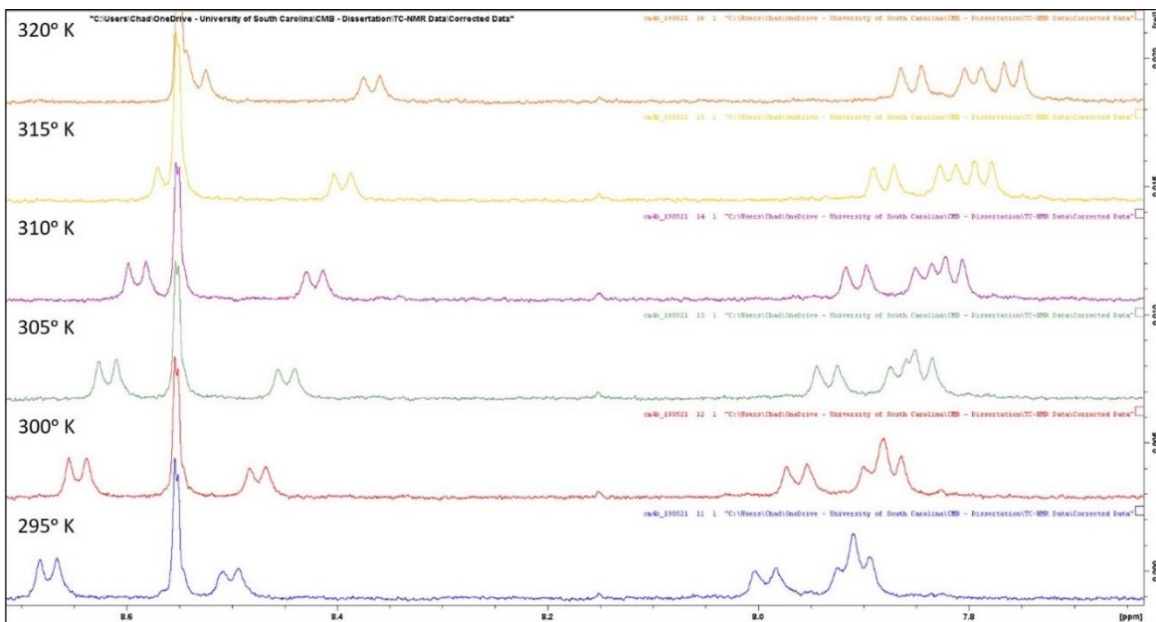


FIGURE 4.2: TC-NMR SPECTRA OF PEPTIDE 44: NMR spectra were taken from 295-320° K showing that all amide protons shifted at temperature-dependent rate faster than that associated with IMHBs.

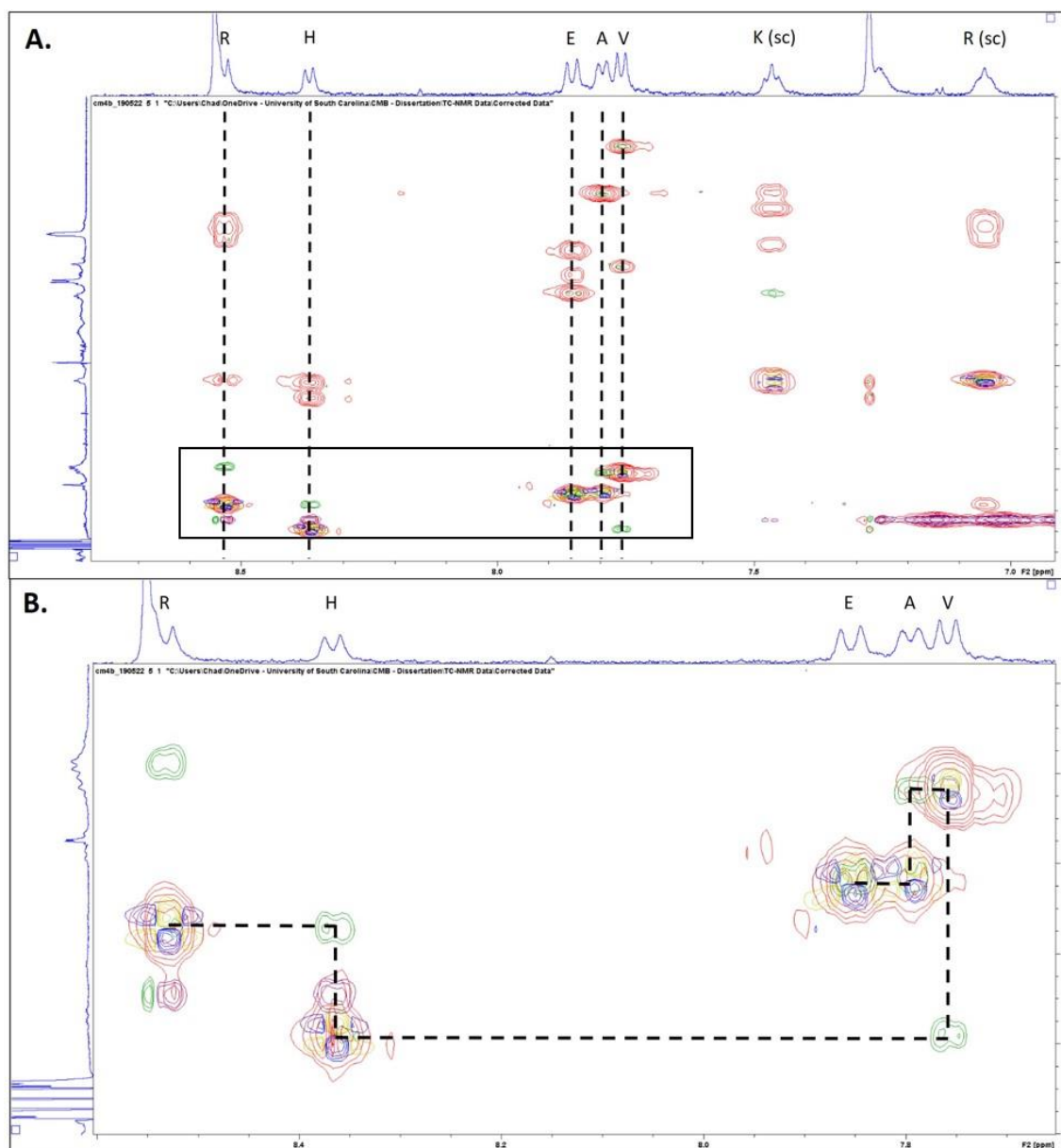


FIGURE 4.3: 2D NMR SPECTRA OF PEPTIDE 44: The above overlapping spectra consist of a DQF-COSY (blue and yellow), TOCSY (red), and ROESY (green and purple). A.) Shows the spin systems in the TOCSY for each 1D amide peak for residue identification. B.) Shows the step-wise correlation of adjacent residues using the DQF-COSY amide peaks and the ROESY spatial correlation peaks. There is not a DQF-COSY peak for the N-terminal amine on the Lys due to rapid deuterium exchange.

CHAPTER 5

OFF-TARGET EFFECTS, CONCLUSIONS, AND FUTURE DIRECTIONS

5.1 Introduction

A major concern in drug discovery is to ensure specificity of clinically relevant compounds for their intended target for the induction of the intended pharmacological response. Small molecules making up most approved drugs generally bind to deep pockets from catalytic sites occupied by substrates or co-factors required for enzymatic activity. For example, Type I kinase inhibitors bind to the ATP binding site to inhibit catalytic phosphorylation of the kinase substrate by blocking ATP. A drawback however is that ATP binding sites are similar in the sense that they natively bind the same compound. As a result, Type I kinase inhibitors have the potential to bind multiple kinases, causing off-target interactions and side effects, thus these types of drugs require extensive optimization to minimize these risks.

Off-target binding can be evaluated through *in silico* modeling through docking of lead compounds into the intended binding sites of similar proteins and calculating binding interactions. Experimentally there are a number of methods, including biochemical screening of compounds against kinase panels using recombinant purified proteins, to determine off-target binding. Cellular assays can be used to determine off target binding

as well using biotinylated ligands; for this experiment, cells would be incubated with tagged compounds, lysed, purified with streptavidin functionalized media, and off-target binders would be identified by western blot analysis.

The target of the developing cyclic peptidomimetics from this research is the BRAF dimer interface, which consists of the highly conserved (among RAF family members and KSR), short reverse- β -turn sequence of BRAF residues 502-521. Dimerization of BRAF is mediated by the key interaction of the arginine handshake motif where R509 of each monomer forms an anti-parallel conformation and a cation-induced dipole interaction with the partial negative charge of the C-terminal end of the α C helix of the adjacent monomer. Though this mechanism of activation is highly conserved between RAF isoforms, as well as KSR proteins, this is not necessarily a common motif of activation of all +500 kinases in the kinome.

Investigation of the BRAF DIF binding motif through sequence similarity searching has led to the identification of several proteins which may be potential off-target binders of the lead DIF inhibitors and these include RIPK3 (Receptor-interacting protein kinase 3), DAPK3 (Death-associated protein kinase 3), and SH2D3C (Sh2 domain-containing protein 3C). Of the three proteins, DAPK3 and SH2D3C contain about 60% sequence identity of the BRAF DIF 500-520 sequence. Upon further investigation of the crystal structures of these similar proteins, neither homologous sequence appears to be directly involved in protein dimerization. Furthermore, the similar region of SH2D3C (PDB 3T6G) appears to be part of two α -helices whereas the sequence associated with DAPK3 (PDB 1YRP)

appears to have a similar secondary structure to that of BRAF with the sequence being found largely in a random coil and bridging between an α -helix and a β -sheet. Though this parallel is interesting, the lack of involvement of this sequence in a dimerization interface with DAPK3 led to the conclusion that the RIPK3 protein was the most relevant since the sequence was encompassed in a dimer interface.

Receptor-interacting protein kinase 3 (RIPK3) is part of a larger family of kinases which regulate the necroptotic cell death pathway. Necroptosis is an inflammatory cell death pathway whereas apoptosis is a non-inflammatory one. In the necroptosis pathway, studies suggest that activated RIPK1 (receptor-interacting protein kinase 1) interacts with RIPK3 through the RHIM (RIP homo-typic interaction motif) to induce autophosphorylation of RIPK3.^{63,64} The activated RIPK3 then recruits and phosphorylates MLKL (mixed lineage kinase domain-like protein), which oligomerizes at the plasma membrane, leading to membrane leakage and cell death. Studies done by Raju et al. show similarities in RIPK3 and BRAF dimerization motifs in which dimerization is centered around an arginine-handshake motif.⁶³ This is not only interesting due to the similarity of the two dimerization motifs, but also since the proteins themselves play opposing roles in cell survival, where BRAF is the gatekeeper kinase for cell proliferation and differentiation, and RIPK3 initiates the necroptosis pathway and is responsible for regulation of programmed cell death. In the scope of the developing BRAF DIF inhibitors, they have the ability to bind the BRAF DIF and inhibit proliferation through the MAPK pathway, but the potential off-target inhibition of RIPK3 may cause opposing effects by inhibition of the necroptosis cell death pathway simultaneously.

5.2 Results

5.2.1 hRIPK3 Homology Model

To qualitatively study the crystal structure of human RIPK3 protein structure, a homology model of the protein was created since there is no previously published crystal structure for hRIPK3. The model was created by alignment of the human RIPK3 sequence to the murine RIPK3 sequence, which already has a crystal structure (PDB 4M66) and is assumed to have a similar secondary and tertiary structure. The protein structure of hRIPK3 was then modeled using the mRIPK3 crystal structure as a template to create the homology model.

5.2.2 Comparison of BRAF/hRIPK3 Dimer Interfaces and DIF Peptides

Comparing the two proteins, each appears to form a dimer in a similar manner with a consecutive sequence forming a reverse-turn between an α -helix and β -sheet at the interface of the two monomers. For BRAF, the dimer interface is composed of residues V504-G518 (VLRKTRHVNILLFMG; **Figure 5.3A**) whereas for hRIPK3, it is made up of residues V48-G64 (VKAMASLDNEFVLRLEG; **Figure 5.3B**). Though the sequence alignment for the dimer interface of the two proteins has a low similarity, it cannot be ignored that the two proteins appear to dimerize in a similar fashion with a continuous reverse-turn encompassing the majority of the dimer interface as well as utilization of an Arg residue in the DIF (**Figure 5.3C**). As a method of confirming similar binding of DIF peptides to the two proteins, a linear peptide of the hRIPK3 DIF (**56**; MASLDNEFVLRLEG) was synthesized and was tested for BRAF direct binding potency in the previously

mentioned intrinsic tryptophan fluorescence assay (Chapter 2). Interestingly, **56** exhibited $K_d = 1.11 \mu\text{M}$ which was a 3-fold increase in potency compared to **1** ($K_d = 3.84 \mu\text{M}$). Granted, it was shown in the linear peptide optimization that minimal changes to the sequence can tremendously influence the binding potency in the linear context, but it cannot be ignored that the linear hRIPK3 DIF peptide did have a legitimate binding interaction to the BRAF protein.

5.2.3 Computational Investigation of Homodimers of BRAF/hRIPK3/mRIPK3

Utilizing the BRAF (PDB 4E26), mRIPK3 (PDB 4M66), and hRIPK3 (Homology Model) homodimer crystal structures, the binding determinants of homodimers were evaluated using Discovery Studio 3.0. The overall interaction energy for the homodimers were -222.2, -208.6, and -160.8 kcal/mol for BRAF, mRIPK3, and hRIPK3, respectively. This data suggests that BRAF and mRIPK3 form more energetically stable homodimers than hRIPK3, but this doesn't necessarily suggest similarity in DIF binding. To compare the DIF sequences specifically, the interaction energy calculation report was focused at the contributions of DIF residues for homodimer formation. Based on the results from this study (**Figure 5.1**), mRIPK3 was shown to rely heavily on DIF residues R69 and E71 (-26.2 and -32.0 kcal/mol respectively) for homodimer formation, of which R69 of mRIPK3 is similar in function and location as R509 in BRAF. As for hRIPK3, homodimer formation appears to rely heavily on E58 (-45.7 kcal/mol) in a similar manner to mRIPK3 binding to a Lys residue outside of the DIF residues in question, and to a lesser extent R62 (-16.3)

which varies dramatically in DIF location from both BRAF and mRIPK3 and appears to bind D56 rather than the induced dipole of the α C-Helix.

5.2.4 Computational Investigation of BRAF/hRIPK3 Heterodimer Interactions

In a similar manner as with the homodimer study, the interactions in a possible BRAF (PDB 4E26) and hRIPK3 (Homology Model) heterodimer were studied by creating a model in which the two monomers were combined, minimized, and the interaction energy of each monomer for the other was calculated (**Figure 5.2**). According to the computational modeling, dimer contributions of the BRAF DIF for hRIPK3 (-92.6 kcal/mol) were strictly dependent on R509 (BRAF) with interaction energy of -55.9 kcal/mol (**Figure 5.2; Figure 5.4**). In the inverse manner, the heterodimer contributions of hRIPK3 DIF for BRAF (-115.6 kcal/mol) were largely reflective of D56 (hRIPK3; -34.2 kcal/mol) and to a lesser extent through A53, L55, E58, and E64 (hRIPK3), with interaction energy calculations of -16.1, -14.3, -19.0, and -18.4 kcal/mol, respectively. Interestingly, the R509 (BRAF) counterpart R62 (hRIPK3) seems to indicate the disfavorable interaction energy of +16.2 kcal/mol.

5.3 Discussion

Based on the BRAF DIF sequence similarity search, DAPK3, SH2D3C, and RIPK3 have sequence identity, but from a qualitative analysis of the similar portions of these crystal structures, DAPK3 and SH2D3C were deemed to have dissimilar secondary and tertiary structure and thus were not considered to be relevant. RIPK3 however from comparison of its crystal structure to BRAF, dimerizes similarly and thus was further

investigated. Due to the human RIPK3 protein not having an available crystal structure, a homology model based on the murine RIPK3 template structure was developed. According to the generated homology model, the hRIPK3 dimer interface has similar secondary structure with a reverse-turn connecting an α -Helix and β -sheet. Upon analyzing the binding interface, it can be observed that the arginine in the hRIPK3 dimer interface is on the opposite side of the reverse-turn in comparison to BRAF and was more likely to bind to an aspartate residue rather than the induced dipole of the α -Helix. Furthermore, homodimer interaction energy calculations of the hRIPK3 homology model suggested that the major contributor to dimer stability was E58 which had a strong electrostatic interaction with a lysine which was not contained in the dimer interface. Additionally, in the BRAF/hRIPK3 heterodimer studies, it appears that in this context, dimer stability is largely reliant on the interaction of R509 (BRAF) with D56 and the C-terminus of the α -helix adjacent to the hRIPK3 DIF (**Figure 5.2; Figure 5.4**). When studying this in the inverse context, it was observed that there are several other hRIPK3 DIF residues which contribute to dimer formation, but to a lesser degree.

Though the homodimer computational studies were informative for dimer interface contributions for hRIPK3, this is only a model and more definitive answers require an experimental crystal structure. Interestingly, the hRIPK3 peptide **56**, when tested for direct binding to BRAF in the ITF assay, **56** had tighter binding than the original peptide **1** which was the linear sequence of the BRAF DIF. Further studies to investigate the reverse, i.e. binding of BRAF DIF peptides to hRIPK3 needs to be done to more completely identify off-target interactions.

5.4 Conclusion

Overall, this study was productive in the sense that the homology model of hRIPK3 was generated and the alignment described by Raju et al was replicated.⁶³ Furthermore, it was found that the hRIPK3 DIF peptide **56** showed binding interactions with BRAF and indicating that there are potential off-target proteins other than RAF family members and KSR proteins which may be influenced by the BRAF DIF peptides. Further experiments still need to be done, such as a kinase panel testing for off-target effects of the lead compounds described previously in the cyclic BRAF DIF peptide library. Other possible experiments could include the use of biotin conjugated DIF peptides for identification of off-target interactions in the cellular context.

5.5 Future Directions

Other than the previously mentioned experiments for off-target interactions of DIF peptides, there are several other areas which need to be addressed for advancement of this project. Firstly, although the peptides have been optimized for binding to the truncated BRAF protein and biochemically tested using the ITF and ITC assay, peptidic and FLIP versions of the cyclic peptide need to be tested in cells to confirm that there is still pharmacological responses under paradoxical activation conditions. Also since it has not been shown that peptides or FLIPs are able to passively enter the cells through diffusion through the PAMPA assay, cellular experiments using electroporation as described in Section 2.2.1 could be repeated with cyclic, lead peptides and FLIPS. Another possibility would be incorporation of the cell penetrating peptide sequence such as TAT to induce

cell penetration without potentially damaging the cell in electroporation. In the peptide context, TAT could be attached through the N-Terminus, additionally, in the FLIP context TAT can be attached through a tri-functionalized cyclization linkage. In the past, the McInnes lab has had some success utilizing cyclization methods through the Ugi 4-component reaction (**57**; $K_d = 0.55 \pm 0.04 \mu\text{M}$; **Figure 5.4**) and through use of a 1,3-dibromobenzene linkage (**58**; K_d not tested; **Figure 5.4**) which could be utilized for incorporation of the TAT sequence in the cyclization linker which does not come into contact with the BRAF DIF binding surface according to molecular modeling data.

The largest area of focus for the progression of this project is the enhancement of cell permeability of the lead peptide and ability of lead compounds to reach the target protein, as well as oral bioavailability. In this sense, the largest contributing factor to this in the peptide or FLIP context would be N-methylation of the backbone amides without interfering with the binding affinity of the compound itself. Another method aside from merely N-methylating the backbone would be the development of peptoids. These are peptide like compounds based on N-substituted glycine which are functionalized through the amide nitrogen rather than the αC of the amino acid. This intrinsically reduces the number of HBDs by removing amide hydrogens. Furthermore, optimization of the macrocycle could be accomplished through further application of the REPLACE strategy to replace it with fragment like molecules which promote increased potency, enhanced cell permeability, and proteolytic stability of the overall compound.

5.6 Experimental

5.6.1 Qualitative Assessment of BLAST Search Hits

Upon BLAST searching for the BRAF DIF sequence to discover potential off-target interactions, hits with greater than 50% identity were examined. Crystal structures were downloaded from the protein data bank and matched sequences were identified. The secondary structure of the hit sequence was then qualitatively scored based on whether the sequence had a reverse- β -turn structure like that of BRAF (PDB 4E26).

5.6.2 Homology Model Development of Human RIPK3

The homology model of hRIPK3 was created in Discovery Studios 3.0. The sequence of hRIPK3 was downloaded from a UniProt search and was aligned with the mRIPK3 sequence (PDB 4M66) in the Discovery Studios program. The dimer sequences were then separated into separate files and monomers of hRIPK3 sequence were separately aligned over the 3D structure of the mRIPK3 crystal structure. Upon alignment, the monomers were then combined back into a single file to create the homology model and were then compared to the BRAF dimer in one window.

5.6.3 Homodimer Interaction Energy Calculations

Each homodimer, whether from a crystal structure or homology model was minimized in the Discovery Studios 3.0 software using the CharmM forcefield, for general protein modeling work, with a max number of steps of 2000 and GBSW solvent algorithm. Once minimized, the interaction energy was calculated as follows: atoms on protomer A

which are 12 Å from protomer B were selected as the binding site, protomer B was selected as the ligand, and the ID-DD dielectric model was used. The resulting report contained contributions of protomer B residues for binding to the dimer interface of protomer A with electrostatic and Van der Waals interaction energy stratification.

5.6.4 Heterodimer Interaction Energy Calculations

Each monomer was combined into the window using Discovery Studio 3.0 and was minimized as previously described in section 5.6.3. The interaction energy was then calculated for one entire protein in relation to the other entire protein. The calculation was then reversed to get contributions of the other for heterodimer formation. Conclusions were then assessed by narrowing the field of view to the contributions of each protein's dimer interface and were then analyzed in conjunction with the homology model of the heterodimer.

5.6.5 Synthesis of hRIPK3 Peptide

See section 3.4.1 Standard Fmoc Chemistry Solid Phase Peptide Synthesis Protocol for details.

BRAF		mRIPK3		hRIPK3	
Residue	IE (kcal/mol)	Residue	IE (kcal/mol)	Residue	IE (kcal/mol)
L505	-1.9	M65	-0.2	M52	-0.7
R506	-2.0	V66	-16.4	A53	-1.0
K507	-24.3	N67	-2.4	S54	-0.8
T508	-19.4	L68	0.4	L55	1.1
R509	-42.6	R69	-26.2	D56	-8.1
H510	-3.3	N70	-3.9	N57	-14.3
V511	-5.1	E71	-32.0	E58	-45.7
N512	0.3	N72	-1.2	F59	-1.2
I513	-1.1	V73	0.4	V60	-2.2
L514	-0.9	L74	-1.8	L61	-0.2
L515	-4.7	L75	-2.7	R62	-16.3
F516	-12.2	L76	-12.7	L63	0.7
M517	-9.3	L77	-5.8	E64	3.7
G518	-0.1	G78	-1.0	G65	-0.4

FIGURE 5.1: HOMODIMER DIF INTERACTION ENERGY CALCULATIONS

Homodimers were either taken from the protein data bank or are a homology model for hRIPK3 based on the mRIPK3 crystal structure. The homodimers were minimized using Discovery Studios 3.0 and the interaction energy was calculated for the second monomer in each complex. Energies are heat mapped with the most favorable interactions presented in green and least favorable in red.

hRIPK3		BRAF	
Residue	IE (kcal/mol)	Residue	IE (kcal/mol)
M52	-1.0	L505	0.3
A53	-16.1	R506	0.1
S54	-3.9	K507	1.4
L55	-14.3	T508	0.7
D56	-34.2	R509	-55.9
N57	-5.5	H510	-5.1
E58	-19.0	V511	-3.9
F59	-1.2	N512	-0.8
V60	-1.0	I513	-0.8
L61	0.3	L514	1.0
R62	16.2	L515	-5.6
L63	-3.7	F516	3.5
E64	-18.4	M517	-2.6
G65	-0.2	G518	-0.2

FIGURE 5.2: BRAF/hRIPK3 HETERODIMER INTERACTION ENERGY CALCULATIONS: The heterodimer for this experiment was a combination of one BRAF protomer from PDB 4E26 and one hRIPK3 protomer from the homology model previously described. Interaction energy values represent the specific residue's calculated value for the opposing protomer as a whole and is not confined to the opposing protomer's dimer interface.

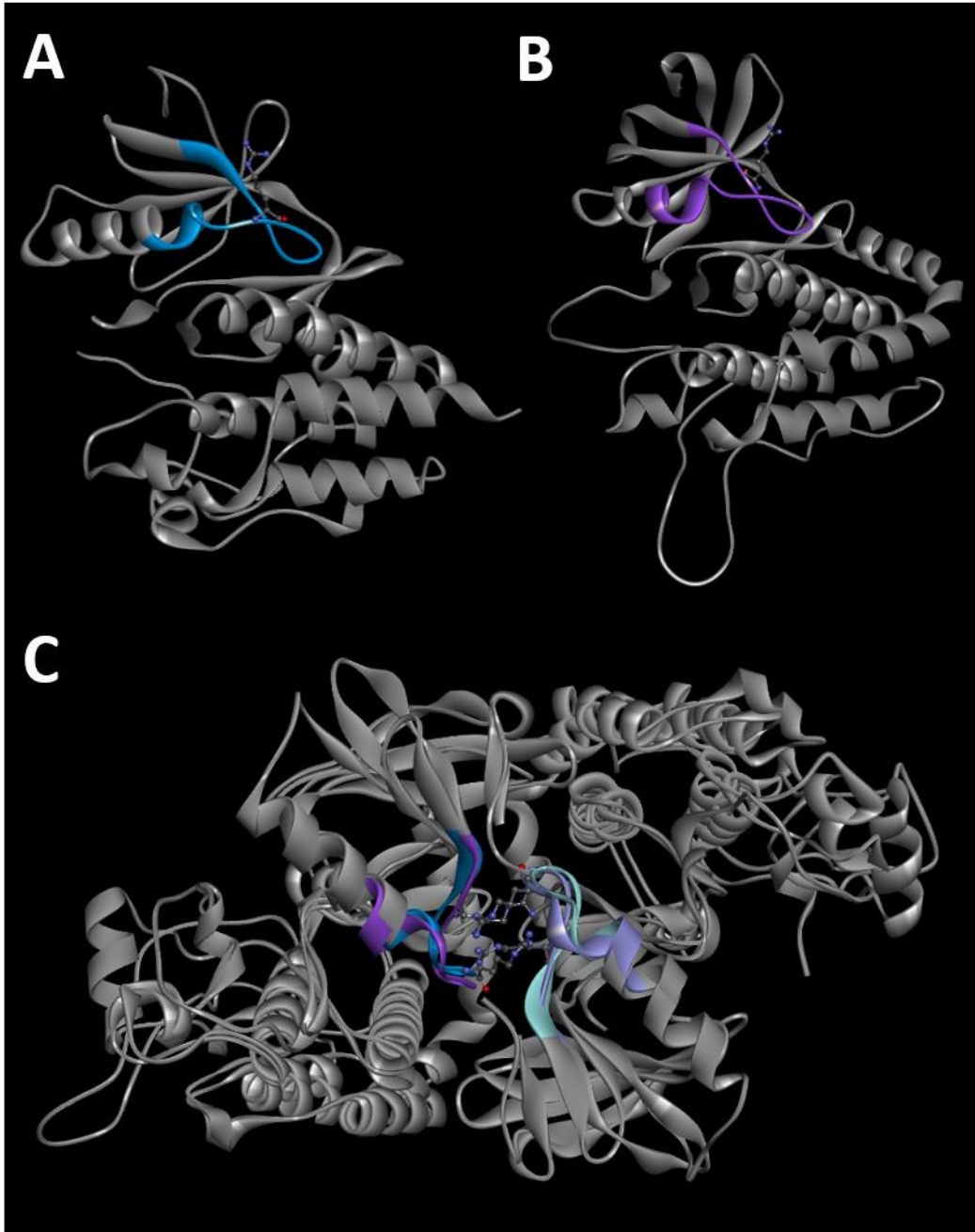


FIGURE 5.3: HUMAN RIPK3 HOMOLGY MODEL AND BRAF CRYSTAL STRUCTURE: A.) Crystal structure (PDB 4E26) of BRAF monomer with dimer interface (DIF) in blue. B.) Homology model of hRIPK3 based on mRIPK3 crystal structure (PDB 4M66) with DIF in purple. C.) Overlay of BRAF and hRIPK3 dimers with DIFs in respective colors and key binding Arg sidechain visible.

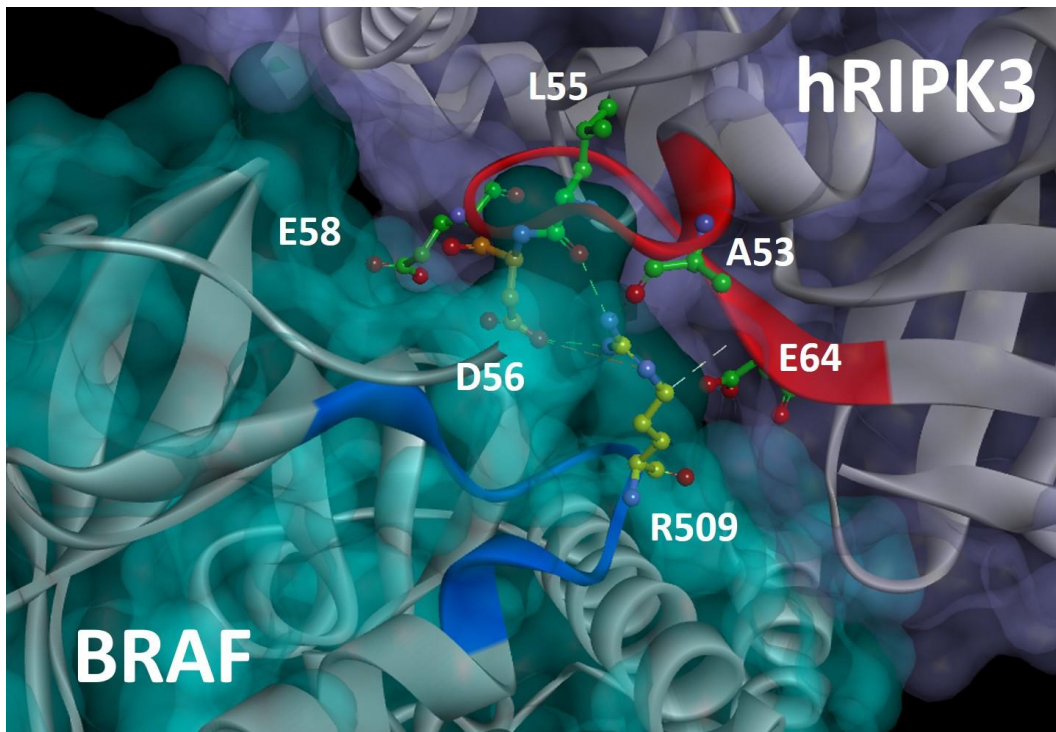


FIGURE 5.4: HETERODIMER OF BRAF AND hRIPK3: Computational modeling of the dimer interface of the BRAF/hRIPK3 heterodimer with the BRAF DIF in blue and the hRIPK3 DIF in red. The major contributing interaction from BRAF include R509 in yellow. The major contributing interaction from hRIPK3 is D56 (orange) and the minor factors A53, L55, E58, and D64 are represented in green.

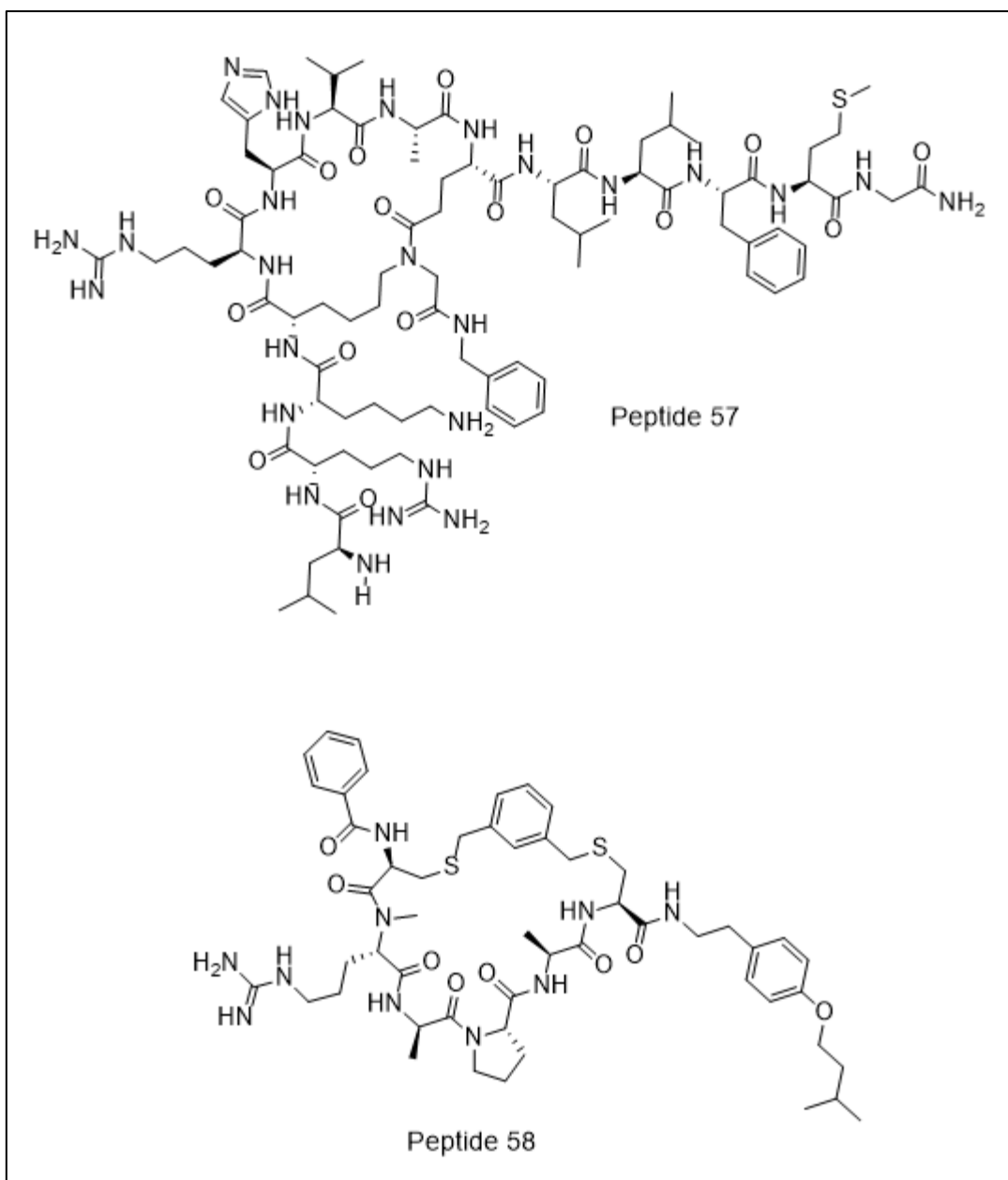


FIGURE 5.5: EXAMPLES OF CYCLIC PEPTIDES WITH POTENTIAL ALTERNATIVE CYCLIZATION METHODS

REFERENCES

- (1) Moore, A. R.; Rosenberg, S. C.; McCormick, F.; Malek, S. RAS-Targeted Therapies: Is the Undruggable Drugged? *Nat. Rev. Drug Discov.* **2020**, *19* (8), 533–552. <https://doi.org/10.1038/s41573-020-0068-6>.
- (2) Canon, J.; Rex, K.; Saiki, A. Y.; Mohr, C.; Cooke, K.; Bagal, D.; Gaida, K.; Holt, T.; Knutson, C. G.; Koppada, N.; Lanman, B. A.; Werner, J.; Rapaport, A. S.; San Miguel, T.; Ortiz, R.; Osgood, T.; Sun, J.-R.; Zhu, X.; McCarter, J. D.; Volak, L. P.; Houk, B. E.; Fakih, M. G.; O’Neil, B. H.; Price, T. J.; Falchook, G. S.; Desai, J.; Kuo, J.; Govindan, R.; Hong, D. S.; Ouyang, W.; Henary, H.; Arvedson, T.; Cee, V. J.; Lipford, J. R. The Clinical KRAS(G12C) Inhibitor AMG 510 Drives Anti-Tumour Immunity. *Nature* **2019**, *575* (7781), 217–223. <https://doi.org/10.1038/s41586-019-1694-1>.
- (3) How Chemotherapy Drugs Work. American Cancer Society 2019.
- (4) Evolution of Cancer Treatments: Chemotherapy. American Cancer Society 2014.
- (5) How Targeted Therapies Are Used to Treat Cancer. American Cancer Society 2019.
- (6) Shu, M.; Yan, H.; Xu, C.; Wu, Y.; Chi, Z.; Nian, W.; He, Z.; Xiao, J.; Wei, H.; Zhou, Q.; Zhou, J. X. A Novel Anti-HER2 Antibody GB235 Reverses Trastuzumab Resistance in HER2-Expressing Tumor Cells in Vitro and in Vivo. *Sci. Rep.* **2020**, *10* (1), 2986. <https://doi.org/10.1038/s41598-020-59818-2>.
- (7) Kannaiyan, R.; Mahadevan, D. A Comprehensive Review of Protein Kinase Inhibitors for Cancer Therapy. *Expert Rev. Anticancer Ther.* **2018**, *18* (12), 1249–1270. <https://doi.org/10.1080/14737140.2018.1527688>.
- (8) Rauch, J.; Volinsky, N.; Romano, D.; Kolch, W. The Secret Life of Kinases: Functions beyond Catalysis. *Cell Commun. Signal.* **2011**, *9* (1), 23. <https://doi.org/10.1186/1478-811X-9-23>.
- (9) Cohen, P. Protein Kinases — the Major Drug Targets of the Twenty-First Century? *Nat. Rev. Drug Discov.* **2002**, *1* (4), 309–315. <https://doi.org/10.1038/nrd773>.

- (10) Feng, Y.; LoGrasso, P. V.; Defert, O.; Li, R. Rho Kinase (ROCK) Inhibitors and Their Therapeutic Potential. *J. Med. Chem.* **2016**, *59* (6), 2269–2300.
<https://doi.org/10.1021/acs.jmedchem.5b00683>.
- (11) Jeong, W.; Doroshow, J. H.; Kummar, S. United States Food and Drug Administration Approved Oral Kinase Inhibitors for the Treatment of Malignancies. *Curr. Probl. Cancer* **2013**, *37* (3), 110–144.
<https://doi.org/10.1016/j.currproblcancer.2013.06.001>.
- (12) Druker, B. J.; Guilhot, F.; O'Brien, S. G.; Gathmann, I.; Kantarjian, H.; Gattermann, N.; Deininger, M. W. N.; Silver, R. T.; Goldman, J. M.; Stone, R. M.; Cervantes, F.; Hochhaus, A.; Powell, B. L.; Gabilove, J. L.; Rousselot, P.; Reiffers, J.; Cornelissen, J. J.; Hughes, T.; Agis, H.; Fischer, T.; Verhoef, G.; Shepherd, J.; Saglio, G.; Gratwohl, A.; Nielsen, J. L.; Radich, J. P.; Simonsson, B.; Taylor, K.; Baccarani, M.; So, C.; Letvak, L.; Larson, R. A. Five-Year Follow-up of Patients Receiving Imatinib for Chronic Myeloid Leukemia. *N. Engl. J. Med.* **2006**, *355* (23), 2408–2417.
<https://doi.org/10.1056/NEJMoa062867>.
- (13) Roskoski, R. Properties of FDA-Approved Small Molecule Protein Kinase Inhibitors. *Pharmacol. Res.* **2019**, *144*, 19–50.
<https://doi.org/10.1016/j.phrs.2019.03.006>.
- (14) Roskoski, R. Classification of Small Molecule Protein Kinase Inhibitors Based upon the Structures of Their Drug-Enzyme Complexes. *Pharmacol. Res.* **2016**, *103*, 26–48.
<https://doi.org/10.1016/j.phrs.2015.10.021>.
- (15) McCain, J. The MAPK (ERK) Pathway: Investigational Combinations for the Treatment Of BRAF-Mutated Metastatic Melanoma. *P T Peer-Rev. J. Formul. Manag.* **2013**, *38* (2), 96–108.
- (16) Guo, Y.; Pan, W.; Liu, S.; Shen, Z.; Xu, Y.; Hu, L. ERK/MAPK Signalling Pathway and Tumorigenesis (Review). *Exp. Ther. Med.* **2020**, *19* (3), 1997–2007.
<https://doi.org/10.3892/etm.2020.8454>.
- (17) ZHANG, W.; LIU, H. T. MAPK Signal Pathways in the Regulation of Cell Proliferation in Mammalian Cells. *Cell Res.* **2002**, *12* (1), 9–18.
<https://doi.org/10.1038/sj.cr.7290105>.
- (18) Brummer, T.; McInnes, C. RAF Kinase Dimerization: Implications for Drug Discovery and Clinical Outcomes. *Oncogene* **2020**, *39* (21), 4155–4169.
<https://doi.org/10.1038/s41388-020-1263-y>.

- (19) Du, Z.; Lovly, C. M. Mechanisms of Receptor Tyrosine Kinase Activation in Cancer. *Mol. Cancer* **2018**, *17* (1), 58. <https://doi.org/10.1186/s12943-018-0782-4>.
- (20) Butti, R.; Das, S.; Gunasekaran, V. P.; Yadav, A. S.; Kumar, D.; Kundu, G. C. Receptor Tyrosine Kinases (RTKs) in Breast Cancer: Signaling, Therapeutic Implications and Challenges. *Mol. Cancer* **2018**, *17* (1), 34–34. <https://doi.org/10.1186/s12943-018-0797-x>.
- (21) Hervieu, A.; Kermorgant, S. The Role of PI3K in Met Driven Cancer: A Recap. *Front. Mol. Biosci.* **2018**, *5*, 86–86. <https://doi.org/10.3389/fmolb.2018.00086>.
- (22) Prior, I. A.; Hood, F. E.; Hartley, J. L. The Frequency of Ras Mutations in Cancer. *Cancer Res.* **2020**, *80* (14), 2969. <https://doi.org/10.1158/0008-5472.CAN-19-3682>.
- (23) Smith, M. J.; Neel, B. G.; Ikura, M. NMR-Based Functional Profiling of RASopathies and Oncogenic RAS Mutations. *Proc. Natl. Acad. Sci.* **2013**, *110* (12), 4574. <https://doi.org/10.1073/pnas.1218173110>.
- (24) Deng, S.; Clowers, M. J.; Velasco, W. V.; Ramos-Castaneda, M.; Moghaddam, S. J. Understanding the Complexity of the Tumor Microenvironment in K-Ras Mutant Lung Cancer: Finding an Alternative Path to Prevention and Treatment. *Front. Oncol.* **2020**, *9*, 1556. <https://doi.org/10.3389/fonc.2019.01556>.
- (25) Leier, A.; Bedwell, D. M.; Chen, A. T.; Dickson, G.; Keeling, K. M.; Kesterson, R. A.; Korf, B. R.; Marquez Lago, T. T.; Müller, U. F.; Popplewell, L.; Zhou, J.; Wallis, D. Mutation-Directed Therapeutics for Neurofibromatosis Type I. *Mol. Ther. - Nucleic Acids* **2020**, *20*, 739–753. <https://doi.org/10.1016/j.omtn.2020.04.012>.
- (26) Röring, M.; Herr, R.; Fiala, G. J.; Heilmann, K.; Braun, S.; Eisenhardt, A. E.; Halbach, S.; Capper, D.; von Deimling, A.; Schamel, W. W.; Saunders, D. N.; Brummer, T. Distinct Requirement for an Intact Dimer Interface in Wild-Type, V600E and Kinase-Dead B-Raf Signalling. *EMBO J.* **2012**, *31* (11), 2629–2647. <https://doi.org/10.1038/emboj.2012.100>.
- (27) Rossi, A.; Roberto, M.; Panebianco, M.; Botticelli, A.; Mazzuca, F.; Marchetti, P. Drug Resistance of BRAF-Mutant Melanoma: Review of up-to-Date Mechanisms of Action and Promising Targeted Agents. *Eur. J. Pharmacol.* **2019**, *862*, 172621. <https://doi.org/10.1016/j.ejphar.2019.172621>.
- (28) Li, P.; He, H.; Wang, Z.; Feng, M.; Jin, H.; Wu, Y.; Zhang, L.; Zhang, L.; Tang, X. Sensitive Detection of Single-Nucleotide Mutation in the BRAF Mutation Site (V600E) of

Human Melanoma Using Phosphate–Pyrene-Labeled DNA Probes. *Anal. Chem.* **2016**, *88* (1), 883–889. <https://doi.org/10.1021/acs.analchem.5b03523>.

(29) Beneker, C. M.; Rovoli, M.; Kontopidis, G.; Röring, M.; Galda, S.; Braun, S.; Brummer, T.; McInnes, C. Design and Synthesis of Type-IV Inhibitors of BRAF Kinase That Block Dimerization and Overcome Paradoxical MEK/ERK Activation. *J. Med. Chem.* **2019**. <https://doi.org/10.1021/acs.jmedchem.8b01288>.

(30) Amaral, T.; Sinnberg, T.; Meier, F.; Krepler, C.; Levesque, M.; Niessner, H.; Garbe, C. MAPK Pathway in Melanoma Part II—Secondary and Adaptive Resistance Mechanisms to BRAF Inhibition. *Eur. J. Cancer* **2017**, *73*, 93–101. <https://doi.org/10.1016/j.ejca.2016.12.012>.

(31) Wagle, N.; Emery, C.; Berger, M. F.; Davis, M. J.; Sawyer, A.; Pochanard, P.; Kehoe, S. M.; Johannessen, C. M.; MacConaill, L. E.; Hahn, W. C.; Meyerson, M.; Garraway, L. A. Dissecting Therapeutic Resistance to RAF Inhibition in Melanoma by Tumor Genomic Profiling. *J. Clin. Oncol.* **2011**, *29* (22), 3085–3096. <https://doi.org/10.1200/JCO.2010.33.2312>.

(32) Hatzivassiliou, G.; Song, K.; Yen, I.; Brandhuber, B. J.; Anderson, D. J.; Alvarado, R.; Ludlam, M. J. C.; Stokoe, D.; Gloor, S. L.; Vigers, G.; Morales, T.; Aliagas, I.; Liu, B.; Sideris, S.; Hoeflich, K. P.; Jaiswal, B. S.; Seshagiri, S.; Koeppen, H.; Belvin, M.; Friedman, L. S.; Malek, S. RAF Inhibitors Prime Wild-Type RAF to Activate the MAPK Pathway and Enhance Growth. *Nature* **2010**, *464* (7287), 431–435. <https://doi.org/10.1038/nature08833>.

(33) Shaw, A. S.; Kornev, A. P.; Hu, J.; Ahuja, L. G.; Taylor, S. S. Kinases and Pseudokinases: Lessons from RAF. *Mol. Cell. Biol.* **2014**, *34* (9), 1538. <https://doi.org/10.1128/MCB.00057-14>.

(34) Zhang, C.; Spevak, W.; Zhang, Y.; Burton, E. A.; Ma, Y.; Habets, G.; Zhang, J.; Lin, J.; Ewing, T.; Matusow, B.; Tsang, G.; Marimuthu, A.; Cho, H.; Wu, G.; Wang, W.; Fong, D.; Nguyen, H.; Shi, S.; Womack, P.; Nespi, M.; Shellooe, R.; Carias, H.; Powell, B.; Light, E.; Sanftner, L.; Walters, J.; Tsai, J.; West, B. L.; Visor, G.; Rezaei, H.; Lin, P. S.; Nolop, K.; Ibrahim, P. N.; Hirth, P.; Bollag, G. RAF Inhibitors That Evade Paradoxical MAPK Pathway Activation. *Nature* **2015**, *526* (7574), 583–586. <https://doi.org/10.1038/nature14982>.

(35) Richmond, C. S.; Vallatharasu, Y.; Deviley, J. A.; Vos, C. R.; Parsons, B. M.; Kenny, P. A. Sequential Treatment Failures in Response to BRAF/MEK and Immune Checkpoint Inhibitors Mediated by MAP2K2 and B2M Mutations in Melanoma. *Exp. Mol. Pathol.* **2019**, *110*, 104260. <https://doi.org/10.1016/j.yexmp.2019.104260>.

- (36) Weber, C. K.; Slupsky, J. R.; Kalmes, H. A.; Rapp, U. R. Active Ras Induces Heterodimerization of CRaf and BRaf. *Cancer Res.* **2001**, *61* (9), 3595.
- (37) Douziech, M. A KSR/CNK Complex Mediated by HYP, a Novel SAM Domain-Containing Protein, Regulates RAS-Dependent RAF Activation in Drosophila. *Genes Dev.* **2006**, *20* (7), 807–819. <https://doi.org/10.1101/gad.1390406>.
- (38) Rajakulendran, T.; Sahmi, M.; Lefrançois, M.; Sicheri, F.; Therrien, M. A Dimerization-Dependent Mechanism Drives RAF Catalytic Activation. *Nature* **2009**, *461* (7263), 542–545. <https://doi.org/10.1038/nature08314>.
- (39) Freeman, A. K.; Ritt, D. A.; Morrison, D. K. Effects of Raf Dimerization and Its Inhibition on Normal and Disease-Associated Raf Signaling. *Mol. Cell* **2013**, *49* (4), 751–758. <https://doi.org/10.1016/j.molcel.2012.12.018>.
- (40) Gunderwala, A. Y.; Nimbvikar, A. A.; Cope, N. J.; Li, Z.; Wang, Z. Development of Allosteric BRAF Peptide Inhibitors Targeting the Dimer Interface of BRAF. *ACS Chem. Biol.* **2019**, *14* (7), 1471–1480. <https://doi.org/10.1021/acscchembio.9b00191>.
- (41) Ghisaidoobe, A. B. T.; Chung, S. J. Intrinsic Tryptophan Fluorescence in the Detection and Analysis of Proteins: A Focus on Förster Resonance Energy Transfer Techniques. *Int. J. Mol. Sci.* **2014**, *15* (12), 22518–22538. <https://doi.org/10.3390/ijms151222518>.
- (42) Herr, R.; Wöhrle, F. U.; Danke, C.; Berens, C.; Brummer, T. A Novel MCF-10A Line Allowing Conditional Oncogene Expression in 3D Culture. *Cell Commun. Signal.* **2011**, *9* (1), 17. <https://doi.org/10.1186/1478-811X-9-17>.
- (43) Weber, A.; Kirejczyk, Z.; Besch, R.; Potthoff, S.; Leverkus, M.; Häcker, G. Proapoptotic Signalling through Toll-like Receptor-3 Involves TRIF-Dependent Activation of Caspase-8 and Is under the Control of Inhibitor of Apoptosis Proteins in Melanoma Cells. *Cell Death Differ.* **2010**, *17* (6), 942–951. <https://doi.org/10.1038/cdd.2009.190>.
- (44) Lakowicz, J. R. *Principles of Fluorescence Spectroscopy*, Third edition, corrected at 4. printing.; Springer: New York, NY, 2010.
- (45) Monitoring of Peptide Coupling and Capping. aapptec.
- (46) Lipinski, C. A.; Lombardo, F.; Dominy, B. W.; Feeney, P. J. Experimental and Computational Approaches to Estimate Solubility and Permeability in Drug Discovery and Development Settings1PII of Original Article: S0169-409X(96)00423-1. The Article Was Originally Published in *Advanced Drug Delivery Reviews* 23 (1997) 3–25.1. *Spec.*

Issue Dedic. Dr Eric Tomlinson Adv. Drug Deliv. Rev. Sel. Most Highly Cited Artic. 1991-1998 **2001**, *46* (1), 3–26. [https://doi.org/10.1016/S0169-409X\(00\)00129-0](https://doi.org/10.1016/S0169-409X(00)00129-0).

(47) Veber, D. F.; Johnson, S. R.; Cheng, H.-Y.; Smith, B. R.; Ward, K. W.; Kopple, K. D. Molecular Properties That Influence the Oral Bioavailability of Drug Candidates. *J. Med. Chem.* **2002**, *45* (12), 2615–2623. <https://doi.org/10.1021/jm020017n>.

(48) Over, B.; Matsson, P.; Tyrchan, C.; Artursson, P.; Doak, B. C.; Foley, M. A.; Hilgendorf, C.; Johnston, S. E.; Lee IV, M. D.; Lewis, R. J.; McCarren, P.; Muncipinto, G.; Norinder, U.; Perry, M. W. D.; Duvall, J. R.; Kihlberg, J. Structural and Conformational Determinants of Macrocyclic Cell Permeability. *Nat Chem Biol* **2016**, *12* (12), 1065–1074.

(49) Doak, B. C.; Over, B.; Giordanetto, F.; Kihlberg, J. Oral Druggable Space beyond the Rule of 5: Insights from Drugs and Clinical Candidates. *Chem. Biol.* **2014**, *21* (9), 1115–1142. <https://doi.org/10.1016/j.chembiol.2014.08.013>.

(50) Nielsen, D. S.; Shepherd, N. E.; Xu, W.; Lucke, A. J.; Stoermer, M. J.; Fairlie, D. P. Orally Absorbed Cyclic Peptides. *Chem. Rev.* **2017**, *117* (12), 8094–8128. <https://doi.org/10.1021/acs.chemrev.6b00838>.

(51) Appiah Kubi, G.; Dougherty, P. G.; Pei, D. Designing Cell-Permeable Macrocyclic Peptides. *Methods Mol. Biol. Clifton NJ* **2019**, *2001*, 41–59. https://doi.org/10.1007/978-1-4939-9504-2_3.

(52) Walport, L. J.; Obexer, R.; Suga, H. Strategies for Transitioning Macrocyclic Peptides to Cell-Permeable Drug Leads. *Chem. Biotechnol. • Pharm. Biotechnol.* **2017**, *48*, 242–250. <https://doi.org/10.1016/j.copbio.2017.07.007>.

(53) Liras, S.; McClure, K. F. Permeability of Cyclic Peptide Macrocycles and Cyclotides and Their Potential as Therapeutics. *ACS Med. Chem. Lett.* **2019**, *10* (7), 1026–1032. <https://doi.org/10.1021/acsmedchemlett.9b00149>.

(54) Rhodes, C. A.; Dougherty, P. G.; Cooper, J. K.; Qian, Z.; Lindert, S.; Wang, Q.-E.; Pei, D. Cell-Permeable Bicyclic Peptidyl Inhibitors against NEMO-I κ B Kinase Interaction Directly from a Combinatorial Library. *J. Am. Chem. Soc.* **2018**, *140* (38), 12102–12110. <https://doi.org/10.1021/jacs.8b06738>.

(55) Deshayes, S.; Morris, M. C.; Divita, G.; Heitz, F. Cell-Penetrating Peptides: Tools for Intracellular Delivery of Therapeutics. *Cell. Mol. Life Sci. CMLS* **2005**, *62* (16), 1839–1849. <https://doi.org/10.1007/s00018-005-5109-0>.

- (56) Dougherty, P. G.; Sahni, A.; Pei, D. Understanding Cell Penetration of Cyclic Peptides. *Chem. Rev.* **2019**, *119* (17), 10241–10287. <https://doi.org/10.1021/acs.chemrev.9b00008>.
- (57) Burton, P. S.; Conradi, R. A.; Ho, N. F. H.; Hilgers, A. R.; Borchardt, R. T. How Structural Features Influence the Biomembrane Permeability of Peptides. *J. Pharm. Sci.* **1996**, *85* (12), 1336–1340. <https://doi.org/10.1021/js960067d>.
- (58) Di, L.; Whitney-Pickett, C.; Umland, J. P.; Zhang, H.; Zhang, X.; Gebhard, D. F.; Lai, Y.; Federico, J. J.; Davidson, R. E.; Smith, R.; Reyner, E. L.; Lee, C.; Feng, B.; Rotter, C.; Varma, M. V.; Kempshall, S.; Fenner, K.; El-kattan, A. F.; Liston, T. E.; Troutman, M. D. Development of a New Permeability Assay Using Low-efflux MDCKII Cells. *J. Pharm. Sci.* **2011**, *100* (11), 4974–4985. <https://doi.org/10.1002/jps.22674>.
- (59) Andrews, M. J. I.; Kontopidis, G.; McInnes, C.; Plater, A.; Innes, L.; Cowan, A.; Jewsbury, P.; Fischer, P. M. REPLACE: A Strategy for Iterative Design of Cyclin-Binding Groove Inhibitors. *ChemBioChem* **2006**, *7* (12), 1909–1915. <https://doi.org/10.1002/cbic.200600189>.
- (60) Liu, S.; Premnath, P. N.; Bolger, J. K.; Perkins, T. L.; Kirkland, L. O.; Kontopidis, G.; McInnes, C. Optimization of Non-ATP Competitive CDK/Cyclin Groove Inhibitors through REPLACE-Mediated Fragment Assembly. *J. Med. Chem.* **2013**, *56* (4), 1573–1582. <https://doi.org/10.1021/jm3013882>.
- (61) Nandha Premnath, P.; Craig, S.; McInnes, C. Development of Inhibitors of Protein-Protein Interactions through REPLACE: Application to the Design and Development Non-ATP Competitive CDK Inhibitors. **2015**, No. 104, e52441. <https://doi.org/10.3791/52441>.
- (62) Sciabola, S.; Goetz, G. H.; Bai, G.; Rogers, B. N.; Gray, D. L.; Duplantier, A.; Fonseca, K. R.; Vanase-Frawley, M. A.; Kablaoui, N. M. Systematic N-Methylation of Oxytocin: Impact on Pharmacology and Intramolecular Hydrogen Bonding Network. *Bioorg. Med. Chem.* **2016**, *24* (16), 3513–3520. <https://doi.org/10.1016/j.bmc.2016.05.062>.
- (63) Raju, S.; Whalen, D. M.; Mengistu, M.; Swanson, C.; Quinn, J. G.; Taylor, S. S.; Webster, J. D.; Newton, K.; Shaw, A. S. Kinase Domain Dimerization Drives RIPK3-Dependent Necroptosis. *Sci. Signal.* **2018**, *11* (544), eaar2188. <https://doi.org/10.1126/scisignal.aar2188>.

(64) Huang, C. S.; Oberbeck, N.; Hsiao, Y.-C.; Liu, P.; Johnson, A. R.; Dixit, V. M.; Hymowitz, S. G. Crystal Structure of Ripk4 Reveals Dimerization-Dependent Kinase Activity. *Structure* **2018**, *26* (5), 767-777.e5. <https://doi.org/10.1016/j.str.2018.04.002>.

APPENDIX A

CHARACTERIZATION OF PEPTIDES

TABLE A.1: LCMS CHARACTERIZATION OF SYNTHETIC PEPTIDES

Peptide	Column Dimensions	Method	Flow Rate	Retention Time	Theoretical MW	Observed MW
1	4.6 x 250 mm	5-65% ACN/water/0.1% TFA/25 min	1 mL/min	20.3	2205.6	2205.0
2	4.6 x 250 mm	5-65% ACN/water/0.1% TFA/25 min	1 mL/min	19.3	2185.5	2186.1
3	4.6 x 250 mm	5-65% ACN/water/0.1% TFA/25 min	1 mL/min	20.7	2205.6	2205.9
4	4.6 x 250 mm	5-65% ACN/water/0.1% TFA/25 min	1 mL/min	17.1	2163.5	2163.3
5	4.6 x 250 mm	5-65% ACN/water/0.1% TFA/25 min	1 mL/min	19.9	2178.6	2178.2
6	4.6 x 250 mm	5-65% ACN/water/0.1% TFA/25 min	1 mL/min	19.4	2162.6	2162.4
7	4.6 x 250 mm	5-65% ACN/water/0.1% TFA/25 min	1 mL/min	18.2	2219.6	2219.4
8	4.6 x 250 mm	5-65% ACN/water/0.1% TFA/25 min	1 mL/min	17.7	2175.6	2175.3
9	4.6 x 250 mm	5-65% ACN/water/0.1% TFA/25 min	1 mL/min	20.2	2215.7	2215.3
10	4.6 x 250 mm	5-65% ACN/water/0.1% TFA/25 min	1 mL/min	18.3	2177.6	2177.2
11	4.6 x 250 mm	5-65% ACN/water/0.1% TFA/25 min	1 mL/min	17.0	2163.6	2163.4
12	4.6 x 250 mm	5-65% ACN/water/0.1% TFA/25 min	1 mL/min	18.6	2205.6	2205.4
13	4.6 x 250 mm	5-65% ACN/water/0.1% TFA/25 min	1 mL/min	20.1	2219.6	2219.4
14	4.6 x 250 mm	5-65% ACN/water/0.1% TFA/25 min	1 mL/min	17.7	2173.6	2173.3
15	4.6 x 250 mm	5-65% ACN/water/0.1% TFA/25 min	1 mL/min	17.7	1854.3	1853.9
16	4.6 x 250 mm	5-65% ACN/water/0.1% TFA/25 min	1 mL/min	17.7	1740.2	1739.9
17	4.6 x 250 mm	5-65% ACN/water/0.1% TFA/25 min	1 mL/min	17.0	1797.2	1797.5
18	4.6 x 250 mm	5-65% ACN/water/0.1% TFA/25 min	1 mL/min	18.9	1796.2	1796.1

Peptide	Column Dimensions	Method	Flow Rate	Retention Time	Theoretical MW	Observed MW
19	4.6 x 250 mm	5-65% ACN/water/0.1% TFA/25 min	1 mL/min	14.8	1839.3	1839.7
20	4.6 x 250 mm	5-65% ACN/water/0.1% TFA/25 min	1 mL/min	15.0	1755.2	1755.2
21	4.6 x 250 mm	5-95% ACN/water/0.1% TFA/30 min	1 mL/min	15.5	1713.1	1712.4
22	4.6 x 250 mm	5-65% ACN/water/0.1% TFA/25 min	1 mL/min	15.9	1740.1	1740.2
23	4.6 x 250 mm	5-65% ACN/water/0.1% TFA/25 min	1 mL/min	19.4	1712.1	1712.0
24	4.6 x 250 mm	5-65% ACN/water/0.1% TFA/25 min	1 mL/min	13.6	1731.2	1731.5
25	4.6 x 250 mm	5-65% ACN/water/0.1% TFA/25 min	1 mL/min	17.5	1754.2	1754.2
26	4.6 x 250 mm	5-65% ACN/water/0.1% TFA/25 min	1 mL/min	17.8	1755.2	1755.3
27	4.6 x 250 mm	5-65% ACN/water/0.1% TFA/25 min	1 mL/min	16.4	1755.2	1755.5
28	4.6 x 250 mm	5-65% ACN/water/0.1% TFA/25 min	1 mL/min	13.9	1721.1	1721.3
29	4.6 x 250 mm	5-65% ACN/water/0.1% TFA/25 min	1 mL/min	15.3	1737.1	1737.2
30	4.6 x 250 mm	5-95% ACN/water/0.1% FA/20 min	1 mL/min	20.5	1886.3	1888.0
31	4.6 x 250 mm	5-95% ACN/water/0.1% FA/20 min	1 mL/min	20.0	1872.3	1872.0
32	4.6 x 250 mm	5-65% ACN/water/0.1% TFA/25 min	1 mL/min	17.5	1684.1	1683.5
33	4.6 x 250 mm	5-95% ACN/water/0.1% TFA/30 min	1 mL/min	17.2	1707.0	1708.0
34	4.6 x 250 mm	5-95% ACN/water/0.1% TFA/30 min	1 mL/min	17.7	1722.1	1724.0
35	4.6 x 250 mm	5-95% ACN/water/0.1% TFA/30 min	1 mL/min	17.4	1664.0	1664.0
36	4.6 x 250 mm	5-95% ACN/water/0.1% TFA/30 min	1 mL/min	18.2	1679.1	1680.0
37	4.6 x 250 mm	5-95% ACN/water/0.1% TFA/30 min	1 mL/min	17.6	1683.1	1682.0
38	4.6 x 250 mm	5-95% ACN/water/0.1% FA/20 min	1 mL/min	17.2	1715.1	1714.9
39	4.6 x 250 mm	5-95% ACN/water/0.1% FA/20 min	1 mL/min	18.3	1679.1	1680.0
40	4.6 x 250 mm	5-95% ACN/water/0.1% FA/20 min	1 mL/min	17.6	1665.1	1668.0
41	4.6 x 250 mm	5-95% ACN/water/0.1% FA/20 min	1 mL/min	17.1	1693.1	1693.0
42	4.6 x 250 mm	5-95% ACN /water/0.1% FA/20 min	1 mL/min	18.9	1281.6	1281.3
43	4.6 x 250 mm	5-95% ACN /water/0.1% FA/20 min	1 mL/min	18.4	1279.6	1279.3

Peptide	Column Dimensions	Method	Flow Rate	Retention Time	Theoretical MW	Observed MW
44	2.1 x 100 mm	10-95% ACN /water/0.1%FA/20 min	0.2 mL/min	1.8	719.8	720.0
45	4.6 x 250 mm	5-95% ACN /water/0.1% FA/20 min	1 mL/min	24.0	1403.7	1403.3
46	4.6 x 250 mm	5-95% ACN /water/0.1% FA/20 min	1 mL/min	24.4	1417.7	1417.3
47	4.6 x 250 mm	5-95% ACN /water/0.1% FA/20 min	1 mL/min	22.1	1431.8	1431.4
48	4.6 x 250 mm	5-95% ACN /water/0.1% FA/20 min	1 mL/min	22.4	1445.8	1445.5
49	4.6 x 250 mm	5-95% ACN /water/0.1% FA/20 min	1 mL/min	21.2	1325.7	1325.6
50	4.6 x 250 mm	5-95% ACN /water/0.1% FA/20 min	1 mL/min	19.7	1325.7	1325.6
51	4.6 x 250 mm	5-95% ACN /water/0.1% FA/20 min	1 mL/min	20.8	1325.7	1325.6
52	4.6 x 250 mm	5-95% ACN /water/0.1% FA/20 min	1 mL/min	25.0	1046.3	1046.1
53	4.6 x 250 mm	5-95% ACN /water/0.1% FA/20 min	1 mL/min	22.1	1014.2	1014.1
54	4.6 x 250 mm	5-95% ACN /water/0.1% FA/20 min	1 mL/min	23.1	960.2	960.1
55	4.6 x 250 mm	5-95% ACN /water/0.1% FA/20 min	1 mL/min	24.1	862.1	862.0
56	4.6 x 250 mm	5-95% ACN /water/0.1% FA/20 min	1 mL/min	20.3	1592.8	1592.4
57	4.6 x 250 mm	5-95% ACN /water/0.1% FA/20 min	1 mL/min	18.9	1826.3	1828.0
58	4.6 x 250 mm	5-95% ACN /water/0.1% FA/20 min	1 mL/min	25.8	1029.3	1029.1

APPENDIX B

TC-NMR DATA

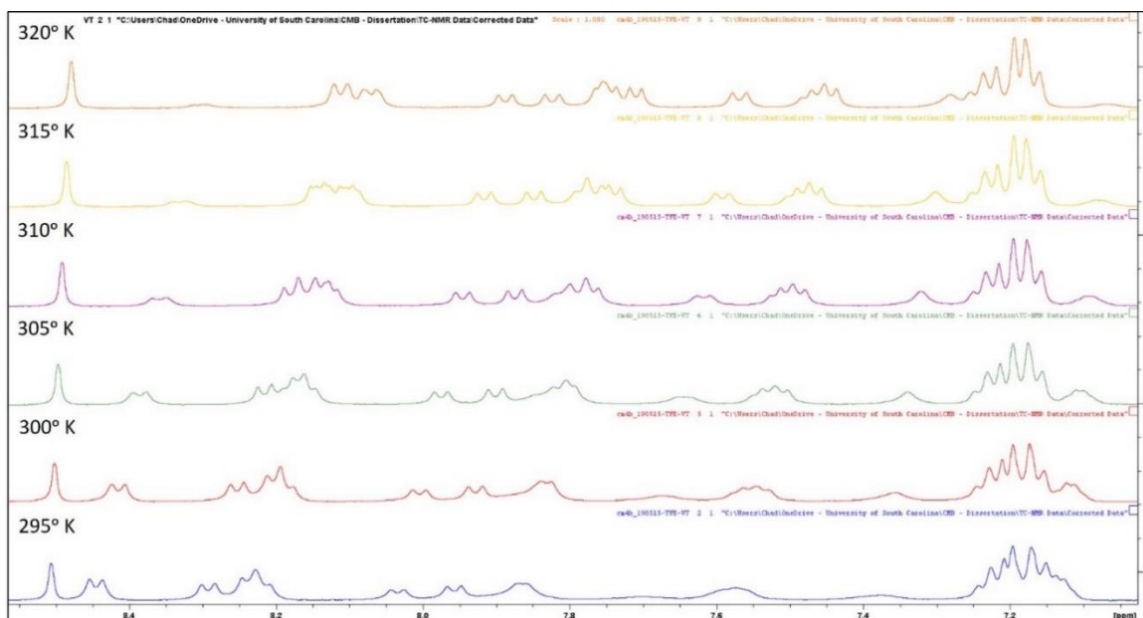


FIGURE B.1: TC-NMR SPECTRA OF PEPTIDE 17: NMR spectra were taken from 295-320° K showing that all amide protons shifted at temperature-dependent rate faster than that associated with IMHBs.